

**Mice of different genetic backgrounds
respond to house dust mite extract
with distinct asthma phenotypes
and microbial changes**

Dissertation

zur Erlangung des Doktorgrades
der Mathematisch-Naturwissenschaftlichen Fakultät
der Christian-Albrechts-Universität zu Kiel

vorgelegt von

Joni Valeska Lund

Borstel, 2020

Erster Gutachter: Prof. Dr. Holger Heine

Zweiter Gutachter: Prof. Dr. Thomas Roeder

Tag der mündlichen Prüfung: 04.06.2020

I. Abstract

Asthma is a multifactorial chronic inflammatory disease of the lungs with pathophysiological and phenotypic heterogeneity. Approximately 339 million individuals worldwide are currently suffering from asthma according to the Global Asthma Report published in 2018. Asthma risk is shaped by a complex interaction of host genetics and environmental influences, which might both affect the host's microbiome. The rise in asthma prevalence over the past decades cannot be explained by genetic changes as these occur over longer periods of time. Thus, it is assumed that changing environmental influences affect the host's microbiome in first instance. This study aimed to obtain a first insight into the relative contribution of the host's genetics versus the host's microbiome in shaping asthma phenotypes. After experimental asthma induction by applying house dust mite (HDM) extract in four mouse strains of different genetic backgrounds (A/J, BALB/cJ, C57BL/6J and C3H/HeJ) the asthma phenotypes and the gut and lung microbial compositions were evaluated.

HDM treatment induced distinct phenotypes in the four mouse strains. C3H/HeJ was identified as a strong Th2-prone, eosinophilic phenotype with pronounced goblet cell hyperplasia and high IgE levels. A/J displayed a similar phenotype with slightly lower levels of Th2-cytokines, whereas BALB/cJ were characterized by a Th2-low phenotype with an overall reduced severity. C57BL/6J showed an intermediate phenotype with higher IL-17A levels in the BAL supernatant than in the remaining strains. Furthermore, it was found that the microbial composition in the gut did not differ among the strains and was also not altered after the induction of experimental asthma. Aside from the A/J and C57BL/6J, the lung microbial composition in the healthy mice showed no marked variation among the strains. However, the abundance of Proteobacteria in the lungs of all HDM-treated groups was increased. Comparing the beta diversity measures of the PBS versus the HDM group revealed a significant difference in the microbial profile only for the C3H/HeJ strain.

These results suggest a contribution of the genetic background on the developing asthma phenotypes. While, the genetics appear to have only a minor impact on the microbial composition in healthy mice. This changes in the disease state where the

lung microbial composition differs among mice of different genetic backgrounds. The obtained results on the microbial composition are purely descriptive, therefore future studies in germ-free mice, including high-resolution sequencing, are required to identify the relevance of single bacteria on lung health.

II. Zusammenfassung

Asthma ist eine multifaktoriell verursachte chronisch entzündliche Lungenerkrankung mit pathophysiologischer und phänotypischer Heterogenität. Laut dem 2018 veröffentlichten Global Asthma Report leiden weltweit etwa 339 Millionen Menschen an Asthma. Das Asthmarisiko wird durch ein komplexes Zusammenspiel von Wirtsgenetik und Umwelteinflüssen geprägt, welche sich beide auf das Mikrobiom des Wirtes auswirken können. Der Anstieg der Asthma-Prävalenz in den letzten Jahrzehnten lässt sich nicht durch Veränderungen der genetischen Ausstattung erklären, da diese über einen längeren Zeitraum erfolgen. Es wird daher angenommen, dass sich verändernde Umwelteinflüsse zunächst primär die mikrobielle Besiedlung beeinflussen. Ziel dieser Arbeit war es daher einen ersten Einblick zu gewinnen, inwiefern die Genetik im Vergleich zur mikrobiellen Besiedlung des Wirtes die phänotypische Ausprägung der Asthmaerkrankung beeinflusst. Nach der experimentellen Asthmaprovokation durch die intranasale Applikation eines Hausstaubmilben-Extraktes in vier Mausstämmen mit unterschiedlichem genetischen Hintergrund (A/J, BALB/cJ; C57BL/6J und C3H/HeJ) wurden die Asthmaphänotypen sowie die mikrobiellen Kompositionen des Darmes und der Lunge untersucht.

In diesem Projekt konnten durch die identische HDM Behandlung in vier verschiedenen Mausstämmen unterschiedliche Asthmaphänotypen charakterisiert werden. C3H/HeJ wurde als ein ausgeprägt eosinophiler Th2-Phänotyp mit erheblicher Bcherzellhyperplasie sowie hohen IgE-Spiegeln im Blut identifiziert. A/J entwickelte einen vergleichbaren Phänotyp jedoch mit erniedrigten Th2-Zytokinen im Überstand der bronchoalveolaren Spülung (BAL). BALB/cJ dahingegen wurde als ein milder Phänotyp mit niedrigen Th2-Zytokinen sowie deutlich verringerten Eosinophilen in der BAL charakterisiert. Die C57BL/6J Mäuse entwickelten einen moderaten Phänotyp, welcher sich insbesondere durch signifikant höhere IL-17A Konzentrationen in dem Überstand der BAL im Vergleich zu den anderen Mausstämmen auszeichnete.

Die Untersuchung des Darmmikrobioms hat keine Unterschiede innerhalb der Kontrollgruppen und der Asthmagruppen der unterschiedlichen Stämme ergeben. Abgesehen von A/J und C57BL/6J Mäusen zeigt die mikrobielle Komposition der Lungen

in den gesunden Mäusen keine erkennbaren Unterschiede zwischen den Mausstämmen. Eine ausgeprägte Veränderung der Zusammensetzung des Lungenmikrobioms wurde jedoch durch den Anstieg von Proteobakterien in den Lungen aller mit HDM behandelten Mäuse verzeichnet. Dennoch führten die Veränderungen in der mikrobiellen Zusammensetzung der Lungen nur in dem C3H/HeJ-Stamm zu einem statistisch signifikanten Unterschied der Betadiversität zwischen den unterschiedlichen Behandlungsgruppen (C3H/HeJ PBS vs. HDM). Die Betadiversität ist ein Maß für die Variation der mikrobiellen Komposition zwischen verschiedenen Gruppen.

Diese Ergebnisse deuten darauf hin, dass die Ausprägung des Asthmaphänotyps von der Genetik des Mausstammes beeinflusst wird. Dahingegen scheint sich die Genetik nur begrenzt auf die Zusammensetzung des Mikrobioms in gesunden Mäusen auszuwirken. Dies verändert sich jedoch im erkrankten Zustand, in welchem sich das Lungenmikrobiom der verschiedenen Mausstämme unterschiedlich verändert.

Die Ergebnisse zur mikrobiellen Zusammensetzung sind bislang rein deskriptiv, daher werden zukünftige Studien in keimfreien Mäusen sowie hochauflösende Sequenziermethoden erforderlich sein, um die Relevanz einzelner Bakterien für die Lungengesundheit zu untersuchen.

III. List of Abbreviations

AAI	allergic airway inflammation
AERD	aspirin-exacerbated respiratory disease
AHR	airway hyperresponsiveness
alum	aluminium hydroxid/magnesium hydroxid
ANOVA	analysis of variance
BAL	bronchoalveolar lavage
BALF	bronchoalveolar lavage fluid
bp	base pair
BSA	bovine serum albumin
C	Celsius
CAST	Computer Assisted Stereology Toolbox
CCL11	Eotaxin
CD	cluster of differentiation
cDNA	complementary DNA
CH	Calinski Harabasz
CLD	chronic lung diseases
cm	centimeter
ddCp	delta delta crossing point
Der f	Dermatophagoides farinae
Der p	Dermatophagoides pteronyssinus
DNA	deoxyribonucleic acid
dNTP	deoxynucleotide triphosphate
ds	double-stranded
e.g.	exempli gratia
EIA	exercise-induced asthma
ELISA	enzyme-linked immunosorbent assay
etc.	et cetera
EtOH	Ethanol
fwd	forward
g	gram

GWAS	genome-wide association studies
HDM	house dust mite
HPRT	Hypoxanthine-guanine phosphoribosyltransferase
HRP	horseradish peroxidase
i. e.	id est
i. n.	intranasal
i. p.	intraperitoneal
IC	inspiratory capacity
ICS	inhaled corticosteroids
IFN	interferon
Ig	immunoglobuline
IL	interleukin
K	Cluster (k-mer)
LPS	Lipopolysaccharids
MDS	multidimensional scaling
mg	milligram
MID	multiplex identifier
min	minutes
ml	milliliter
mm	millimeter
MUC5B	Mucin 5B
n	number of animals
NaCl	sodium chloride
NEC	negative extraction control
ng	nanogram
NGS	next-generation sequencing
NRNA	non-RNA sample
NRT	non-reverse transcriptase sample
μl	microliter
μm	micrometer
OD	optical density
ORMDL3	orosomucoid 1-like 3

OTU	operational taxonomic unit
OVA	ovalbumin
padj	adjusted <i>p</i> value
PAS	periodic acid-Schiff
PBS	Phosphate buffered Saline
PERMANOVA	permutational multivariate analysis of variance
pg	picogram
qRT-PCR	quantitative real-time polymerase chain reaction
rDNA	ribosomal DNA
rev	reverse
rpm	rounds min ⁻¹
rRNA	ribosomal RNA
SCFA	short chain fatty acids
SD	standard deviation
s	seconds
SNP	single nucleotide polymorphism
TBP	TATA sequence binding protein
TH	T helper cell
TNF	tumor necrosis factor
TSLPR	thymic stromal lymphopoietin receptor
vs.	versus
WHO	World Health Organisation
WT	wild-type

IV. Table of Contents

I. Abstract	I
II. Zusammenfassung	III
III. List of Abbreviations	V
IV. Table of Contents	VIII
1 Introduction	1
1.1 Asthma bronchiale	1
1.1.1 Definition and incidence rates	1
1.1.2 Phenotypes and pathogenesis of asthma.....	2
1.1.3 Host genetics and environmental factors influencing asthma risk.....	4
1.2 The Microbiome	6
1.2.1 Definition, sequencing approaches	6
1.2.2 Lung Microbiome	7
2 Aims and Research Questions	10
3 Materials and Methods	11
3.1 Materials.....	11
3.1.1 Chemicals and reagents	11
3.1.2 Buffer and solutions	13
3.1.3 Antibodies.....	14
3.1.4 Oligonucleotides	14
3.1.5 Commercial kits	16
3.1.6 Consumables	16
3.1.7 Mouse strains	17
3.1.8 Devices and equipment.....	18
3.1.9 Software	19
3.2 Methods.....	20
3.2.1 Animals	20
3.2.2 Asthma treatment protocol	20
3.2.3 Characterization of asthma phenotype.....	20
3.2.4 Microbiome analysis.....	25
3.3 Statistical analysis	28
3.4 Bioinformatic analysis	29
3.4.1 Analysis of raw sequences.....	29
3.4.2 Analysis in R.....	30

4	Results	32
4.1	Asthma phenotype.....	32
4.1.1	Airway inflammation.....	32
4.1.2	Lung function.....	37
4.1.3	Total IgE in serum.....	40
4.1.4	Histology.....	40
4.1.5	Gene expression in lung homogenates	42
4.2	Microbiome analysis.....	45
4.2.1	Analysis of caecum in R.....	45
4.2.2	Analysis of lungs in R	53
5	Discussion	63
5.1	Characterization of asthma phenotypes	63
5.2	Microbial composition in a murine asthma model.....	69
5.2.1	The murine gut and lung microbiome – methodological challenges	70
5.2.2	Analysis of lung and gut microbiome in healthy mice.....	73
5.2.3	Analysis of lung and gut microbiome in murine experimental asthma	74
5.3	Conclusion	77
5.4	Future perspective	78
6	Bibliography	80
7	Appendix	99
7.1	Supplemental results	99
7.2	List of Figures	103
7.3	List of Tables.....	104
7.4	Eidesstattliche Erklärung.....	105
7.5	Curriculum vitae.....	106
7.6	Acknowledgements	107

1 Introduction

1.1 Asthma bronchiale

1.1.1 Definition and incidence rates

According to the latest report of the Global Initiative for Asthma (GINA), asthma is a “heterogeneous disease, usually characterized by chronic airway inflammation. It is defined by the history of respiratory symptoms such as wheeze, shortness of breath, chest tightness and cough that vary over time and in intensity, together with variable expiratory airflow limitation”¹. Airway hyperresponsiveness and inflammation are generally associated with the disease, but are neither a prerequisite nor sufficient themselves for the diagnosis of asthma¹. The 2018 Global Asthma Report estimates that about 339 million persons worldwide are currently affected by asthma. In Europe, 3-9% of the population aged 18 to 45 are diagnosed with asthma and thereby present a major socioeconomic burden for both society and health care systems². Moreover, asthma frequently starts in childhood and can persist lifelong, the World Health Organization (WHO) ranks asthma as the most common chronic disease in children. The incidence of childhood asthma in European children was estimated to be 17 % in 2008³. The global numbers of asthmatics in all age groups have been observed to be on a rise, this applies particularly for low- and middle-income countries, whereas first evidences were found that the prevalence in high-income states is rather declining^{4,5}. The age at disease onset can vary widely, meaning it can occur during early childhood or later in life during adulthood. Early onset asthma can either fully recover or further persist into adulthood. Known risk factors which increase the likelihood of the transition from childhood to adulthood asthma have been identified as the severity of childhood asthma, female gender, smoking and atopy⁶. Interestingly, before puberty asthma is more prevalent in boys, while in adults this is reversed and more women are diseased than men. One explanation for this change that is presumably involved in this reversal after puberty is the influence of sex hormones⁷.

1.1.2 Phenotypes and pathogenesis of asthma

Asthma is no longer considered a single disease entity, but rather a multifactorial syndrome encompassing different phenotypes that are caused by distinct pathogenic pathways. When the underlying mechanisms are considered, phenotypes are further referred to as endotypes^{8,9}. This debate is not a purely academic one, as different phenotypes might require different “personalized” therapies and thus might be of clinical relevance as well. Classically, asthma has been sub-classified in allergic (non-intrinsic) and non-allergic (intrinsic) asthma. Allergic asthma is more frequent in children and triggered by inhalant allergens such as house dust mite (HDM), pet dander, pollen and others while non-allergic asthma is independent from allergen exposure. Non-allergic asthma is more often seen in adults than in children and attacks can be triggered by cold air, exercise, viral infection or other substances such as aspirin¹⁰⁻¹². Non-allergic asthma thus lacks detectable sensitization via allergen-specific immunoglobulin (Ig)E¹³. However, the dichotomy of allergic *versus* (vs.) non-allergic asthma is nowadays considered an oversimplification and insufficient to fully describe the heterogeneity of asthma¹⁴⁻¹⁶. According to the GINA report in 2019 asthma phenotypes are defined as “recognizable clusters of demographic, clinical and/or pathophysiological characteristics”¹. Thus, the sub-classification of asthma is further evolving and the underlying molecular mechanisms are thought to be responsible for the different phenotypic manifestations. This led to the description of two major asthma endotypes: a T helper(Th)2-high endotype with high numbers of eosinophils and a Th2-low, non-eosinophilic rather neutrophilic or mixed endotype and the respective associated Th2 vs. non-Th2 inflammatory cytokines as measured in blood, bronchoalveolar lavage (BAL) or sputum samples^{17,18}. Accordingly, the Th2-high type shows a good treatment response to inhaled corticosteroids (ICS) which is less in non-Th2 type asthma¹⁷. Beyond that, the Th2-high group has been sub-classified into either early or late onset both manifesting a wide range of severity¹⁹. Late-onset eosinophilic asthma as well as aspirin-exacerbated respiratory disease (AERD) are proposed to belong to the Th2-high cluster. Both phenotypes have been described to show a more pronounced severity compared to the much milder form of the disease in the exercise-induced asthma (EIA), although all belong to the category of Th2-high phenotypes¹⁹⁻²³. Some patient characteristics such as obesity and smoking, are mainly

found in the non-Th2 asthma cluster^{24,25}. The vast majority of very late-onset asthmatics are predominately found to be women with a neutrophilic non-Th2 asthma phenotype²⁶. Furthermore, this phenotype is often characterized by higher disease severity with less reversible airflow obstruction and resistance to steroid treatment²⁷⁻³¹. A paucigranulocytic phenotype is characterized by the absence of increased inflammatory cells in blood or airways but presence of hypertrophic smooth muscle tissue mediating airway obstruction³².

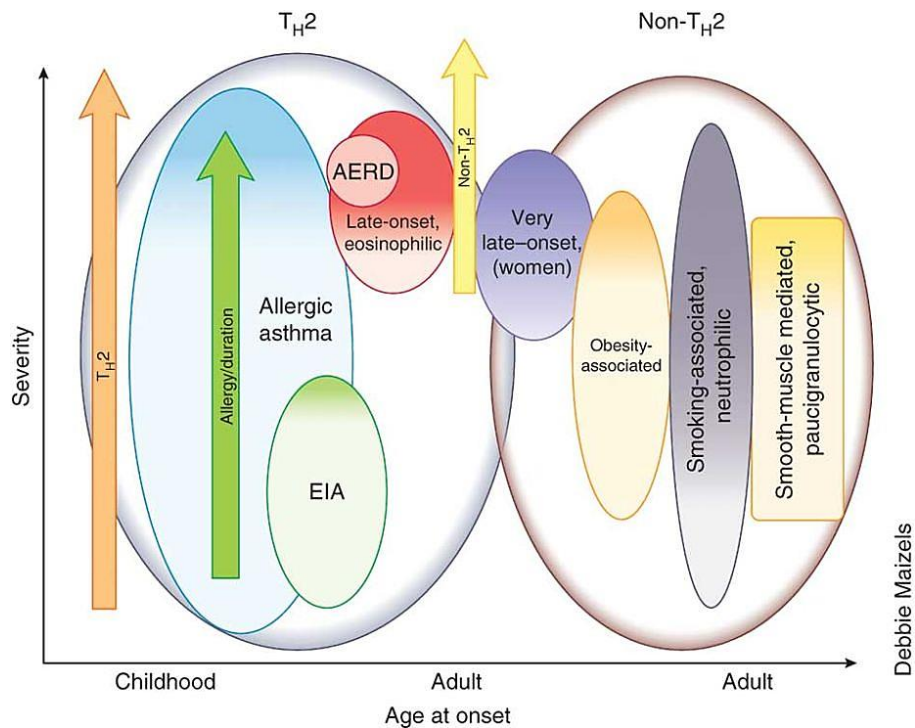


Figure 1.1: Categorization of the asthma disease in Th2-high and non-Th2 phenotypes.

Further classification is based on the consideration of the following factors; severity, age at onset, triggers, as well as patient related factors. Picture taken from Wenzel et al., Nat Med., 2012¹⁶.

As already described above, the pathogenesis of asthma is highly complex where the underlying molecular processes can differ widely– and are therefore not yet understood in all detail. Hence, asthma can be classified as Th2-high mediated eosinophilic asthma and Th2-low mediated asthma. Th2-high asthma is characterized by the presence of Th2 helper cells and the Th2-cytokines IL-4, IL-5 and IL-13³³. The presence of IL-5 stimulates and activates the function of eosinophils³⁴. IL-4 and IL-13 induce the IgE class switch in B cells and amplify Th2 cells^{35,36}. Th2-low asthma is mainly characterized by Th1- and Th17-inflammatory pathways and often accompanied by neutrophil influx into the airways or a mixed granulocytic immunopathology^{27,28,37,38}. In neutrophilic asthma increased Th1- (INF-gamma, IL-2

and TNF-alpha) and Th17- (mainly IL-17) cytokines are detected in the lungs and systemically³⁹⁻⁴³. Beneath airway inflammation, narrowing of the airways is caused by the contraction of the airway smooth muscle (ASM). The increase of ASM is accompanied by mast-cell infiltration, and has been identified to be further correlated with bronchial constriction⁴⁴. Both chronic airway inflammation and airway hyperresponsiveness (AHR) are usually enduring, even during times when symptoms are gone. As stated above, airway remodeling is another major feature of asthma. The remodeling process comprises various structural changes such as thickening of the airway epithelium⁴⁵ *exempli gratia* (e. g.) goblet cell hyperplasia^{46,47}, increased subepithelial collagen, submucosal matrix, ASM tissue^{48,49}, and mast cell localization in the latter one. The positive association of asthma severity and the degree of remodeling processes, e. g. airway thickening, has previously been shown⁵⁰.

1.1.3 Host genetics and environmental factors influencing asthma risk

The risk to develop asthma results from a complex interaction of host genetics and the environment which especially occurs during critical developmental windows in life. In addition, several observations suggest that modifications of early life microbial exposure can alter immune development thereby modifying the risk for allergic disease^{51,52}. Further, other non-asthma related patient factors such as lifestyle, nutrition, environment *et cetera* (etc.) can contribute to the disease development or severity⁶. Ante- and perinatal factors enhancing asthma risk include amongst others low birth weight, *in utero* exposure to tobacco smoke⁵³ and cesarean section⁵⁴. All these factors have also been related to the risk for allergic disease⁵⁵. Vice versa, the contact of younger children to older siblings at home or playfellows in daycare has been inversely correlated with the risk for asthma⁵⁶. Similarly breastfeeding has been identified as a protective factor as it is related to lower asthma risk during the first four years of life⁵⁷. Growing up with pets in the same household has been associated with protection from sensitization and the development of asthma. This association exists for dog owners, in contrast close contact to cats increases rates of sensitization⁵⁸. The observation that children born to atopic parents are more likely to develop allergic sensitization and asthma suggested a genetic contribution to atopic asthma⁵¹. Later on, several single nucleotide polymorphisms (SNPs) related to asthma susceptibility were identified in genome-wide association studies (GWAS). For

example, SNPs on chromosome 2 (IL18R1 and IL1RL1), chromosome 6 (HLA-DQ region of the major histocompatibility complex gene), chromosome 9 (flanking the IL33 gene), chromosome 15 (SMAD3) and chromosome 22 (IL2RB) have been identified as genetic risk factors in the development of asthma^{59,60}. In particular, a SNP in the orosomucoid 1-like 3 (ORMDL3) gene locus is a strong predictor of childhood asthma in GWAS⁶¹⁻⁶⁷. Various effects of gene-environment interactions on asthma susceptibility have been examined by genotyping SNPs in candidate genes. On the one hand, children who were exposed to passive smoke during their childhood present a linkage of asthma and AHR to chromosome 5q⁶⁸ and environmental smoke exposure has further been linked to an increased risk for early-onset asthma, inasmuch SNPs of the 17q21 are present⁶⁹. On the other hand, the same genotype of 17q21 locus was identified to interact with animals shed exposures as well as the number of siblings during the time of wheezing and acts as an asthma protective manner⁷⁰. Another asthma-protective effect linked to gene-environment interaction, detected in farmers' children exclusively, was associated with a genetic variation characterised by the SNPs of one to two T alleles on the TLR2 gene⁷¹. Many epidemiological studies showed that growing up on a farm with livestock protects from asthma susceptibility⁷²⁻⁷⁴. In a hallmark study by Stein et al. Amish and Hutterite communities were compared. The Amish immigrated to the USA from 1720 onwards, mainly from Germany and Switzerland. Similarly, the Hutterite populations migrated in the late 18th century from various European regions to the USA. Both populations have a similar genetic background and still live today like their ancestors sharing a similar lifestyle. However, the Amish community performs traditional farming while the Hutterite do industrialized farming. The Amish children showed a significant lower susceptibility to develop asthma, compared to the Hutterite children reporting four times more asthma cases⁷⁴. In dust samples collected in their homes, endotoxin levels were nearly seven times higher in Amish homes as compared to those from Hutterites. To investigate this difference further, a murine model was applied to induce experimental allergic asthma under the influence of intranasal instillations of either Amish or Hutterite homes' dust extracts. The Amish house dust significantly inhibited the provocation of an AHR and eosinophilia, further on applying the same model in mice absent of MyD88 and TRIF signaling, both

molecules are important for innate signaling, these protective effects were no longer existent. These findings among others strongly suggest that early life exposure to a microbe-rich farm environment has a preventive influence on asthma development⁷⁵, attributing genetics a secondary role, whereas the involvement of the innate immune system plays a major role⁷⁴.

1.2 The Microbiome

1.2.1 Definition, sequencing approaches

The term “microbiota” refers to the collection of all microorganisms within a specific environment, whereas “microbiome” describes the genes of all microbes being present on a particular body site^{76,77}. However, in daily practice these terms are used interchangeably and it is popular to apply the term microbiome to microorganisms colonizing the human body or any other ecosystem. Throughout this dissertation the term “microbiome” will be used for the collection of bacteria present on a body site. The human microbiome encompasses a broad variety of microorganisms including bacteria, archaea, viruses and fungi. Surfaces of the body such as skin, mouth, nose, gut, vagina, stomach and lung harbor characteristic populations of microbes with commensal, symbiotic and facultative pathogenic properties on the different body sites^{78–83}. With the help of new analytical methods such as 16S ribosomal DNA (rDNA) or ribosomal RNA (rRNA) analysis and metagenomics, it is now possible to investigate the function and composition of the microbiome in health and disease. An important advantage of these techniques is the possibility to identify microorganisms which are not cultivable and thus have been neglected in the past^{84–86}. One of the innovations of this method is the use of highly specific, ubiquitous primers that bind to the highly conserved regions of the 16S rRNA gene, which is present in all bacterial cells. Through the identification of the universal targets the classification of the phylogeny was greatly simplified⁸⁷. The possibility to identify bacteria through 16S ribosomal sequencing is already known for more than three decades^{85,86}. However, early methodologies only allowed to analyze single sequences and therefore were unable to distinguish multiple bacteria in a single complex sample. During the past 15 years, advanced next-generation sequencing (NGS) technologies, such as pyrosequencing

and DNA sequencing methods based on amplification, have been used for deep analysis of complex microbial compositions⁸⁷⁻⁹⁰. These new developments in microbiological profiling, nowadays allow the massive parallel sequencing of amplified DNA molecules which are analyzed as spatial separated single-stranded DNA on a flow cell and sequences are achieved by fluorescent “reversible-terminating” deoxynucleotide triphosphate (dNTP)⁹¹. The application of these sequencing approaches has been broadly used to analyze the microbiomes of healthy individuals and patients in various disease states.

1.2.2 Lung Microbiome

The respiratory tract is lined by several types of epithelial cells covering a large area of ~120-140 m² which is topographically located at the body surface. Thus, it is exposed directly and with every breath to a wide range of environmental aerosolized materials, including gases, microbes and particulate matter from car emissions, tobacco smoke, pollens, or house dust. Of note, lung epithelial cells do not simply act as physical barrier, but exert important immune regulatory and first-line defense functions thereby controlling tissue homeostasis. Lung resident microbes are located in close proximity to the apical side of airway epithelia, thus forming an intimate interface between the latter and the external environment. Hilty et al. were among the first to describe in 2010 that healthy lungs are not sterile but harbor microorganisms⁸³. Thus, the longstanding dogma of sterile lungs has been progressively refuted. Since that time investigations of the lung microbiome have rapidly emerged⁹²⁻⁹⁷ and still presents a growing field of research. In contrast to the bacterial communities identified on other body sites, e. g. distal gut being colonized with 10¹¹-10¹² organisms per ml luminal content, the density of bacteria in the lungs is relatively small with only 10³-10⁴ bacterial genomes per cm² of lung tissue^{77,83,98}. The low bacterial burden in the lung was one factor keeping the controversial discussion on the existence of the lung microbiome and the proof of its existence ongoing for some time. By now, many observations support the role of the human lung microbiome as a potentially influential player in shaping the pathogenesis of asthma⁹⁹⁻¹⁰¹ and also other chronic lung diseases (CLD)¹⁰²⁻¹⁰⁴. However, characterizing a consistent distinct lung microbiome in healthy individuals remains a challenge as even healthy persons show a high inter-person individuality in the lung microbial composition^{98,105,106}. These observations have been

consistent, nevertheless the main phyla – Firmicutes, Bacteroidetes, Proteobacteria, Fusobacteria and Actinobacteria – were unanimously described to colonize the lungs^{83,94,105,107–109}. Technically, the study of the lung microbiome is demanding. It requires specific adaptations for the complete process from sample collection, library preparation, sequencing to the subsequent biostatistics approach and the inclusion of many controls as the sequencing of the lung microbiome has a higher risk to be influenced by contaminations due to the low bacterial burden. It is speculated that the microbiome composition could influence allergic asthma development¹¹⁰. In this regard, the gut microbiome has already been shown to be associated with chronic inflammatory diseases, such as Crohn's disease or diabetes^{111,112}. For the lung microbiome, however, the relevance of the colonization with single bacteria for the development of chronic lung diseases, such as asthma, needs to be further established. First clinical parameters have been shown to correlate with bacterial taxa, thus it might become relevant as a marker for disease severity, to predict exacerbations and treatment efficacy¹¹³. The mechanism of changes in the microbiome could most likely be due to microaspiration into the lungs which would be cleared under normal conditions via coughing, mucociliary clearance or immune cells, but this function is partly impaired in the disease state^{105,114,115}. Studies so far have shown that asthmatic patients' lung microbiomes were associated with higher proportions of Proteobacteria for all severities. More specifically *Haemophilus* subspecies were identified to be more frequent⁸³ and from Actinobacter phylum *Klebsiella* species were detected in a higher abundance in the more severe cases¹¹⁶. Further other bacterial species, such as *Pseudomonas*, *Neisseria* and *Burkholderia* and additional taxonomy belonging to *Enterobacteriaceae* family were found to be stronger represented in asthmatics^{52,83,117–121}. Different studies showed that in neutrophilic asthma the lung microbiome has a reduced bacterial diversity with higher bacterial prevalence of *Haemophilus* and for one study also the *Moraxella* taxa^{119,122}. From an evolutionary perspective, the symbiosis between host genetics and the microbiome is the result of coevolution. In the last decades, the incidence and prevalence of asthma have been rapidly increasing in wealthy countries¹²³. However, the underlying cause for this rapid rise cannot be explained by genomic changes as these would require many generations to be manifested in the genetics¹²⁴. Therefore, one can speculate that the increased prevalence of asthma could

be explained by the large changes of our environment in westernized countries, with reduced exposure to microbe-rich environments and altered dietary habits. Many factors have been described to negatively affect the microbiome development in early childhood: as e. g. C-section vs. vaginal delivery¹²⁵, the shift to more frivolous prescription of antibiotics in early life¹²⁶ and formula milk vs. breastfeeding¹²⁷ (Figure 1.2). These factors are suggested to delay the colonization with health-promoting bacteria, decrease the diversity of the microbiome and lead to an increase of *Escherichia coli* and *Clostridium difficile* counts^{127,128}. Along this line, the microbiome is more dynamic than genetics and hence could more rapidly respond to environmental changes. This process, however, could lead to a mismatch of the actual microbiome and the microbiome that the human body and the immune system is evolutionary prepared for by the respective genetic background. Accordingly, there is a highly dynamic interaction of the environment, the genetics and the asthma susceptibility.

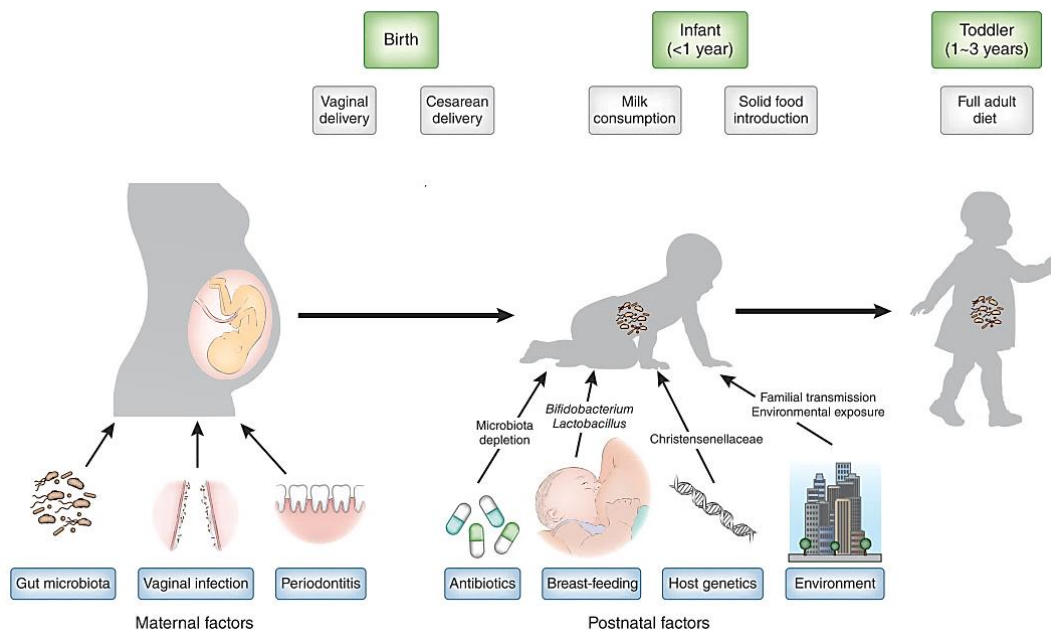


Figure 1.2: Microbiome development in early life.

Prenatal and postnatal influences shape the microbial composition, those include maternal, host genetics as well as the environment factors (e. g. antibiotic usage, nutrition requirements, contact with siblings and pets, etc.). Picture modified from Tamburini et al., *Nat Med.*, 2016¹²⁹.

2 Aims and Research Questions

As outlined above, asthma is a multifactorial disease shaped by a highly complex interaction of host's factors and the environment, which complicates the development of precision medicine approaches. Gaining an initial insight into this potential relationship might be of high relevance for the translation to humans, *id est* (i. e.) if the microbiome can be modulated independently of the genetic background or is associated with disease susceptibility. This knowledge would be the prerequisite to develop strategies that target the microbiome in early life. If, however, the microbial composition is mainly driven by the genetic background, such strategies will not be effective in humans. The aim of this thesis is, therefore, to obtain a first insight into the relative contribution of the host's genetics vs. the host's microbiome in shaping asthma phenotypes.

To this end, we investigated the response to HDM extract, as a defined and uniform environmental challenge, in four different mouse strains. In particular, we addressed the following questions:

1. a) Do mouse strains with genetically different backgrounds exhibit distinguishable asthma phenotypes as defined by lung function and inflammatory cells in response to identical HDM treatment?
b) If so, do levels of Th1-, Th2- and T_{reg} associated cytokines differ in BAL supernatant in response to HDM?
c) Do these differences associate with different IgE levels?

2. a) Does the composition of the gut and lung microbiomes in mice of different genetic backgrounds differ at baseline even before experimental asthma induction?
b) Does the HDM treatment in different genetic backgrounds shift the gut and lung microbiomes?
c) If so, is the shift similar across the strains or does it vary?

3 Materials and Methods

3.1 Materials

3.1.1 Chemicals and reagents

Table 3.1: Chemicals and reagents

Substance	Manufacturer	Country
3,3',5,5'-Tetramethylbenzidine (TMB) (Cat. No. 6350.1)	Carl Roth	Karlsruhe (GER)
Agar-Agar, Bioscience, granulated (CAS: 9002-18-0)	Carl Roth	Karlsruhe (GER)
Bovine serum albumin (Cat. No. A7030-50G)	Sigma-Aldrich	St.Louis, MO (USA)
Dermatophagoides pteronyssinus extract (Nr. 218234)	Greer	Lenoir (USA)
DNA-free water (PCR-grade)	Molzymb GmbH & Co. KG	Bremen (GER)
Ethanol >99.8 %	Carl Roth	Karlsruhe (GER)
FastRuler Low Range DNA Ladder	Thermo Fisher Scientific	Waltham, MA (USA)
Gel Loading Dye, Purple (6x), no SDS	New England BioLabs	Ipswich, MA (USA)
Hydrogen peroxide 30 % (Cat. No. 1.07210.0250)	Merck	Darmstadt (GER)
Ketamine (Ketamindor 100 mg/ml)	WDT (Wirtschaftsgenossenschaft deutscher Tierärzte eG)	Garbsen (GER)
Liquid nitrogen, GER	Westfalen AG	Münster (GER)
Methacholine chloride (1396364)	Sigma-Aldrich	St.Louis, MO (USA)
Pancuronium bromide (P1918)	Sigma-Aldrich	St.Louis, MO (USA)
Phosphate-buffered formaldehyde solution 4 % (Roti-Histofix, Nr. P087.3)	Carl Roth	Karlsruhe (GER)
QIAzol Lysis Reagent	Qiagen	Hilden (GER)
Rotiphorese 10xTBE buffer	Carl Roth	Karlsruhe (GER)

Sevoflurane (SevoFlo)	Zoetis	Ottignies-Louvain-la-Neuve (B)
Sodium acetate (Cat. No. 1.06268.1000)	Merck	Darmstadt (GER)
Sodium carbonate (Cat. No. 1.06398.1000)	Merck	Darmstadt (GER)
Sodium chloride (Cat. No. 3957.1)	Carl Roth	Karlsruhe (GER)
Sodium dihydrogen phosphate monohydrate (CAS 10049-21-5)	Merck	Darmstadt (GER)
Sodium hydrogen car- bonate (Cat. No. 1.06329.1000)	Merck	Darmstadt (GER)
Sodium hydroxide (CAS: 1310-73-2)	Merck	Darmstadt (GER)
Sulfuric acid (Cat. No. 1.00731.1000)	Merck	Darmstadt (GER)
SYBR Green II	Lonza	Basel (CHE)
Tryptan Blue (CAS: 72-57-1; T6146)	Sigma-Aldrich	St.Louis, MO (USA)
Tween 20 (Cat. No. P1379-500)	Sigma-Aldrich	St.Louis, MO (USA)
UltraPure™ Agarose	Invitrogen™ Thermo Fisher	Carlsbad, CA (USA)
Xylazin (Xylavet 20 mg/ml)	CP-Pharma GmbH	Burgdorf (GER)
Zymbiomics Microbial Community DNA Standard (D6305) 1:10 dilution with sterile water	Zymo Research	Irvine, CA (USA)
Zymbiomics Microbial Community Standard (D6300)	Zymo Research	Irvine, CA (USA)

3.1.2 Buffer and solutions

Table 3.2: Buffer and solutions

Name		Substance	Volume
Blocking + detection buffer	1 % bovine serum albumin (BSA); 0.05 % Tween20 in phosphate-buffered saline (PBS)	BSA	1.00 g
		PBS	up to 1000 ml
		Tween20	0.5 ml
Coating buffer (carbonate buffer, pH9.6)	15 mM Na ₂ CO ₃ , 35 mM NaHCO ₃	Na ₂ CO ₃	0.11 g
		NaHCO ₃	2.94 g
		H ₂ O	up to 1000 ml
PBS-Buffer, sterile filtered, pH7.2	10 mM NaH ₂ PO ₄ 0.15 M NaCl	NaH ₂ PO ₄	1.37 g
		NaCl	8.76 g
		H ₂ O	up to 1000 ml
Sodium acetate solution	0.1 M C ₂ H ₃ NaO ₂	C ₂ H ₃ NaO ₂	8.20 g
		H ₂ O	up to 1000 ml
Sodium hydroxid - Buffer for library denaturation	0.2 N NaOH	NaOH	0.8 g
		H ₂ O	up to 100 ml
Stop solution	1 M H ₂ SO ₄	H ₂ SO ₄	98.08 g
		H ₂ O	up to 1000 ml
TBS-Tween buffer, pH7.4	0,1 M NaCl 0.1 M Tris 0.5 mM MgCl ₂ × 6 H ₂ O	NaCl	29.22 g
		Tris	60.57 g
		MgCl ₂ × 6 H ₂ O	2.54 g
		H ₂ O	up to 5000 ml
		Tween	2 ml
Tetramethylbenzidine (TMB) buffer, pH5.5	10 µg/ml in 0.1 M Sodium acetat H ₂ O ₂ (30 %, 1:5000), added to TMB solution shortly before use	TMB	0.01 g
		0.1M C ₂ H ₃ NaO ₂	up to 1000 ml
		H ₂ O ₂ (30%)	0.2 g
Trypan blue 0.5 % in 0.9 % NaCl		NaCl	0.9 g
		H ₂ O	up to 100 ml
		Trypan blue	0.5 g
Tetramethylbenzidine (TMB) buffer, pH5.5	10 µg/ml TMB in 0.1 M C ₂ H ₃ NaO ₂ H ₂ O ₂ (30 %, 1:5000), added to TMB solution shortly before use	TMB	0.01 g
		0.1M C ₂ H ₃ NaO ₂	up to 1000 ml
		H ₂ O ₂ (30%)	0.2 g

3.1.3 Antibodies

Table 3.3: Antibodies

Antibody	Application	Manufacturer	Country
Horseradish peroxidase (HRP)-labeled rat anti-mouse IgE (Clone 23G3, Cat. No. 1130-05, Lot: H021-TF39F)	enzyme-linked immunosorbent assay (ELISA)	Southern Biotech	Birmingham, AL (USA)
Mouse IgE (clone C38-2, Cat. No. 03231D, Lot M042555)	ELISA	BD Pharmingen	Franklin Lakes, NJ (USA)
Rat anti-mouse IgE (2 µg/ml, clone R35-72, Cat. No. 553413, Lot: 3081842)	ELISA	BD Pharmingen	Franklin Lakes, NJ (USA)

3.1.4 Oligonucleotides

Table 3.4: Primer sequences for qRT-PCRs

Gene name (species)	fwd 5'→3'	rev 5'→3'
CCL11 (mmu)	TTCTATTCCTGCTGCTCACGG	GGAAGTTGGGATGGAGCCTGG
HPRT (mmu)	AATTGTACCGCAGCTTCAAAAT	ATGATGACTGCAGCAAATCG
MUC5B (mmu)	ACCGGAGACAGTCAGAGAGT	GGTGTAAGGCGCTCATGCTA
TBP (mmu)	CAGGCCAGACTTTGTTGGAT	ACGTGATTCAAATCCCTGAAGT

Table 3.5: 16S rRNA amplicon primer

Target region	Name	Sequence 5'→3'
Test primer		
16S rRNA gene V1-V2 (bac)	27F	TATGGTAATTGTAGAGTTTGATCCTGGCTCAG
Test primer		
16S rRNA gene V1-V2 (bac)	338R	AGTCAGTCAGCC TGCTGCCTCCCGTAGGAGT
16S rRNA gene V1-V2 (bac)	27F	AGAGTTTGATCCTGGCTCAG
16S rRNA gene V1-V2 (bac)	338R	TGCTGCCTCCCGTAGGAGT
Linker sequence	fwd	TATGGTAATTGT
Linker sequence	rev	AGTCAGTCAGCC
Flowcell binding side	p5 (fwd)	AATGATACGGCGACCACCGAGATCTACAC
Flowcell binding side	p7 (rev)	CAAGCAGAAGACGGCATACGAGAT

Table 3.6: Multiplex identifier (MID) indexes

338R		27F	
Code	Sequence	Code	Sequence
A	TTCCGGTT	1	AACCGCAT
B	GTCACTCT	2	AAGGCCTT
C	ACCAGTTG	3	AGAGTGTG
D	AACGAACG	4	CACAAGTC
E	GTGAACAG	5	CGTTCCTA
F	TTGCAAGC	6	GCTTGGAT
G	CAGTTGAC	7	GTCAACAC
H	CATGAGGA	8	GTCACTGA
I	CTAGTCGA	9	TCTCGTCA
J	GCTTGCAA	10	TTGGTACG
K	AGAGGTGT	11	CGTTGGAT
L	GCTACGAT	12	CGTTAAGC
M	GTCAAGAG	13	ACAGCTCA
N	ATGGTAGG	14	GACAAGTG
O	GACTTCAG	15	GCATTAGC
P	ACGATCGT	16	TGTGGACT
Q	GGCCATAT		
R	CCATCGAA		
S	CGTACGTA		
T	ACGTGATC		

3.1.5 Commercial kits

Table 3.7: Commercial kits

Kit	Provider	Country
Agencourt® AMPure®	Agencourt Bioscience Corporation	Beverly, MA, USA
Direct-zol™ RNA Mini-prep Plus Kit (R7073)	Zymo Research	Irvine, CA (USA)
enhanced sensitivity cytometric bead array (Flex Set Kits)	BD Biosciences	Franklin Lakes, NJ (USA)
Maxima First Strand complementary DNA (cDNA) Synthesis Kit with double-stranded (ds)DNase	Thermo Fisher Scientific	Waltham, MA (USA)
LightCycler® 480 SYBR® Green I Master	Roche Diagnostics GmbH	Mannheim (GER)
miRNeasy Mini	Qiagen	Hilden (GER)
MiSeq Reagent Kit v3 600	Illumina	San Diego, CA (USA)
OneStep™ PCR Inhibitor removal	Zymo Research	Irvine, CA (USA)
PAS (Periodic Acid Schiff's) Staining Kit (HP01)	Carl Roth	Karlsruhe (GER)
PhiX Control v3	Illumina	San Diego, CA (USA)
Qiagen MinElute Gel Extraction Kit	Qiagen	Hilden (GER)
Quant-iT™ dsDNA BR Assay Kit.	Invitrogen	Carlsbad, CA (USA)
RAL Diff-Quik™ (REF:720555-0000)	RAL Diagnostics	Martillac (FR)
ZR BashingBead Lysis Tubes ((0.1 & 0.5 mm), S6012-50)	Zymo Research	Irvine, CA (USA)

3.1.6 Consumables

Table 3.8: Consumables

Consumables	Provider	Country
1 ml syringe	BD	Heidelberg (GER)
1.5 ml reaction tube	Eppendorf	Hamburg (GER)
10 ml syringe	BD	Heidelberg (GER)
2 ml safe-cap tube	Sarstedt	Nümbrecht (GER)
2 ml syringe	BD	Heidelberg (GER)
5 ml syringe	BD	Heidelberg (GER)

cannula 20G x 1 1/2"; 0.9 x 40 mm	BD	Heidelberg (GER)
cannula 26G x 3/8"; 0.45 x 10 mm	BD	Heidelberg (GER)
cannula 27G x 3/4"; 0.4 x 19 mm	BD	Heidelberg (GER)
Cytofuge filter	Thermo Scientific	Runcorn (UK)
DNA free water, PCR-grade	Molzym	Bremen (GER)
DNAZap™ PCR DNA Degradation Solution	Invitrogen	Carlsbad, CA (USA)
PCR plates	Roche Diagnostics GmbH	Mannheim (GER)
Seal film for PCR plates	Roche Diagnostics GmbH	Mannheim (GER)
Slide	Langenbrinck	Emmendingen (GER)
Stericup and Steritop 0.22 µm	millipore	Burlington, MA (USA)
Sterile Water for clean- ing surgical tools	Braun water	Melsung (GER)
Superfrost Slide	Langenbrinck	Emmendingen (GER)
Swingsette biopsy em- bedding cassettes	Carl Roth	Karlsruhe (GER)
Tissue embedding sponge	Kartell S.p.A.	Milano (ITA)
Tube 15 ml, 120 x 17 mm, PP	Sarstedt	Nümbrecht (GER)
Tube 50 ml, 114 x 28 mm, PP	Sarstedt	Nümbrecht (GER)

3.1.7 Mouse strains

Table 3.9: Mouse strains

Strain	Provider	Country
A/J	Jackson Laboratory	Bar Harbor, Maine (USA)
BALB/cJ	Jackson Laboratory	Bar Harbor, Maine (USA)
C57BL/6J	Jackson Laboratory	Bar Harbor, Maine (USA)
C3H/HeJ	Jackson Laboratory	Bar Harbor, Maine (USA)

3.1.8 Devices and equipment

Table 3.10: Devices and equipment

Device/equipment	Name	Provider	Country
Blood cell differential blood counter	Counter AC-8	Glaswarenfabrik Karl Hecht GmbH & Co KG	Sondheim vor der Rhön (GER)
Cameras	Olympus DP-25	Olympus	Waltham, MA (USA)
	DS-Ri1	Nikon	Tokio (JPN)
Cannuale	tracheal cannuale (Nr. 730029)	Harvard Apparatus	Cambridge (UK)
Centrifuges	Eppendorf centrifuge 5415 R	Eppendorf AG	Hamburg (GER)
	Plate centrifuge Multifuge X1R Centrifuge	Heraeus Holding GmbH	Hanau (GER)
	Cytospin centrifuge Cytospin 3	SHANDON	Cambridge (UK)
Embedding machine	Histostar Embedding Workstation	Thermo Fisher Scientific	Mariette, OH (USA)
Flow Cytometer	BD Accuri C6 Flow-Cytometer	BD Biosciences	Franklin Lakes, NJ (USA)
Fluorospectrometer	NanoDrop 3300 fluorospectrometer	Thermo Fisher Scientific	Mariette, OH (USA)
Fume Hood	Köttermann Systemlabor Typ 2-453-DAND	Köttermann Systemlabor	Uelze-Hänigsen (GER)
Freezer/Fridges	-20°C Freezer Privileg öko Energiesparer	Quelle GmbH	Fürth (GER)
	4°C Fridge/Freezer Privileg de lux	Quelle GmbH	Fürth (GER)
	-80°C Freezer VWR60086V-80°C	Thermo Fisher Scientific	Mariette, OH (USA)
Gel imager	ChemiDoc Touch Imaging system doc	Bio-Rad	Hercules, CA (USA)
Hemocytometer	Neubauer counting chamber (REF:0610130)	Paul Marienfeld GmbH&Co.KG	Lauda-Königshofen (GER)
Incubator	C02-AUTO-ZERO	Heraeus Holding GmbH	Hanau (GER)
Lung function machine	Flexivent	Scireq	Montreal (CAN)
Microplate reader	Infinite® M200	Tecan	Männerdorf (CHE)
Microscopes	BX40	Olympus	Hamburg (GER)
	BX51	Olympus	Hamburg (GER)

	Primostar	Zeiss	Jena (GER)
	Zeiss microscope	Zeiss	Jena (GER)
Microtom	Microm HM340E (with waterslide and cooling block)	Thermo Fisher Scientific	Waltham, MA (USA)
Mouse cage system	IVC Greenline SEALSAFE® PLUS	Tecniplast	Buguggiate (IT)
Multichannel Pipettes	Eppendorf multi-channel pipettes (200 µl, 100 µl, 10 µl)	Eppendorf AG	Hamburg (GER)
Spectrometer	DeNovix®, DS-11 Spectrophotometer	DeNovix Inc.	Wilmington, DE (USA)
Thermocyclers	DNA Engine Tetrad® 2 Thermal Cycler	Bio-Rad	Hercules, CA, (USA)
	Real-timer Thermocycler Light Cycler 480 II	Roche	Basel (CH)
	TProfessional TRIO Thermocycler	Biometra biomedizinische Analytik GmbH	Göttingen (GER)
Tissue lysers	FastPrep-24™ 5G	MP Biomedicals	Santa Ana, CA (USA)
	Tissue Lyser II	Qiagen	Hilden (GER)
Warming plate	ThermoLux Warming plate	Witte+Sutor GmbH	Murrhardt (GER)
Workstations	PCR Workstation, UVT-S-AR DNA/RNA UV-Cleaner Box	Kisker Biotech GmbH & Co	Steinfurt (GER)
	Sterile hood Scanlaf MARS	Labogene (Scandinavia by Design)	Allerød (DNK)

3.1.9 Software

Table 3.11: Software

Name	Version/Package	Company/Person
FastQC	Version 0.10.1 (linux)	Babraham Bioinformatics ¹³⁰
Flexivent software	flexiWare Version 7.2, Service pack 2, build 728	Scireq, Montreal, Canada
Graphpad Prism	Version 6	GraphPad Software, Inc.
Image Lab	Version 2.0.1 build 18,	Bio-Rad Laboratories
Mega7	Version 7.0.26	Mega Software
R	v. 3.5.2	R Foundation ¹³¹
	vegan (v. 2.5-5)	Oksanen et al. ¹³²
	phyloseq (v. 1.24.2)	McMurdie et al. ¹³³
	Rhea pipeline	Lagkouvardos et al. ¹³⁴
RDP database	rdp_16s_v16 (v.16)	Ribosomal Database Project ¹³⁵
USEARCH	v 10.0.240_i86linux64 (linux)	Edgar et al. ¹³⁶

3.2 Methods

3.2.1 Animals

Female A/J, BALB/cJ, C57BL/6J and C3H/HeJ mice were obtained from Jackson Laboratory (Bar Harbor, Maine, USA) at the age of six weeks and housed in individually ventilated cages (Sealsafe PLUS, Green Line, Tecniplast, Italy) in a specific pathogen free (SPF) facility. A standard pellet diet and water were provided *ad libitum*. The study was conducted under the German federal guidelines for the use and care of laboratory animals and was approved by the Ministry of energy system transformation, agriculture, environment and rural areas of the District of Schleswig-Holstein (V 244 – 1867/2017 (28-2/17)).

3.2.2 Asthma treatment protocol

Eight-week-old female mice were treated intranasally three times per weeks for three weeks with 20 µg HDM extract (HDM, Dermatophagoides pteronyssinus extract, Nr. 218234, Greer, USA) in 30 µl PBS under sevoflurane (SevoFlo, Zoetis, ecuphar, Belgium) anesthesia. Control groups were treated with PBS only. All mice were sacrificed one day after the last treatment. Mice were *intraperitoneal* (i. p.) anaesthetized with ketamine (140 mg/kg) and xylazine (7 mg/kg).



Figure 3.1: HDM-treatment scheme to induce allergic airway inflammation.

Eight-week-old mice were treated intranasally with 20 µg HDM extract in 30 µl PBS or 30 µl PBS three times a week for a duration of three weeks. The mice were anaesthetized using sevoflurane prior to the i. n. administration. One day after the last treatment the mice were sacrificed.

3.2.3 Characterization of asthma phenotype

3.2.3.1 BAL cell total number

After lung function measurement, 0.8 ml of cold PBS was instilled into the lungs through the intratracheal tube and immediately recollected. The bronchoalveolar lavage fluid was centrifuged (1200 rpm, 10 min, 4 °C (Eppendorf centrifuge 5415 R, Eppendorf, Hamburg)). The cell pellet was resuspended in 200 µl cold PBS and 10 µl

were counted in a 1:2 dilution mixed with trypan blue using a hemocytometer. The absolute number of BAL cells was calculated according to the following formula: absolute cell number = (counted cells in 4 squares \times 2 (dilution factor with trypan blue)/4 squares) \times dilution (200 μ l used for suspension) \times 10⁴ cells/ml).

3.2.3.2 BAL cell differentiation

100 μ l of the resuspended cells from the BAL were spun on a slide at 900 rpm for 8 min (SHANDON, Cytospin 3, Cambridge, UK). After drying the slide over night at room temperature the cells were stained according to the manufacturer's instructions (RAL Diff-Quik™, RAL Diagnostics, Martillac, France). The cell populations were differentiated in macrophages, eosinophils, lymphocytes and neutrophils under the microscope (BX40, Olympus, Hamburg, Germany) using a 40-fold magnification and counting a minimum of 300 cells. The dye stains the cytoplasm in a light blue and the acidophilic granules are stained pink with eosin and characterizes the eosinophils. The granules present in neutrophils appear unstained, as the milieu doesn't have acidophilic properties. The differentiation of macrophages and lymphocytes was performed based on the cell, nuclei and cytoplasm size. Macrophages show a distinctive big cytoplasm, in contrast lymphocytes are smaller and dominated by the dark stained nucleus.

3.2.3.3 Cytokines in BAL supernatant

Cytokine levels of interleukin (IL)-1 β , IL-4, IL-5, IL-6, IL-10, IL-12p70, IL-13, IL-17A, interferon (IFN)- γ and tumor necrosis factor (TNF)- α were assessed in the supernatant of bronchoalveolar lavage fluid (BALF). The measurement was performed, according to the manufacturer's guidelines, by using an enhanced sensitivity cytometric bead array (Flex Set Kits; BD Biosciences, Franklin Lakes, NJ, USA) on a flow cytometer (BD Accuri C6 FlowCytometer, BD Biosciences, Franklin Lakes, NJ, USA). Using this method single cytokines can be captured by a bead coupled with a specific antibody for each analyte and next a specific detection antibody binds to the individual analyte. This detection antibody is conjugated with a fluorochrome which sends a signal that relies on specific fluorescent intensities for each of the individual cytokines. The samples can be measured on a standard flow

cytometer. It enables the simultaneous measurement of multiple proteins in one reaction and small volumes¹³⁷.

3.2.3.4 Lung function

The mice were tracheostomized and intubated with tracheal cannulae (Harvard Apparatus U.K., Nr. 730029, Cambridge, UK) and subsequently placed on a warming plate and ventilated at a frequency of 150 breaths/ min. with a tidal volume of 10ml/kg. Once connected to the Flexivent ventilation system (SCIREQ Inc, Montreal, Qc, Canada) pancuronium was injected i. p. to stop own breathing. The Flexivent software was used to record the measurement (flexiWare version 7.2, Service pack 2, build 728). To assess airway hyperresponsiveness, the mice were challenged with increasing doses of methacholine (0, 6.25, 12.5, 25, 50, 100 mg/ml) for 10 s. The highest value of airway resistance and corresponding values after each applied dose within 2 min after application was plotted against the methacholine concentration (Figure 4.10). Values for the airway resistance, compliance of the airway and the inspiratory capacity (IC) were recorded.

3.2.3.5 Total IgE in serum

A sandwich ELISA was used for the measurement of IgE concentration in mouse serum. 96-well ELISA plates were coated with rat anti-mouse IgE (2 µg/ml, clone R35-72, BD Pharmingen), diluted in 50 mM carbonate buffer, pH 9.6. After overnight incubation at 4 °C plates were blocked with 1 % BSA in PBS with 0.05 % Tween20. Serum samples were pre-diluted and analyzed in duplicates. Purified mouse IgE (clone C38-2, BD Pharmingen) was used as a standard. For the detection of IgE, HRP-labeled rat anti-mouse IgE (Clone 23G3, Southern Biotech) was used. Dilution of serum samples and detection antibodies was performed in 1 % BSA in PBS with 0.05 % Tween20. For the colorimetric detection TMB was used as a substrate. Optical density (OD) was measured at 450 nm with 570 nm reference measurement in a microplate reader (Infinite® M200, Tecan, Männerdorf, CHE). IgE concentration in samples was calculated according to standard curve.

3.2.3.6 Histology

3.2.3.6.1 Embedding, cutting, staining the slides

For the analysis of the lung structure, airway remodeling and inflammation the histological features of the whole lung were analyzed. Therefore, the lungs were perfused with 5 ml cold PBS applied with a syringe and then fixed under constant pressure with phosphate-buffered formaldehyde solution 4% via the trachea and subsequently stored in the reagent. Next, lungs were embedded in 2% Agar-Agar for pre-cutting and finally embedded in paraffin. 2.0 μm thick tissue sections were cut (ThermoSCIENTIFIC, Microm HM340E, Waltham, MA, USA) and the slides were stained with the PAS reagent according to the manufacturer's instructions (Pas Staining Kit, Carl Roth, Karlsruhe, Germany) after drying for one night in the incubator at 37°C. The PAS staining detects carbohydrates by covalent binding of Schiff's reagent to the aldehyde structures which result from the oxidation of the hydroxyl groups after periodation with periodic acid^{138,139}. The histological analysis of the lung section was separated in two different methods; Firstly, the quantification of changes in lung sections based on a scoring system and secondly, the quantitative Computer Assisted Stereology Toolbox (CAST) analysis. For the scoring system pictures were taken under the microscope (BX40, Olympus, Hamburg, Germany) using a 2- and 10-fold magnification and for the severity of goblet hyperplasia and cell infiltrates around the airways scores from 1-10 were selected. Number 0 means no changes to PBS control and 10 very strong changes that are visibly observed.

3.2.3.6.2 CAST analysis

Mucus production and inflammatory cells surrounding the airways were evaluated in a blinded manner with respect to the treatment groups in PAS-stained slides by using the CAST method. Pictures were recorded using a digital camera (DP-25, Olympus, Tokyo, Japan) attached to a microscope (BX-51, Olympus) at 40- and 100-fold magnification using Olympus cell^A software. Systemic uniform random samples of the lungs were prepared according to standard method for mucus quantification¹⁴⁰. By applying the CAST (newCAST, Visiopharm, Hoersholm, DK)^{141,142} the surface area of mucin-containing goblet cells (S_{gc}) per total surface area of airway epithelial basal membrane (S_{ep}) and the volume of PAS-stained epithelial

mucin (V_{mucin}) per S_{ep} were determined according to following equation: $S_{\text{ge}}/S_{\text{ep}} = \sum I_{\text{gc}}/\sum I_{\text{ep}}$ and $V_{\text{mucin}}/S_{\text{ep}} = LP \times (\sum P_{\text{mucin}}/2) \times \sum I_{\text{ep}}$. $\sum I_{\text{gc}}$ being the sum of intersection of a grid with goblet cells, $\sum I_{\text{ep}}$ is the sum of all intersections of test-lines with the epithelial basal membrane, $\sum P_{\text{mucin}}$ is the sum of all points hitting mucin and LP is the test-line length at final magnification.

3.2.3.7 Gene expression in lung homogenates

Total RNA was isolated from homogenized lung tissue (Tissue lyser II, Qiagen, Hilden, Germany) using the miRNeasy Mini Kit according to the manufacturer's instructions (Qiagen, Hilden, Germany). RNA concentrations were determined using a DeNovix® DS- 11 Spectrometer (DeNovix Inc., Wilmington, USA). In the next step, total RNA was first converted to cDNA using the QuantiNova Reverse Transcription Kit (Qiagen, Hilden, Germany) and subsequently gene expression levels were evaluated by performing a quantitative real-time polymerase chain reaction (qRT-PCR). The qRT-PCR was performed on a LightCycler 480 system (Roche, Mannheim, Germany) utilizing the LightCycler 480 SYBR Green I Master Mix kit (Roche Diagnostics GmbH, Mannheim, Germany) and additional primers for the target genes (metabion, Planegg, Germany). All steps were performed as described in the manufacturer's manual. For the detailed Light cycler protocol see the Table 3.12 below. The levels of gene expression for MUC5B and CCL11 were calculated based on the ddCt method using the mean values of TBP and HPRT as references gene. The specific primers sequences for the regions of interest are provided in Table 3.4.

Table 3.12: Light cycler protocol for qRT-PCR

Step		Time {min}	Temperature {°C}
Denaturation		10:00	95
Amplification	for 50 cycles	00:10	95
		00:15	60
		00:10	72
		00:01	78
		Melting Curve	00:05
		01:00	60
	0.11°C/sec	continuous	99
Cool down		00:10	40

3.2.4 Microbiome analysis

3.2.4.1 RNA extraction, Purification and cDNA transcription for 16S preparations

Caecum and lungs were harvested under sterile conditions and stored in bashing bead tubes filled with Trizol. Tools were disinfected between different steps and organs; therefore, they were first cleaned in 70 % ethanol (EtOH) and then rinsed in sterile water. The caecum was collected from all animals; lungs on the other hand only from the microbiome group as the lungs of the BAL group were used for BAL and histological analysis. Prior to RNA isolation the tissues were homogenized five times for 50 s using the Fastprep-24TM5G (MP Biomedicals, Santa Ana, CA, USA). Samples were stored on ice in between the homogenization steps to allow the device to cool down until it was ready to be used again. The RNA isolation was performed according to manufacturer's instructions (Direct-zol™ RNA Miniprep Plus Kit, Zymo Research, Irvine, CA, USA). RNA was eluted in 50 µl of DNA-free water (Molzymb GmbH & Co. KG, Bremen, Germany). Next, RNA was purified by using the OneStep™ PCR Inhibitor Removal Kit (Zymo Research, Irvine, CA, USA) and subsequently the RNA concentration was measured on the DeNovix spectrometer (DeNovix®, DS-11 Spectrophotometer, DeNovix Inc., DE, USA). The RNA was diluted to the required concentration for the cDNA transcription and the transcription was performed according to kit's instructions (Maxima First Strand cDNA Synthesis Kit with dsDNAse, Thermo Fisher Scientific, Waltham, MA, USA). From extraction to sequencing various negative controls were included. The controls were as followed: 1. Negative extraction controls (NEC) rinsed surgical tools were dipped in bashing bead tube filled with Trizol under the bench on the day of organ collection; 2. Trizol used as template for the RNA extractions (Trizol); 3. Next, during cDNA transcription negative reverse transcriptase samples (NRT) and non-RNA templates (NRNA) were included. In addition, mock community standards were isolated and a mock community DNA standard included for library preparation, starting from amplicon PCR and sequenced along with the samples.

3.2.4.2 Library preparation and 16S rRNA sequencing

From this point onwards the library preparation was performed by the author in the collaborator's (John Baines) lab in the Max Planck institute in Plön. The first step was to amplify the cDNA with test primers for the V1-V2 region (Table 3.5) and subsequently load the PCR-product with added loading buffer on a 2 % agarose gel to verify that only one product of the expected size was detected. The standard for size comparison used was the FastRuler Low Range DNA Ladder (Thermo Fisher Scientific Waltham, MA, USA). The 27F and the 338R primers were used to target the broadly conserved bacterial 16S gene. The test PCR amplification was performed according to kit's specification (Phusion® Hot Start II DNA High-Fidelity DNA Polymerase, Finnzymes, Espoo, Finland) and the PCR plates were run simultaneously on a multiplate thermal cycler (DNA Engine Tetrad® 2 Thermal Cycler, Bio-Rad, Hercules, CA, USA) using the protocol provided in Table 3.13. The generated test 16S rRNA amplicons were then tested using SYBR green detection with the Bio-Rad fluorescence system to confirm good quality. After the absence of additional bands was confirmed, the dual-index amplicon PCR was performed. The V1-V2 region was amplified using a dual indexing approach for all samples with specific primers. The Illumina P5 (forward) and P7 (reverse) binding to the MiSeq flow cell is characterized in *italic* and the underlined sequence represents the primer binding side (27F and 338R) and for the conserved bacterial regions, both are part of the specific primers. The underlined part of the primer sequence shows the 12-base linker sequence which was included in the sequence to increase annealing temperature; this procedure was recommended by Illumina. To allow identification, each sample was tagged with an individual eight base multiplex identifier (MID). This sequence is represented by XXXXXXXX for detailed sequences see Table 3.6.

To summarize, the V1-V2 primer pair appears as followed: forward primer (5' - *AATGATACGGCGACCACCGAGATCTACAC XXXXXXXX TATGGTAATTGT AGAGTTTGATCC TGGCTCAG-3'*) and the corresponding reverse primer sequence for the V1-V2 (5' - *CAAGCAGAAGACGGCATAACGAGAT XXXXXXXX AGTCAGTCAGCC TGCTGCCTCCCGTAGGA GT -3'*). The PCR amplification was performed with 100 ng of cDNA template in a 25 µl volume in accordance with kit's specification (Phusion® Hot Start II DNA High-Fidelity DNA Polymerase, Finnzymes, Espoo, Finland). All dilutions were carried out

using DNA-free water with PCR-grade (Molzym GmbH & Co. KG, Bremen, Germany). All PCR samples were pipetted under a PCR workstation (Kisker Biotech GmbH & Co, Steinfurt Germany) after decontaminating surfaces and pipettes with DNAZap™ (Invitrogen, Carlsbad, CA, USA) and UV irradiation for 30 min. Cycling conditions were as followed for all caecum samples: initial denaturation for 30 s at 98 °C; 10 cycles of 9 s at 98 °C, 30 s at 55 °C, and 90 s at 72 °C for DNA; and for final extension 10 min. at 72 °C. The same temperature steps were applied for the lung samples; hence the cycle number was increased to 30 cycles.

Table 3.13: Amplicon-PCR program

A: Caecum samples			B: Lung samples		
Temperature {°C}	Time {min.}	Cycle number	Temperature {°C}	Time {min.}	Cycle number
98	00:30		98	00:30	
98	00:09	10x	98	00:09	30x
55	00:30		55	00:30	
72	01:30		72	01:30	
72	10:00		72	10:00	
12	∞		12	∞	

Template-free reactions were performed by using PCR-grade water combined with every available primer combination to test for contamination. These products were then transferred to a 1,5 % agarose gel and it was an inclusion criterion of each primer pair used for the regular samples, that no product was detected on the agarose gel using Image Lab software (version 2.0.1, build 18, Image Lab, Bio-Rad). As required, all combinations were found negative. Furthermore, various controls were included as mentioned above. In the next step, the concentrations of all the PCR-products were quantified by taking pictures on the ChemiDoc Touch Imaging system and referring them to standard bands applying the Image Lab quantification approach. After quantification, all samples loaded on the same gel were mixed together according to calculated concentrations to obtain an equimolar subpool. This procedure was performed separately for each gel. The subpools were in the following step extracted from the agarose gel with the Qiagen MinElute Gel Extraction Kit (Qiagen, Hilden, Germany) and subsequently quantified using the Quant-iT™ dsDNA BR Assay Kit on NanoDrop 3300 fluorospectrometer (Thermo Fisher Scientific, Mariette, OH,

USA). Finally, all subpools were pooled into one final equimolar pool representing the library. The equimolar pool was further purified using Agencourt® AMPure® Beads (Agencourt Bioscience Corporation, Beverly, MA, USA) and the final library was run on an Agilent Bioanalyzer prior to calculate the final concentration for the sequencing. The sample is diluted to 4 nM and denatured with 0.2 N NaOH for 5 min. For sequencing on the MiSeq it is brought to the final concentration of 10 pM. Next, the PhiX control (PhiX Control v3, Illumina, San Diego, CA, USA) spike-in at 10 % (12.5 pM) is added to the sample library and sequenced on the MiSeq platform using the Miseq Reagent Kit v3 600 cycles sequencing chemistry. The library was clustered to a density of approximately 1000 K/mm².

3.3 Statistical analysis

For all statistics performed $p < 0.05$ was considered to be *-significant. All tests performed on the data collected for murine phenotypic characterization were performed in Graphpad Prism (version 6, GraphPad Software, La Jolla, USA) and are stated below each corresponding figure throughout the course of this thesis. All shown data presented in dot plots include the mean values shown as a solid line, each animal is represented by one data point. If the data are not shown as a dot plot, the mean values plus the standard deviation is presented. If appropriate parametric analyses were performed; with two-way analysis of variance (ANOVA) and Tukey's multiple comparisons test and the corresponding p values were stated (* $p < 0.05$, ** $p < 0.01$, *** $p < 0.001$, **** $p < 0.0001$). For the measurement of the resistance values (Figure 4.10) a two-way ANOVA was performed followed by the Sidak's multiple comparisons test with the following significance levels: (* $p < 0.05$, ** $p < 0.01$, *** $p < 0.001$, **** $p < 0.0001$). The gene expression levels in lung homogenates comparing the PBS- vs. HDM-treated group of one strain (Figure 4.15 A-B) were determined by a one-way ANOVA followed by the Sidak's multiple comparisons test with the following significances: (* $p < 0.05$, ** $p < 0.01$, *** $p < 0.001$, **** $p < 0.0001$). For statistics on the fold change values for gene expression a one-way ANOVA was selected, followed by the Tukey's multiple comparisons test with the corresponding p values (* $p < 0.05$, ** $p < 0.01$, *** $p < 0.001$, **** $p < 0.0001$).

3.4 Bioinformatic analysis

The Rhea package was used for the analysis by using the R software (v. 3.5.2)¹³⁴. The operational taxonomic unit (OTU) table, a mapping file containing all relevant information, the OTUs-Seqs file in fasta format and an OTUs-Tree, generated in Mega7 software (Mega version 7.0.29), were imported to start the data analysis. The workflow as described¹³⁴ was performed with the following modifications.

3.4.1 Analysis of raw sequences

The CASAVA software from Illumina was used for de-multiplexing and no mismatch of the barcodes was allowed. The quality of the fastq sequences was checked randomly by generating quality files and visualization of the sequences in the FastQC program (version 0.10.1). In the next step, the trimming of the reads was performed using the following software version: Trimmomatic-0.36, nine bases from the start and three bases from end were cut off if under a threshold, reads were discarded if below a specific length of 100 base pair (bp). For the further processing USEARCH (v.10.0.240_i86linux64) was applied to merge the forward and reverse read: to start, both reads were processed and a maximum error (E=1) was allowed; the minimum length of the reads post truncation was set to 200bp; for the overlap region the minimum length was 150bp; minimum length post merging was set to 270bp, maximum length to 350bp. The merged reads were filtered by the parameter of expected error (E=1), as recommended in the literature¹³⁶. Subsequently, a table with unique sequences was generated with the `-fastx_uniques` command using USEARCH. The OTU clusters were created using the unique sequences and the `-cluster_otus` in USEARCH based on 97% similarity of the OTUs. This command includes chimera filtering and their exclusion, next the `-otutab` command was run in USEARCH for the generation of the OTU table. Taxonomy was assigned using RDP Multi-Classifer (v.16) from phylum- to genus-level at a confidence level of 0.8¹⁴³. A phylogenetic tree was built using the fasta sequences post quality filtering with the MEGA7 program (Version 7.0.26). Initially, the sequences were imported and next aligned by MUSCLE, an integrated tool to perform multiple sequence alignment¹⁴⁴ and finally a maximum likelihood tree was generated and exported in the TRE format.

3.4.2 Analysis in R

To continue, the output data from USEARCH and the phylogenetic tree were imported into R studio to carry out the statistical analysis and data visualization. Two different R packages were utilized to process the files generated previously: Phyloseq package¹⁴⁵ and the Rhea pipeline¹³⁴.

3.4.2.1 Rhea pipeline

The Rhea pipeline was executed for the lungs and caecum samples individually, as the library preparation differed in some steps. To begin this process, the total numbers of reads were transformed to relative values to compensate for differences in sequencing efficiency; these values were used throughout all calculations in the Rhea script. A rarefaction curve was generated to estimate the sufficiency of sequencing depth. Alpha diversity was calculated based on the Simpsons effective values. Broadly, the alpha diversity is the species richness present in each individual sample; Simpson diversity accounts for the abundance of the detected OTUs and once converted to Simpson effective, values behave linear and improve graphic visualization by making it easier to intuitively understand and compare values¹⁴⁶. The same applies for the Shannon diversity values, only this value adds less weight to abundance, in contrast to this the measure Richness does only consider total species counts and neglects the abundance completely. Beta diversity measures similarity between microbial profiles of different samples. Within the Rhea script beta diversity is calculated using the generalized UniFrac distances. In general, UniFrac distance considers the shared composition of the samples and further takes the distance in the phylogenetic tree into calculation. The applied generalized UniFrac enables not to over- or underestimate the relevance of rare nor dominate species¹⁴⁷. The multidimensional scaling (MDS) plots visualize the calculated matrix in a two-dimensional space. The `vegan::adonis` command calculates the distance matrices, these distances are further used to perform the permutational multivariate analysis of variance (PERMANOVA) to statistically test if the separation of two groups being compared is significant¹⁴⁸, for multiple testing the Benjamini-Hochberg method was used¹⁴⁹. The MDS plots annotate the p values of the PERMANOVA and the grid distance of $d=0.05$ represents 5% and $d=0.1$ represents 10% of dissimilarity. The two-dimensional visualization in the

MDS plot might not be sufficient to display the proper separation of clusters, which has been calculated using the PERMANOVA. This analysis is executed for all groups combined and pairwise to compare to groups. Further de-novo clustering was carried out. Hereby, samples are not assigned to groups initially but each sample is assigned to one cluster based on similarity¹⁵⁰. For serial comparison different variables among groups of samples e. g. OTU or taxonomic assignments were compared among groups. The non-parametric Kruskal-Wallis Rank Sum Test was used, as OTU data are normally not normal distributed, for multiple testing the Mann-Whitney Test was applied. The obtained p values are again corrected for multiple testing using the Benjamini-Hochberg method¹⁴⁹. Finally, Pearson correlation coefficients of meta and taxonomic variables are calculated and displayed in a graphic output¹⁵¹.

3.4.2.2 Phyloseq and corresponding packages

Phyloseq is an R package used to analyze microbiological communities. It allows importing, storing, analyzing and visualizing large sequencing data sets starting from an OTU table. This OTU table, mapping file, taxonomy assignments and the sequences are combined in one phyloseq object. The number of reads were rarefied to 10,000 reads for lung samples and 20,000 reads for caecum samples to equalize the number of reads. Most controls could be excluded through this step as they had less reads. To analyze the controls further they were visualized before and after rarefying to allow to identify all potential contaminations. After this, the different phyloseq objects were subsampled according to the different organs (gut and lung) and treatments. Next, bar plots of Top10 detected taxa (phylum- to genus-level) among all different groups were generated.

4 Results

4.1 Asthma phenotype

To investigate if mouse strains of four different genetic backgrounds (A/J, BALB/cJ, C57BL/6J and C3H/HeJ) respond differently an airway inflammation was induced in the mice (Figure 3.1). The airway inflammation was provoked by using a standard experimental asthma mouse model, applied concentration was adapted to 20 μg HDM in 30 μl PBS^{152,153}.

4.1.1 Airway inflammation

4.1.1.1 BAL cell numbers

Inflammatory cell numbers in the BAL were counted to evaluate the airway inflammation in the HDM-treated groups. As expected, for all HDM-treated mice significantly higher total cell counts compared to the respective PBS controls were observed. Within the “asthmatic” groups BALB/cJ mice had the lowest total cell counts among all strains after the HDM application (Figure 4.1), whereas C3H/HeJ showed the highest number of total BAL cells.

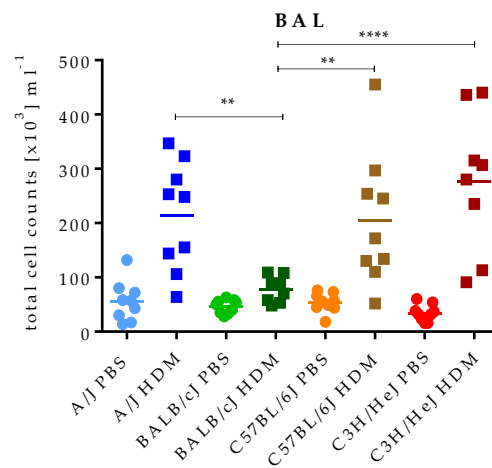


Figure 4.1: Total BAL cell numbers.

Total cell numbers counted in the BAL. $n=8-9$ animals per group; Two-way ANOVA (strain vs. PBS/PBS and HDM/HDM) and Tukey's multiple comparisons test; * $p < 0.05$, ** $p < 0.01$, *** $p < 0.001$, **** $p < 0.0001$.

4.1.1.2 BAL cell differentiation

Similarly, to total BAL cells, eosinophils were significantly lower in HDM-treated BALB/cJ mice compared to the asthma-induced groups of other three strains (Figure

4.2). Numbers of macrophages and lymphocytes did not differ among the strains, except that the relative cell count of macrophages were higher in BALB/cJ HDM-treated group (Figure 4.3 and Figure 4.4). The percentage of neutrophils were increased in BALB/cJ already at baseline (PBS) compared to C57BL/6J and C3H/HeJ (both PBS). Further, also the relative neutrophil numbers were higher in the BALB/cJ HDM-treated group than in the C3H/HeJ HDM group (Figure 4.5 B).

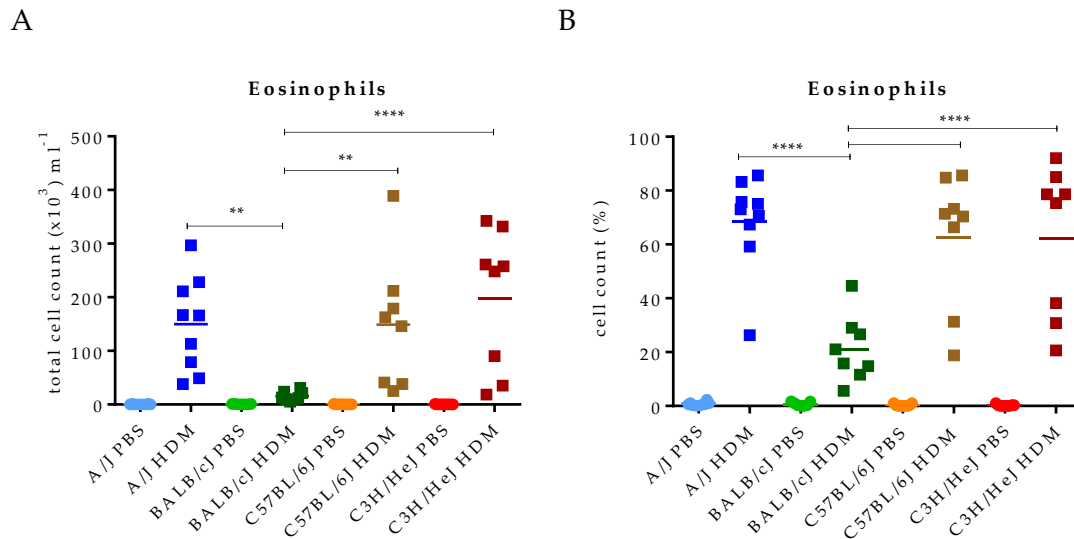


Figure 4.2: Eosinophils in BAL.

A. Total cell counts. B. Relative cell counts.

$n=7-9$ animals per group; Two-way ANOVA (strain vs. PBS/PBS and HDM/HDM) and Tukey's multiple comparisons test; * $p < 0.05$, ** $p < 0.01$, *** $p < 0.001$, **** $p < 0.0001$.

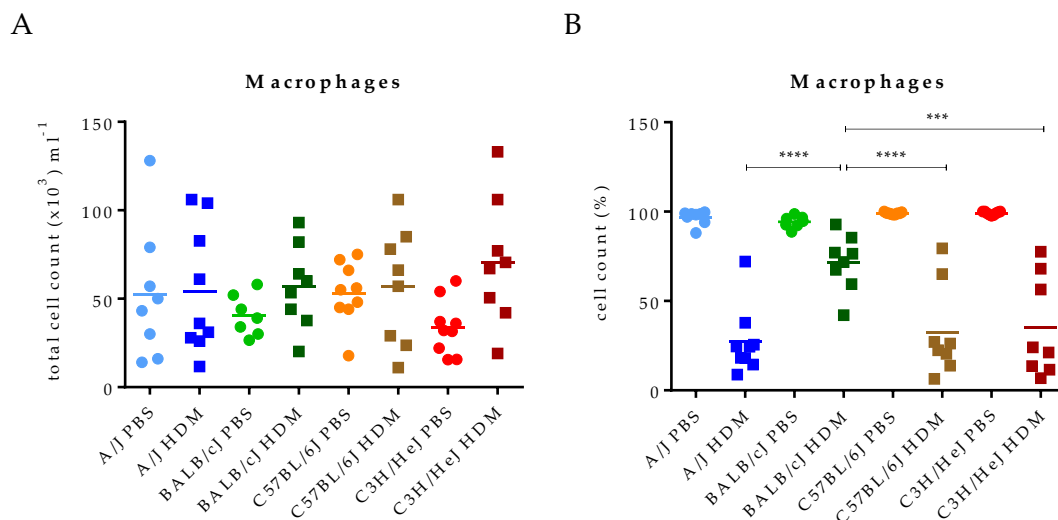


Figure 4.3: Macrophages in BAL.

A. Total cell counts. B. Relative cell counts.

$n=7-9$ animals per group; Two-way ANOVA (strain vs. PBS/PBS and HDM/HDM) and Tukey's multiple comparisons test; * $p < 0.05$, ** $p < 0.01$, *** $p < 0.001$, **** $p < 0.0001$.

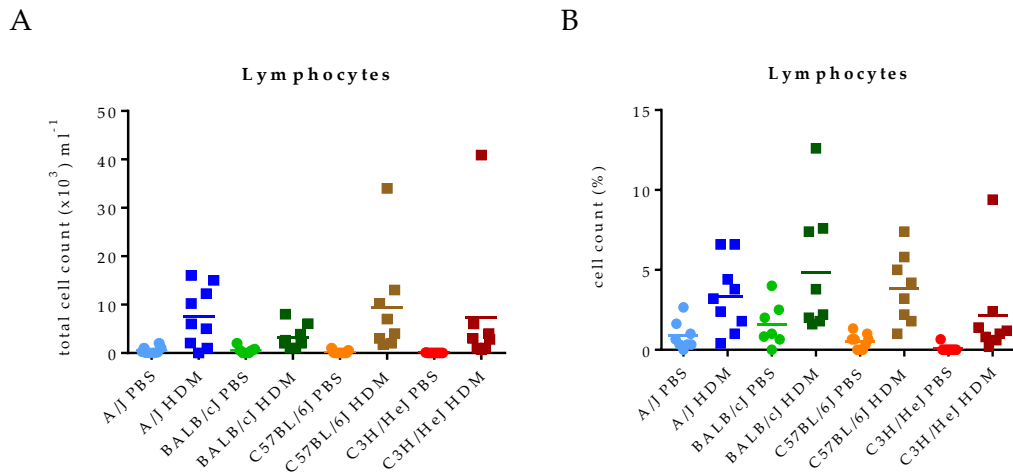


Figure 4.4: Lymphocytes in BAL.

A. Total cell count. B. Relative cell counts.

$n=7-9$ animals per group; Two-way ANOVA (strain vs. PBS/PBS and HDM/HDM) and Tukey's multiple comparisons test; * $p < 0.05$, ** $p < 0.01$, *** $p < 0.001$, **** $p < 0.0001$.

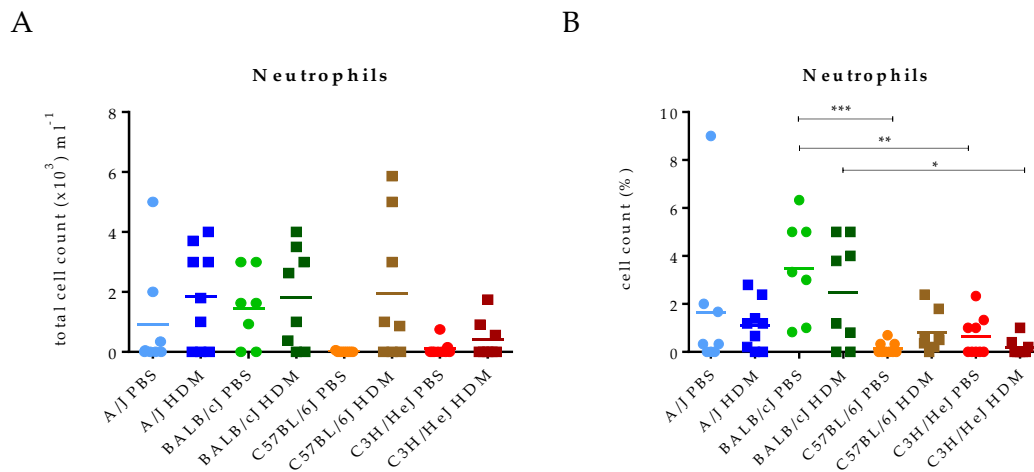


Figure 4.5: Neutrophils in BAL.

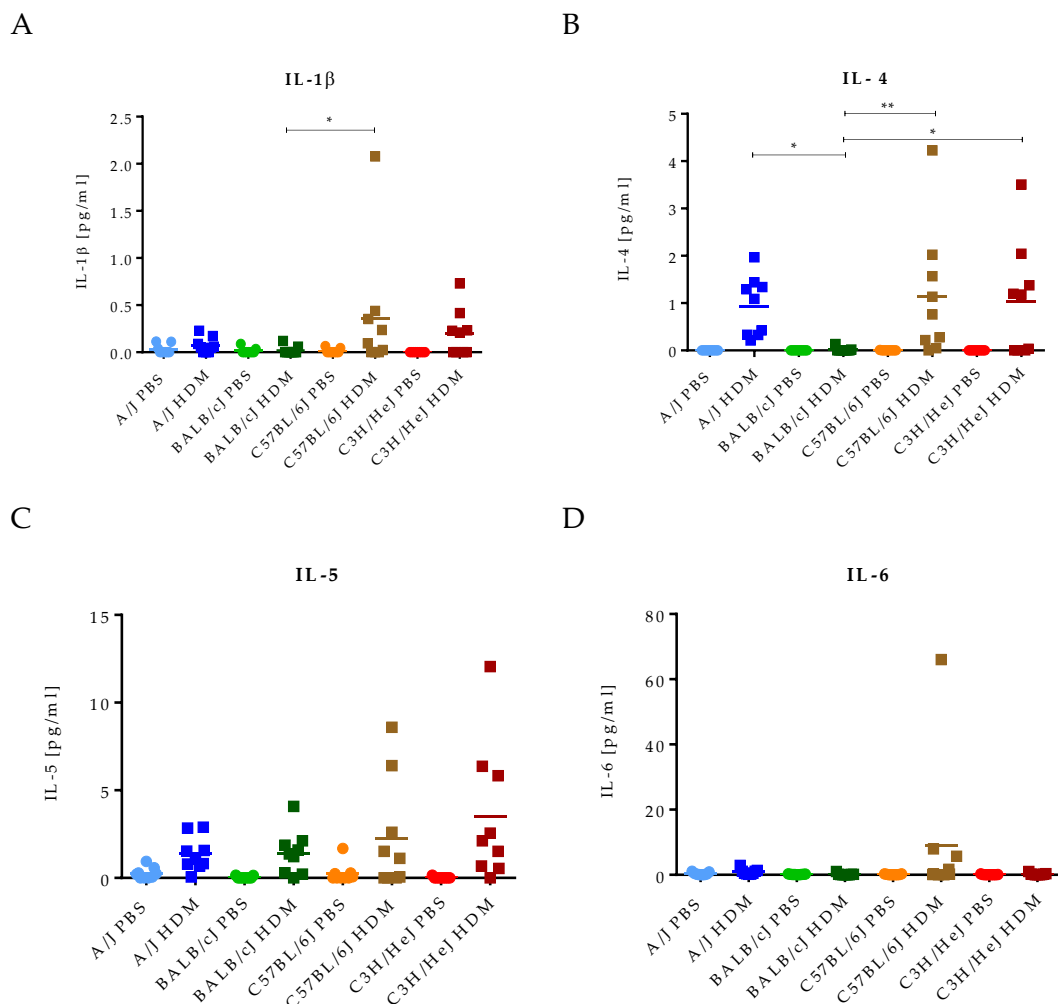
A. Total cell counts. B. Relative cell counts.

$n=7-9$ animals per group; Two-way ANOVA (strain vs. PBS/PBS and HDM/HDM) and Tukey's multiple comparisons test; * $p < 0.05$, ** $p < 0.01$, *** $p < 0.001$, **** $p < 0.0001$.

4.1.1.3 Cytokines in BAL supernatant

To assess if the observed airway inflammation was accompanied by alterations in asthma related signaling molecules, several Th1-/Th2-/Th17- and T_{reg}-associated cytokines (IL-1 β , IL-4, IL-5, IL-6, IL-10, IL-12p70, IL-13, IL-17A, IFN- γ and TNF-alpha) were quantified in cell-free supernatants of BALF (Figure 4.6). IL-1 β concentration were found to be slightly increased for the HDM-treated group of C57BL/6J compared to BALB/cj (Figure 4.6 A). Levels of Th2-cytokines IL-4, IL-5 and IL-13 were increased in all HDM-treated groups with one exception. The IL-4 concentrations were detected to be negative for the HDM-treated BALB/cj mice. Logically, all remaining HDM-

treated groups revealed significantly higher levels in the BALF compared to the BALB/cj strain (Figure 4.6 B). Next, comparing the HDM-treated groups of BALB/cj and C3H/HeJ discovered higher IL-13 levels for the latter one (Figure 4.6 G). The Th17-associated cytokine IL-17A was significantly elevated only in the C57BL/6J HDM group, but not in any other HDM-treated strain (Figure 4.6 H). IL-6, IL-12p70 and INF-gamma did not differ among different strains (Figure 4.6 D, F; I). The anti-inflammatory cytokine IL-10 was increased in the A/J PBS compared to C3H/HeJ PBS group. Furthermore, the TNF-alpha level was elevated in the PBS-treated group of BALB/cj mice compared to the respective group of the C57BL/6J strain (Figure 4.6 J). Overall, a strain-dependent cytokine production was observed with main differences detected in response to the HDM sensitization.



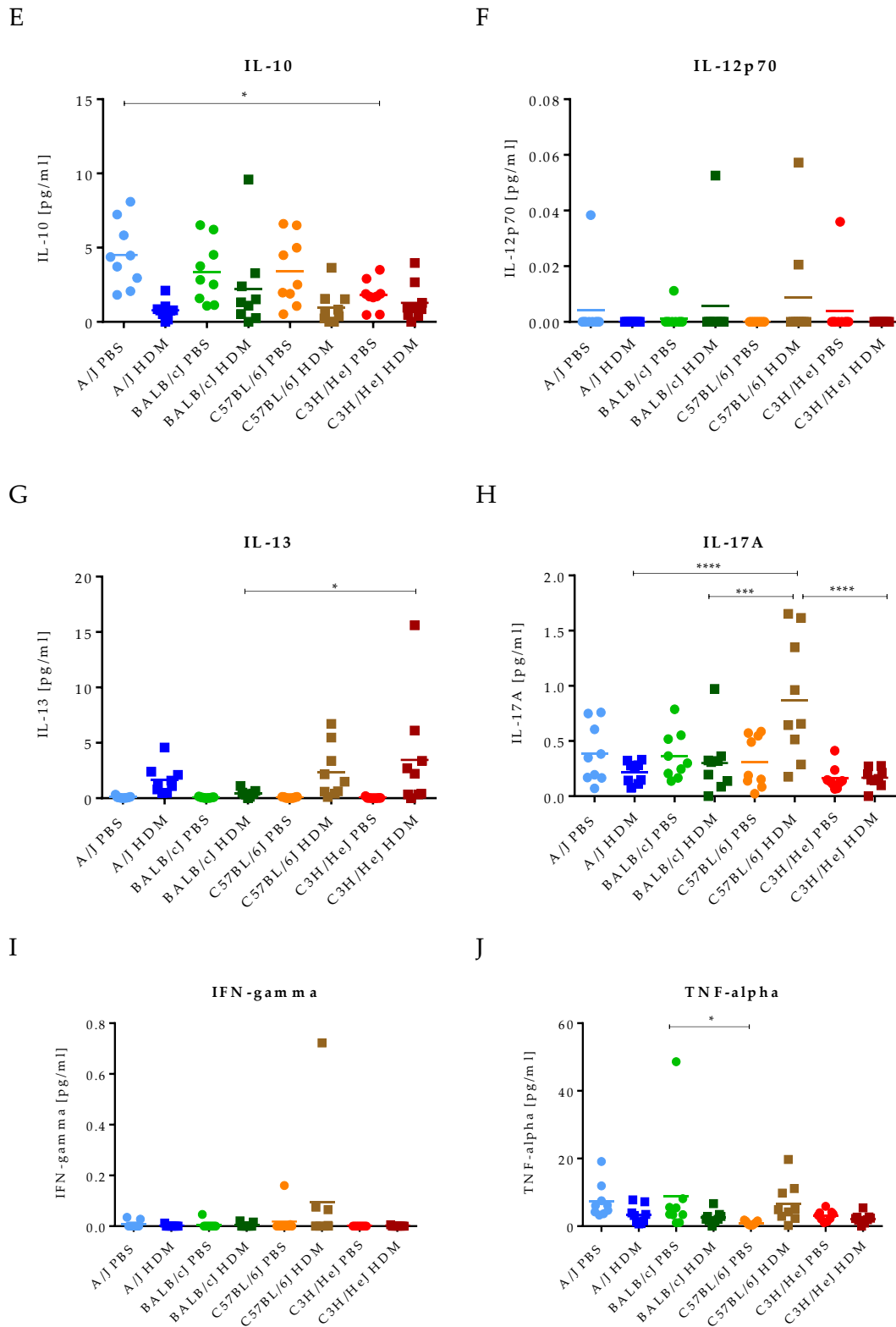


Figure 4.6: Cytokines measured in BAL supernatant.

A. IL-1 β . B. IL-4. C. IL-5. D. IL-6. E. IL-10. F. IL-12p70. G. IL-13. H. IL-17A. I. IFN-gamma. J. TNF-alpha. $n=9$ animals per group; Two-way ANOVA (strain vs. PBS/PBS and HDM/HDM) and Tukey's multiple comparisons test; * $p < 0.05$, ** $p < 0.01$, *** $p < 0.001$, **** $p < 0.0001$.

4.1.2 Lung function

To measure the different lung function parameters, invasive lung function measurements were performed at baseline, and the AHR was assessed in response to increasing doses of the bronchoconstricting agent methacholine. AHR is defined by significantly higher values of airway resistance for at least two concentrations of applied methacholine in the HDM compared to PBS group of same strain. During the measurement IC, airway compliance and airway resistance were monitored and recorded. The IC was significantly higher for C3H/HeJ than for A/J and C57BL/6J comparing the PBS-treated control groups (Figure 4.7). Multiple significant differences were further observed for the baseline values of the compliance, both among PBS- and HDM-treated groups. Both treatment groups of C3H/HeJ showed the highest values, whereas C57BL/6J showed the lowest compliance values, for detailed information see Figure 4.8 A. The compliance of the airways is decreasing in all groups in response to the increasing methacholine doses applied, further the graph of the HDM-groups is slightly below the PBS graph for the same strain (Figure 4.8). The measurement of airway resistance at baseline did not reveal differences among the strains (Figure 4.9 A). For all HDM-treated groups a trend towards increased airway resistance (Figure 4.9 B) and decreased compliance (Figure 4.8 B) was observed compared to the respective PBS controls.

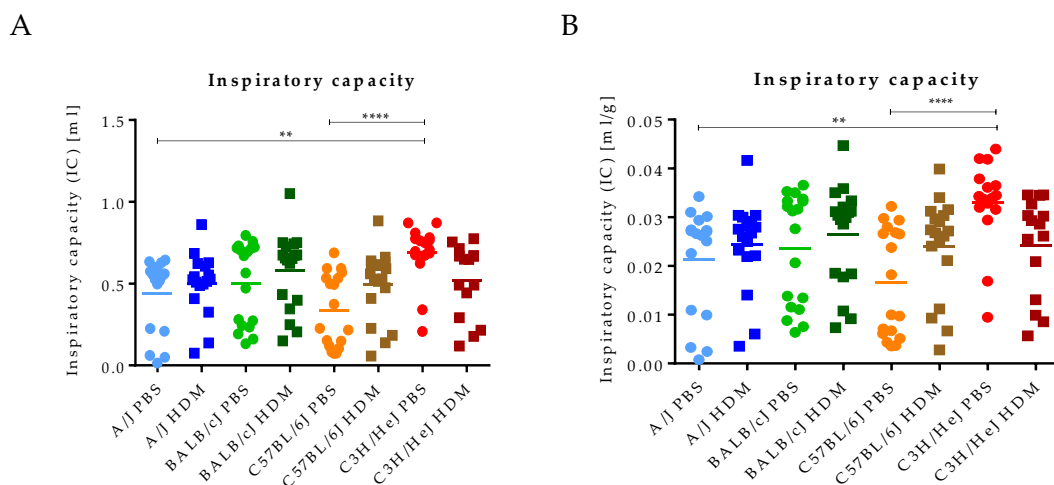


Figure 4.7: Inspiratory capacity measurement.

A. Absolute values for IC (IC/ml). B. IC related to the bodyweight (IC ml/g), $n=15-18$ animals per group; Two-way ANOVA (strain vs. PBS/PBS and HDM/HDM) and Tukey's multiple comparisons test; * $p < 0.05$, ** $p < 0.01$, *** $p < 0.001$, **** $p < 0.0001$.

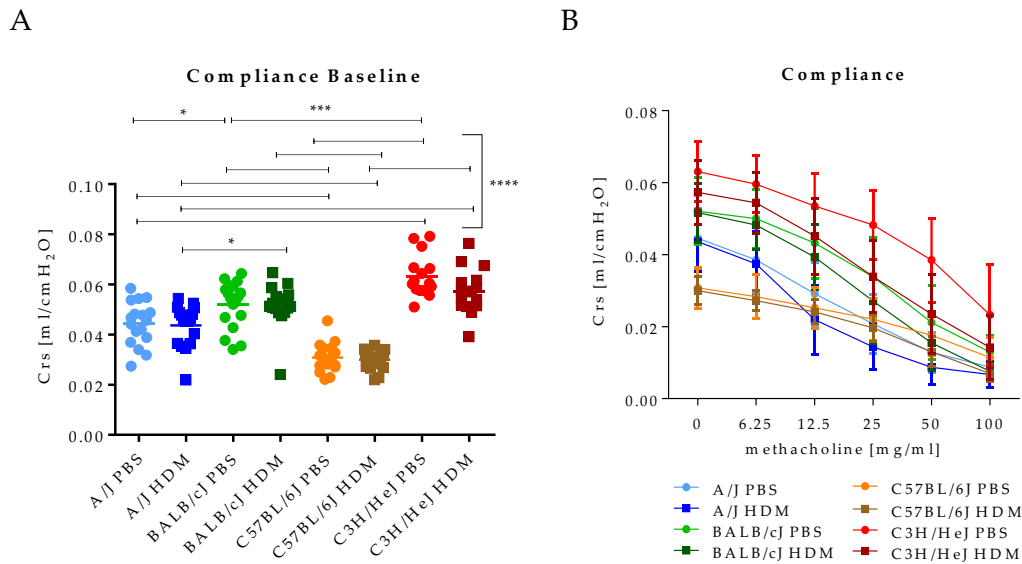


Figure 4.8: Compliance measurement.

A. Compliance at Baseline, $n=16-18$ animals per group; Two-way ANOVA (strain vs. PBS/PBS and HDM/HDM) and Tukey's multiple comparisons test; $*p < 0.05$, $**p < 0.01$, $***p < 0.001$, $****p < 0.0001$.

B. Analysis of compliance in response to increasing doses of methacholine, $n=2-18$ animals per group.

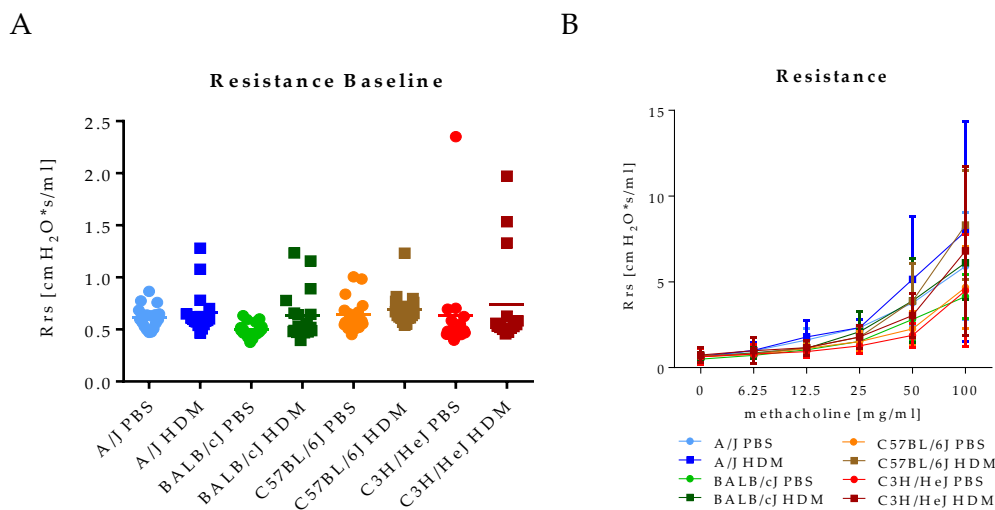


Figure 4.9: Resistance measurement.

A. Resistance at Baseline, $n=16-18$ animals per group; Two-way ANOVA (strain vs. PBS/PBS and HDM/HDM) and Tukey's multiple comparisons test; $*p < 0.05$, $**p < 0.01$, $***p < 0.001$, $****p < 0.0001$.

B. Analysis of resistance in response to increasing doses of methacholine, $n=2-18$ animals per group.

However, an AHR, defined by resistance values differing significantly for at least two concentrations of applied methacholine comparing PBS to HDM group were only observed for the C57BL/6J strain (Figure 4.10 C). For the three remaining strains, a trend was observed but no statistical significance was reached (Figure 4.10 A, B and D).

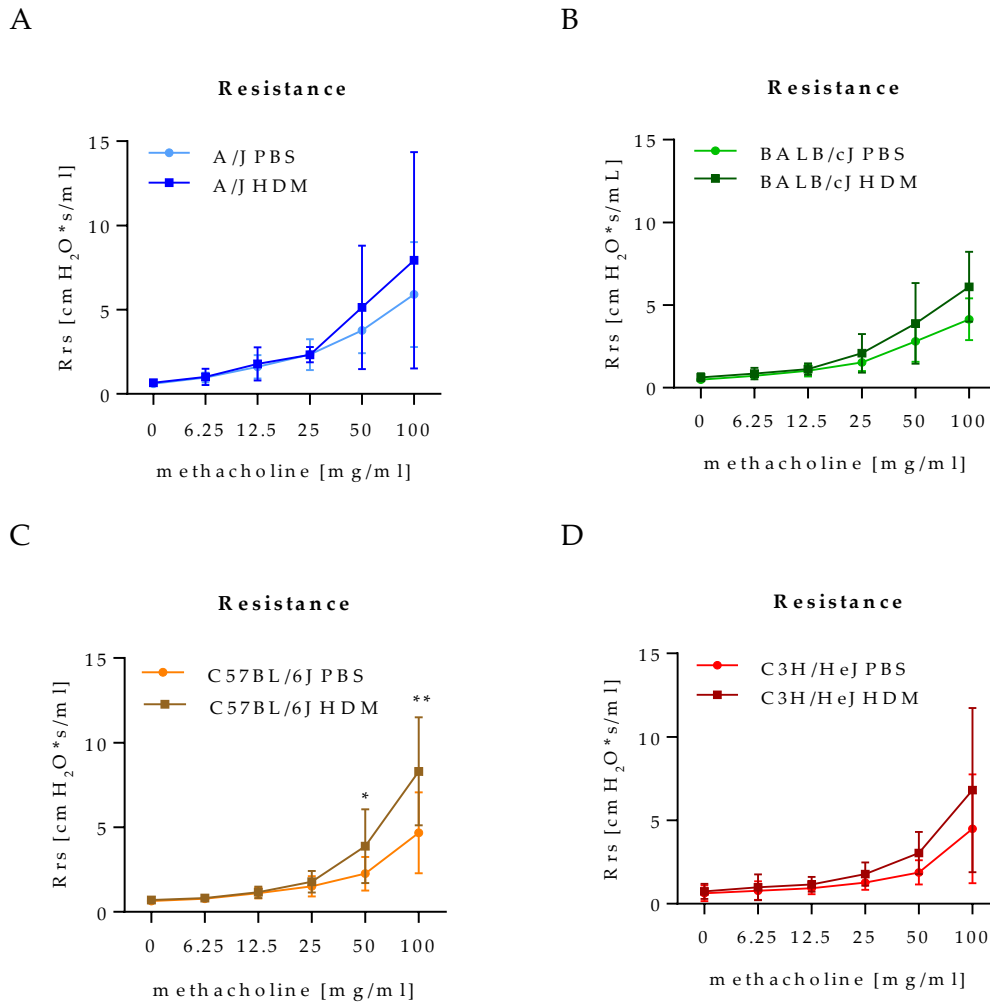


Figure 4.10: AHR measurement for each strain.

A. A/J, $n=2-18$ animals per group (100 mg/ml only two valid values); B. BALB/cJ, $n=12-18$ animals per group; C. C57BL/6J, $n=16-18$ animals per group; D. C3H/HeJ, $n=11-16$ animals per group.

Statistics: Mean \pm SD shown; Two-way ANOVA (PBS/HDM vs. methacholine dose) followed by Sidak's multiple comparisons test; * $p < 0.05$, ** $p < 0.01$, *** $p < 0.001$, **** $p < 0.0001$.

4.1.3 Total IgE in serum

Since IgE levels partly reflect the severity of the allergic response and are relevant for the characterization of allergic asthma, the sensitization status was assessed in all four mouse strains. Total IgE was increased in all treated groups with clear differences among the strains: C3H/HeJ and A/J developed the highest levels while BALB/cJ mice showed a slight rise only (Figure 4.11). One out of three experiments didn't show an increase of IgE concentrations for the HDM-treated BALB/cJ group compared to the PBS-only treated control group.

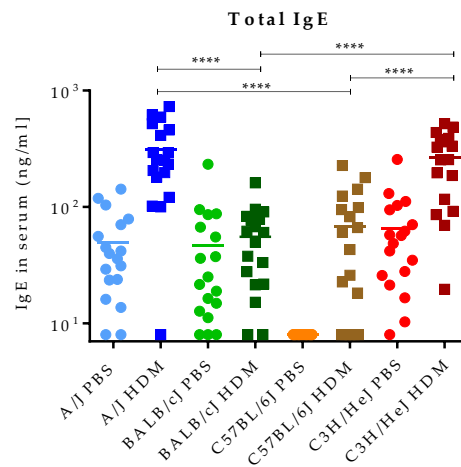


Figure 4.11: Total IgE levels in serum.

Total IgE levels measured by ELISA in serum, $n=17-18$ animals per group, Two-way ANOVA (strain vs. PBS/PBS and HDM/HDM) and Tukey's multiple comparisons test; * $p < 0.05$, ** $p < 0.01$, *** $p < 0.001$, **** $p < 0.0001$.

4.1.4 Histology

The PAS staining revealed changes in histological feature in the HDM-treated mice compared to PBS-treated mice. The staining revealed cellular infiltrates of immune cells, shown in blue, surrounding main airways and goblet cells filled with mucus stained in pink in the HDM-treated groups. The severity of cell infiltrates and goblet hyperplasia increased in the following order (analyzed by giving score for each individual sample): BALB/cJ < C57BL/6J = C3H/HeJ < A/J. When comparing goblet cell hyperplasia and pulmonary cell infiltration in response to HDM-treatment, A/J mice showed both the most prominent mucus production and airway inflammation, while both parameters were lowest in BALB/cJ (Figure 4.12 and Figure 4.13). These observations were partly confirmed by using the CAST system for a quantitative analysis.

The CAST analysis detected that numbers of mucus producing goblet cells were significantly higher in A/J and C3H/HeJ than in BALB/cJ and C57BL/6J mice (Figure 4.14 A).

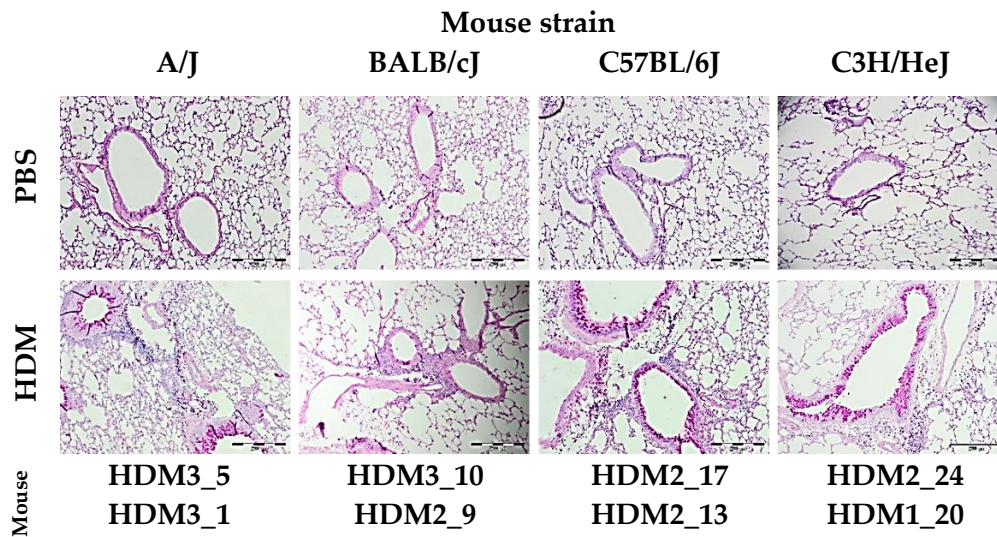


Figure 4.12: PAS histology staining of lung sections (10-fold magnification).

HDM treatment induces mucus production in goblet cells and the infiltration of inflammatory cells around the airways. Representative images of PAS-stained lung sections of the HDM- and the PBS-treated group.

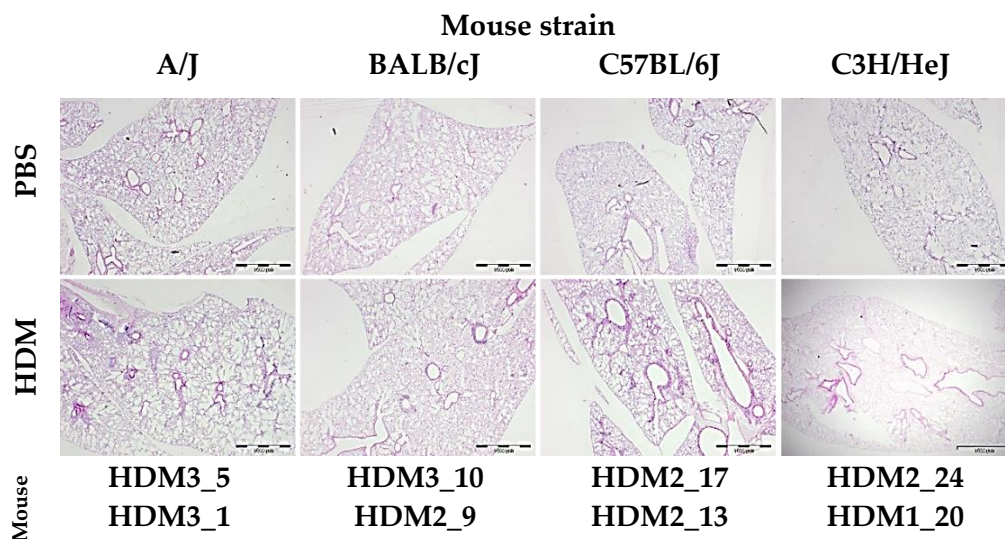


Figure 4.13: PAS histology staining of lung sections (2-fold magnification).

HDM treatment induces mucus production in goblet cells and the infiltration of inflammatory cells around the airways. Representative images of PAS-stained lung sections of the HDM- and the PBS-treated group.

A similar order was seen for the volume of PAS-stained epithelial mucin ($V_{s \text{ mucin}}$) per total area of airway epithelial basal membrane, except that C3H/HeJ and C57BL/6J did not differ significantly (Figure 4.14 B). The quantification of infiltrating cells ($V_{s \text{ inf}}$)

around the peribronchial epithelium in the HDM-treated groups did not differ significantly among the strains (Figure 4.14 C).

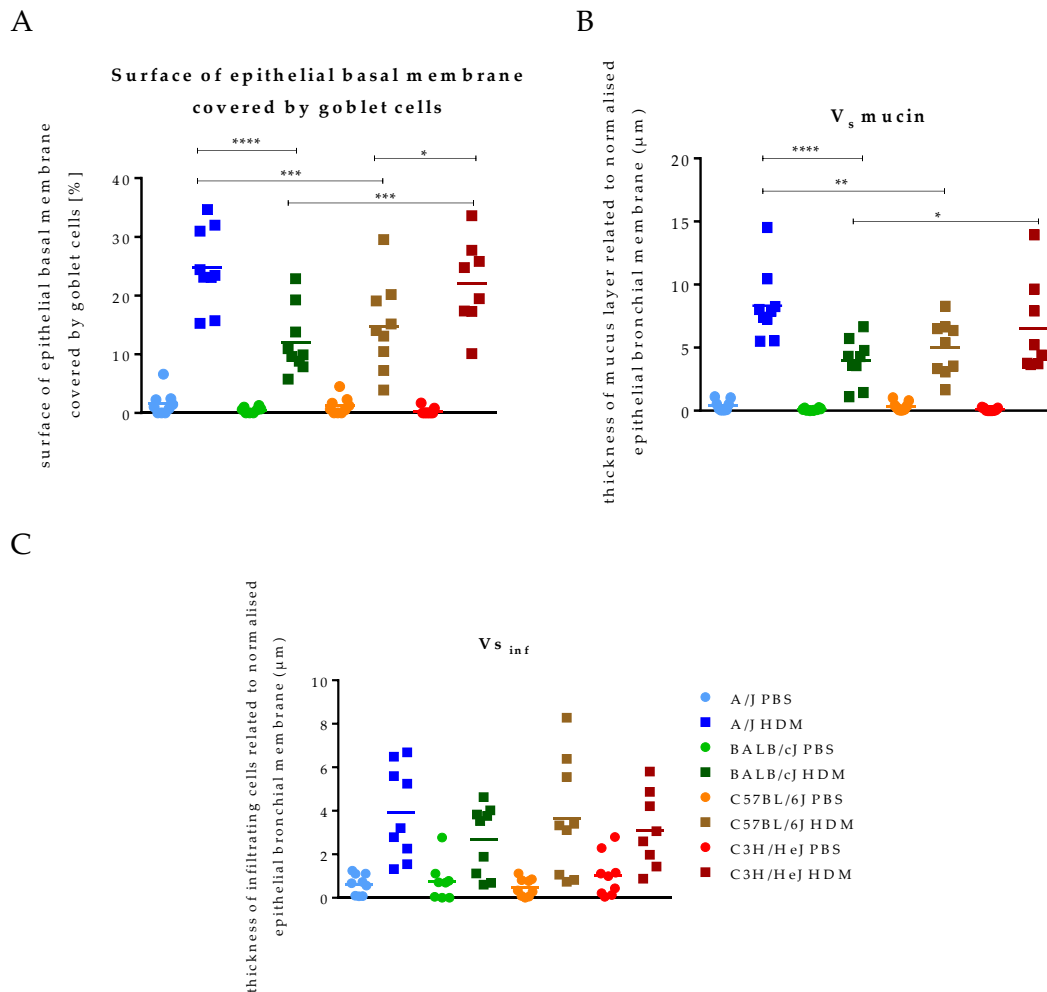


Figure 4.14: CAST analysis of histological features.

A. Surface of epithelial basal membrane covered by goblet; B. Volume of PAS-stained epithelial mucin (V_s mucin); C. Volume of infiltrating cells in the peribronchial epithelium ($V_{s\ inf}$); $n=8-9$ animals per group; Two-way ANOVA (strain vs. PBS/PBS and HDM/HDM) and Tukey's multiple comparisons test; * $p < 0.05$, ** $p < 0.01$, *** $p < 0.001$, **** $p < 0.0001$.

4.1.5 Gene expression in lung homogenates

To corroborate these findings, MUC5B and CCL11 expression was measured in lung homogenates by qRT-PCR analysis. Both genes were elevated in lung homogenates of all HDM-sensitized groups (Figure 4.15 A-B) with the strongest increase for A/J and C3H/HeJ. These findings thus confirmed previous results of the CAST analysis (Figure 4.15 A-B). The analysis of the obtained values for the fold change of MUC5B and CCL11 gene expression of the HDM groups showed that CCL11 was only significantly higher in A/J HDM than in BALB/cj HDM group.

In summary, all mice treated with HDM showed the development of an “asthmatic” phenotype in contrast to the corresponding PBS controls. Interestingly, the severities of individual readouts differed among the mice of the four strains. Applying the identical HDM treatment scheme in four different mouse strains led to distinct phenotypic manifestations of asthma in the strains.

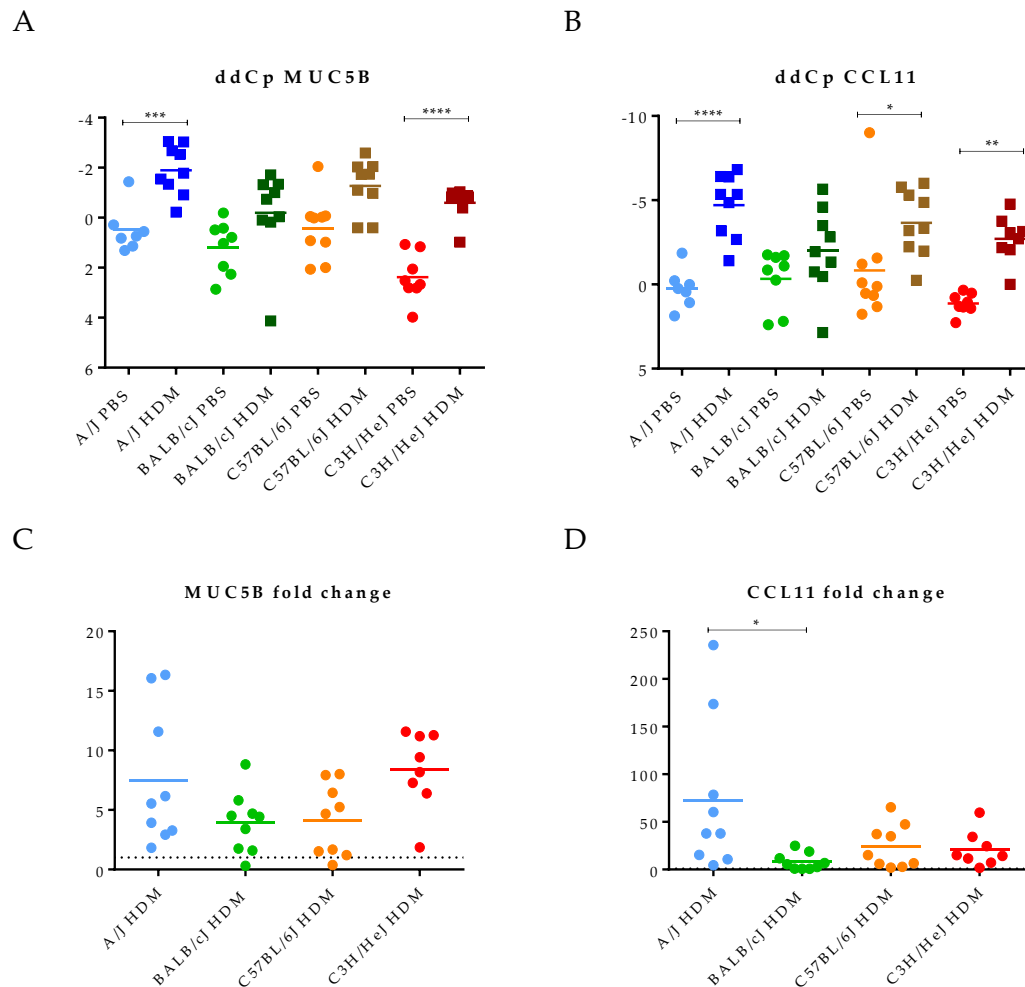


Figure 4.15: Gene expression of MUC5B and CCL11 in lung homogenates.

A-B. Delta delta crossing point (ddCP) values of MUC5B (A) and CCL11 (B) gene expression in lung homogenates, $n=7-9$ animals per group; One-way ANOVA with Sidak's multiple comparisons test, PBS/HDM of same strain; * $p < 0.05$, ** $p < 0.01$, *** $p < 0.001$, **** $p < 0.0001$.

C-D. Fold change to PBS control of gene expression levels of MUC5B (C) and CCL11 (D) in lung homogenates; $n=7-9$ animals per group; One-way ANOVA with Mann Whitney's multiple comparisons test, HDM groups of different strains; * $p < 0.05$, ** $p < 0.01$, *** $p < 0.001$, **** $p < 0.0001$.

BALB/cj has been identified as a relatively mild (low eosinophilic, Th2-low) and C3H/Hej as a severe strong phenotype, mainly eosinophilic, Th2-dominated with pronounced changes in lung histology. The A/J strain developed a phenotype with comparable characteristics as C3H/Hej albeit less pronounced Th2-cytokines in the

BAL supernatant. For C57BL/6J the severity was ranked as intermediate, characteristic for this strain was the significantly higher IL-17A concentration detected in the BAL supernatant. The different manifestation of asthma using the same HDM treatment in four different mouse strains allowed identification of distinct asthma phenotypes. A summary of the results is shown in Figure 4.16 below.





A/J		<p>Eosinophilic (67%) moderate IL-4, IL-17A low Strong goblet cell hyperplasia IgE high</p>
BALB/cJ		<p>Eosinophilic (21%) IL-4 negative, IL-5 and IL-17A moderate, IL-13 low IgE low</p>
C57BL/6J		<p>Eosinophilic (63%) IL-4 high, IL-5 and IL-13 moderate, IL-17A high IgE low</p>
C3H/HeJ		<p>Eosinophilic (62%) IL-4 and IL-5 moderate, IL-13 high, IL-17A low Strong goblet cell hyperplasia IgE high</p>

Figure 4.16: Characterization of asthma phenotypes in four strains.

Summary of relevant readouts used for characterization of different “asthmatic” phenotypes identified in the four different mouse strains. Pictures taken from the Jackson Laboratory web page, 2020¹⁵⁴.

4.2 Microbiome analysis

4.2.1 Analysis of caecum in R

4.2.1.1 Rhea pipeline

4.2.1.1.1 Rarefaction curve

The graph below shows the rarefaction curve of all caecum samples and the corresponding controls. The curve has not reached a final plateau for each individual sample, thus deeper sequencing might have yielded further species. Although, the sequencing depth could be improved, the number of species was considered to be sufficient to perform subsequent analysis of the composition. The number of identified species in caecum samples are between 150 to 350 detected species.

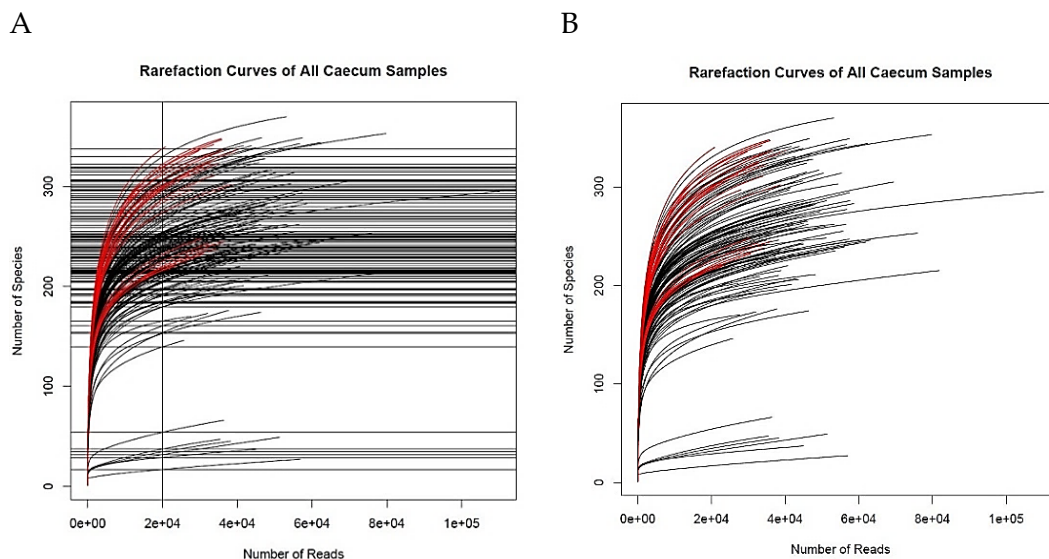


Figure 4.17: Rarefaction curve of all caecum samples.

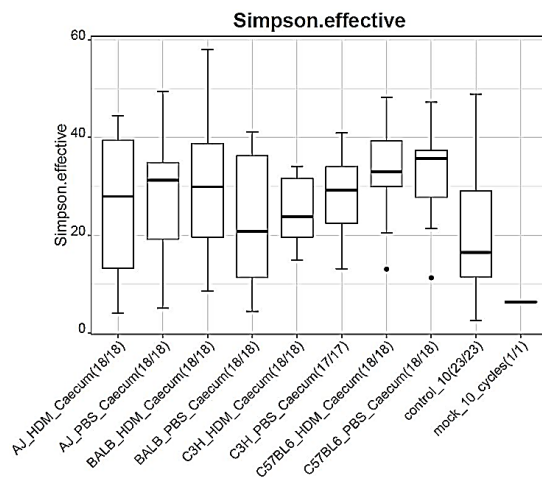
A. The vertical line shows the number of 20,000 reads the caecum samples are normalized to in Phyloseq and the horizontal lines the number of species detected in the individual sample post normalization. 20 undersampled cases are highlighted in red. B. 20 undersampled cases are highlighted in red. Graphs are generated with Normalization script in Rhea pipeline.

4.2.1.1.2 Alpha diversity

Alpha diversity is a value representing the diversity of the detected operational taxonomic units within one sample. From Figure 4.18 A the mean Simpson effective value of the controls group 9 (includes NEC/ Trizol/ NRNA/ NRT control samples) shows the trend to be less diverse than the values for the caecum sample of the differently treated strains. Further, the diversity differs among strains: The C57BL/6J PBS-treated group showed pronounced higher alpha diversity values comparing the

values to the C3H/HeJ HDM group. Statistical testing did not show significant difference of alpha diversity measures neither at baseline, nor after the induction of experimental asthma, for the caecum microbial composition across the four strains. Analyzing the statistics in a broader view, based on the different sample-type (Figure 4.18 B), revealed significantly lower Simpson effective value for the controls (group 1, controls) than for the caecum sample (group 3, RNA).

A



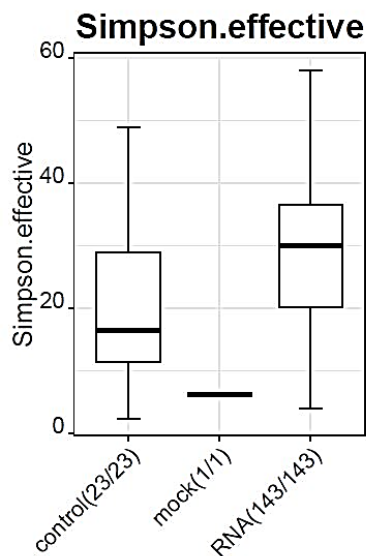
Kruskal-Wallis Rank Sum Test – all groups

	p-value	Adj. p-values
Simpson effective	0.0067	0.0148

Wilcoxin Rank Sum Test - pairwise

Groups	p-value	Adj. p-values
3-9	0.0175	0.1517
4-7	0.0315	0.1772
4-8	0.0205	0.1517
5-7	0.0119	0.1339
5-8	0.0008	0.0255
6-9	0.0236	0.1517
7-9	0.0014	0.0255
8-9	0.0017	0.0255

B



Kruskal-Wallis Rank Sum Test – all groups

	p-value	Adj. p-values
Simpson effective	0.0059	0.0218

Wilcoxin Rank Sum Test - pairwise

Groups	p-value	Adj. p-values
1-3	0.005	0.015

Figure 4.18: Alpha diversity (Simpson effective values) of caecum samples.

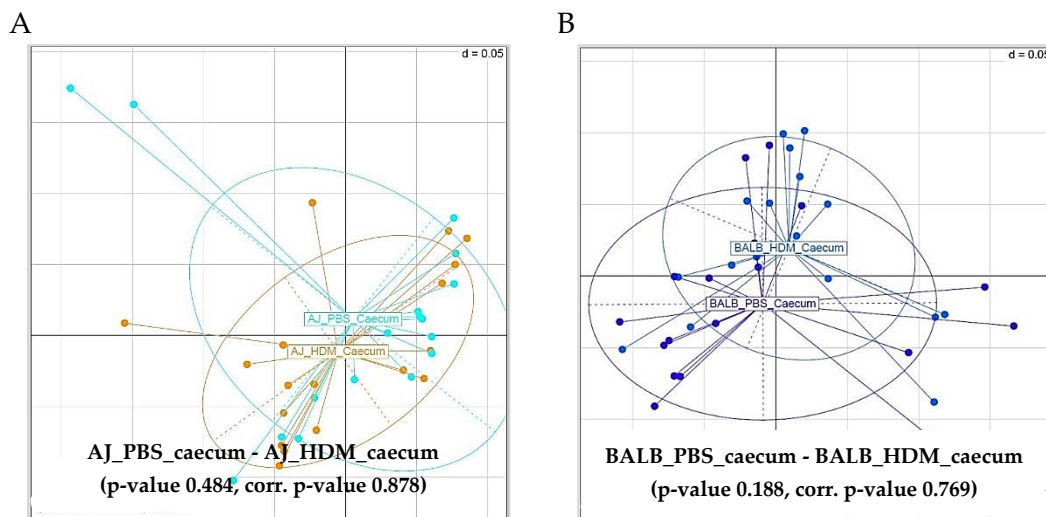
A. Alpha diversity (Simpson effective values) of caecum samples compared among different treated groups and corresponding controls. Group 1-10 represent the groups counting left to right in the x-axis of the figure. Statistics: animals per group ($n=17-18$); controls ($n=23$); mock=mock community ($n=1$)

B. Alpha diversity (Simpson effective values) of caecum samples compared based on sample_type. Statistics: controls ($n=23$), RNA ($n=143$), mock=mock community ($n=1$);

Kruskal-Wallis Rank Sum Test, multiple testing by Mann-Whitney Test, and correction of p -values by Benjamini Hochberg method.

4.2.1.1.3 Beta diversity

The beta diversity based on the generalized UniFrac distances was compared between the PBS- and HDM-treated mice of the same strain in a pairwise manner. As visualized in the MDS plot and stated by the corrected p values, this analysis did not detect significant changes in the microbial composition of the caecum, with respect to the received treatment in mice of the same genetic background (Figure 4.19 A-D). Figure 4.19 E presents all groups, including controls and the mock community, combined in one MDS plot. For this statistical approach an overall difference was stated with a p value of 0.001. Figure 4.19 E illustrates the clusters of the different caecum treatment groups although, it appears that C57BL/6J forms a distinct cluster, this was not statistically relevant based on the comparison of beta diversity measures of the C57BL/6J to the corresponding treatment groups of the other strains (Figure 7.1, page 100, supplement). Further, as visualized in the same figure the microbial composition of the caecum builds a separate cluster, irrespective of the received treatment, compared to other strains. Also, the mock community sample and controls clustered separately (Figure 4.19 E-F). Generating clusters based on the different sample types (RNA, control and mock community (mock)) confirmed that controls vs. caecum samples (RNA) cluster significantly different with a corr. p value of 0.003 (Figure 4.19 G).



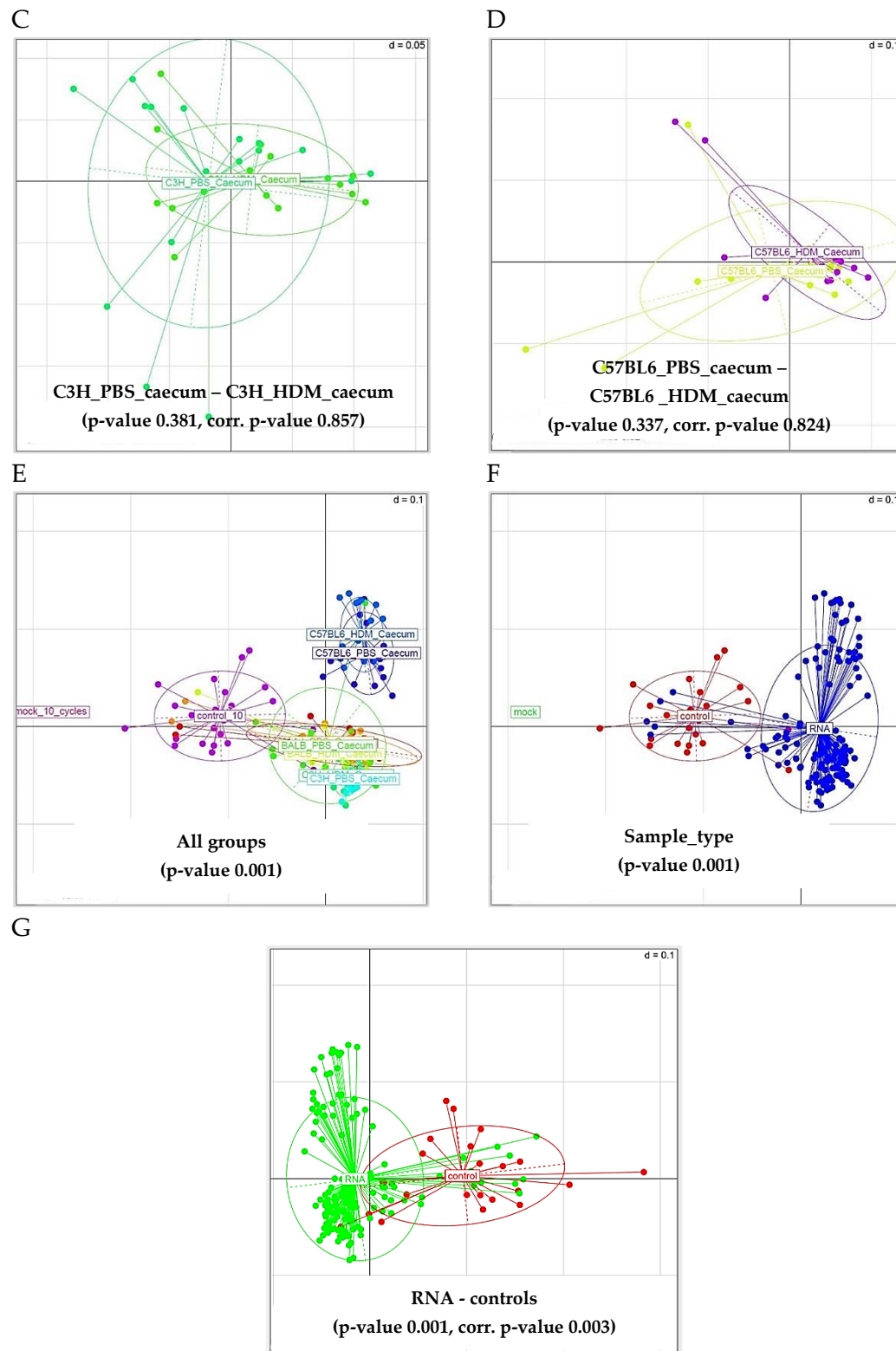


Figure 4.19: MDS plots comparing beta diversity in caecum samples.

MDS plots representing the beta diversity comparing among groups ($n=17-18$ animals per group; mock=mock community ($n=1$); controls ($n=23$)); A. A/J; B. BALB/cJ; C. C3H/HeJ; D. C57BL/6J; E. all groups; F. clustering based on sample type; G. pairwise comparison of RNA vs. controls.

Distances matrices calculated with `vegan::adonis`, subsequently PERMANOVA was applied, followed by Benjamini-Hochberg method for multiple testing for corr. p value. MDS plots annotate the p values of the PERMANOVA, $d=0.05$ represents 5% and $d=0.1$ represents 10% of dissimilarity in the grid distance.

4.2.1.1.4 Correlation plots

The plot below states the correlation between different alpha diversity measures vs. single-identified taxa. The color of the dot explains the direction of the correlation; blue, positive; red, negative. The circle size represents the uncorrected p value of the corresponding correlation. Positive and negative correlations of alpha diversity values and taxa at different taxonomic hierarchy could be identified. On class-level *Clostridia*, on order-level *Clostridiales* and on family-level *Ruminococcaceae* are found to be positively correlated with a higher alpha diversity based on both the Shannon effective and Simpson effective values. The two identified genera *Clostridium XIVa* and *Clostridium XIVb* are from the same phylum but show a negative correlation with the Shannon effective and Simpson effective values, whereas the cluster *Clostridium XIVa* correlated positively with richness measures. All mentioned taxa belong to the phylum Firmicutes; therefore, it becomes clear that the assignment on phylum-level could neglect differences which occur at lower taxonomic levels. This means that the effect single identified genera have on alpha diversity measures can lead to opposing or compensating effects for the same measures on the phylum-level. These findings highlight the relevance of changes within the same phylum and the need to investigate at lower taxonomic levels thus those effects cannot be accounted for on phylum level.

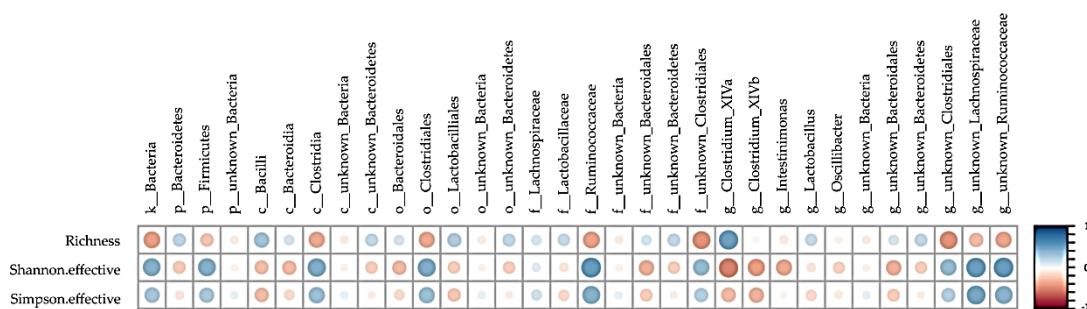


Figure 4.20: Correlation plot of alpha diversity in caecum samples.

Correlation plot of alpha diversity measures and taxonomy of caecum samples. Dot color states direction of the correlation (blue, positive; red, negative), circle size represents uncorrected p value of correlation. Correlation calculated based on Pearson's coefficient of correlation.

4.2.1.2 Phyloseq

4.2.1.2.1 Top10 assignments to taxonomic hierarchy

The assignment of the ten most abundant phyla (Top10) in the caecum samples are summarized in Figure 4.21 below. The taxonomic distribution on phylum-level shows

that the caecum microbiome is mainly composed of bacteria belonging to the phylum Firmicutes, followed by a lower abundance of the phylum Bacteroidetes. The remaining eight assigned phyla, plotted in the diagram, account on the whole population for less than 5% of the total identified microbes. Comparing the HDM and PBS group of the same strain no differences could be identified. Thus, it can be deduced that the treatment does not affect the distribution of phyla in the caecum in the four strains. On family-level (Figure 4.21 B) in both C57BL/6J groups *Bacteroidaceae* and *Erysipelotrichaceae* are more abundant in contrast to the other three strains. The proportion of *Blautia* is clearly higher for the A/J samples than for the other strains, as seen in Figure 4.21 C showing the assignment of taxa on genus level.

Throughout the process, various controls were included. The controls are as followed: includes NEC/ Trizol/ NRNA/ NRT control samples. In addition, one mock community was isolated and sequenced along with the caecum samples. All controls included throughout the processing of the caecum samples showed very low number of reads. Out of the 23 controls 21 lead to less than 100 reads and the remaining two less than 250 samples, so still very low numbers. All of them were removed by rarefying. The only control remaining after rarefying was the mock community represented in both figures (Figure 4.22 A-B). The isolated mock community sample presents the accurate composition, all eight bacterial genera are detected and correctly assigned according to the product specification of the ZymoBIOMICS™ Microbial Community Standard.

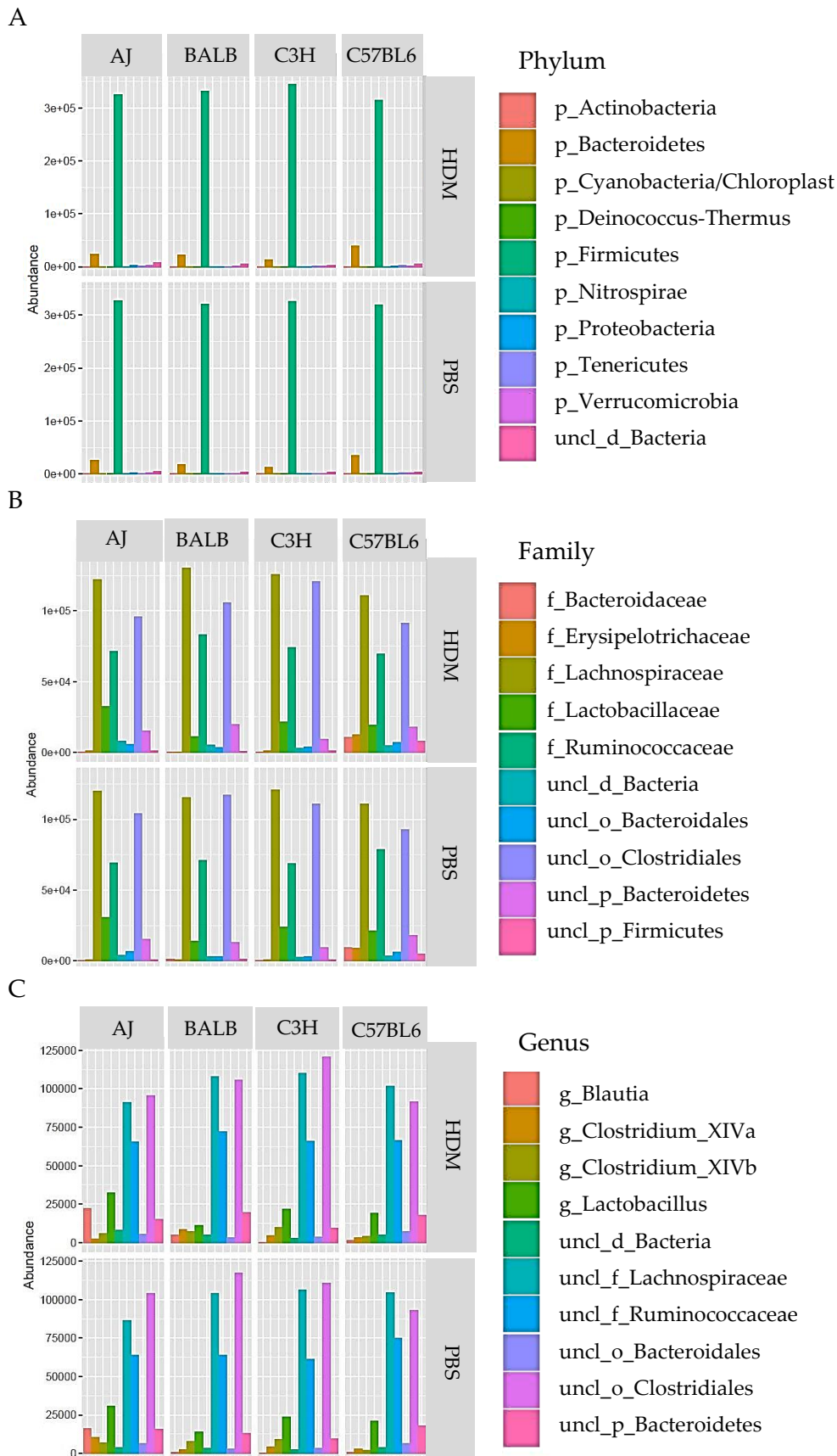


Figure 4.21: Top10 detected Taxonomy in caecum samples comparing PBS and HDM groups.

A: Phylum-level, B: Family-level; C: Genus-level.

$n=17-18$ animals per group; generated using Phyloseq in R.

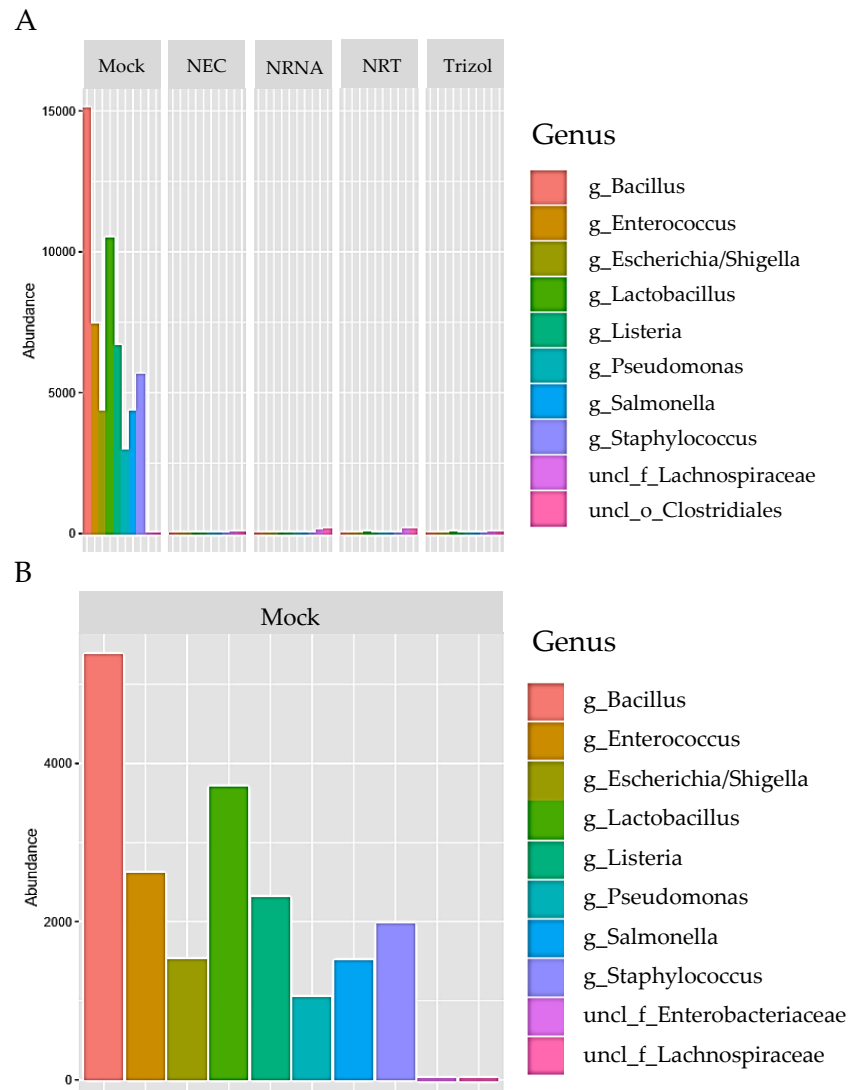


Figure 4.22: Top10 detected Genera in different subgroups of control caecum samples.

A. Raw reads without normalization B. Post normalization to 20,000 reads per samples.

(Mock=Mock community isolated starting from Fastprep step onwards ($n=1$); NEC ($n=3$); NRNA ($n=5$); NRT ($n=11$); Trizol=Trizol extraction control, post Fastprep isolation ($n=4$)). Generated using Phyloseq in R.

4.2.2 Analysis of lungs in R

4.2.2.1 Rhea pipeline

4.2.2.1.1 Rarefaction curve

The rarefaction curve of all lung samples, including the corresponding controls, is shown in Figure 4.23. For most of the samples the curve has reached a final plateau proofing sufficient sequencing depth. The 20 most undersampled samples are highlighted in red color. The number of identified species shows mainly 150 to 450 identified species per sample which is a slightly higher range compared to the caecum samples.

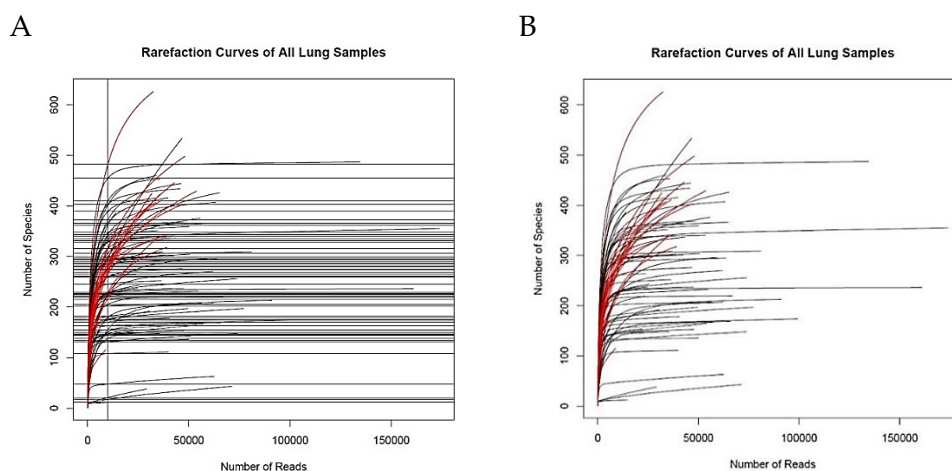


Figure 4.23: Rarefaction curve of all lung samples.

A. The vertical line shows the number of 10,000 reads the lung samples are normalized to in Phyloseq and the horizontal lines the number of species detected in the individual sample post normalization. 20 undersampled cases are highlighted in red. B. 20 undersampled cases are highlighted in red. Graphs are generated with Normalization script in Rhea pipeline.

4.2.2.1.2 Alpha diversity

Simpsons effective values as a measure of within sample diversity in the lung samples reveal a wide range within the same group (Figure 4.24). Overall, median values observed in the lungs are lower than in the caecum. The trend that the PBS groups have higher values for alpha diversity which was previously observed for caecum samples, could also be seen for the lung samples. Due to the high variation within each group no statistically significant difference among the groups was calculated.

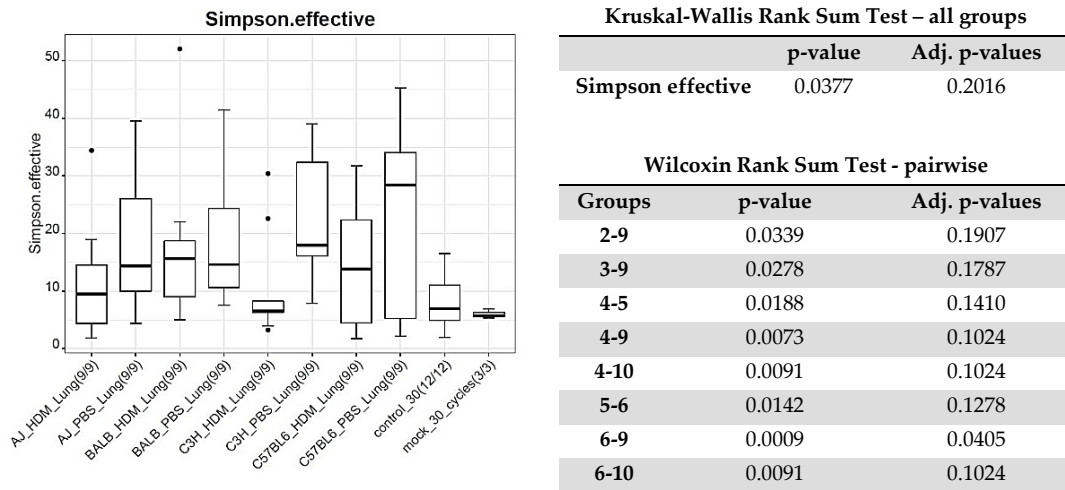


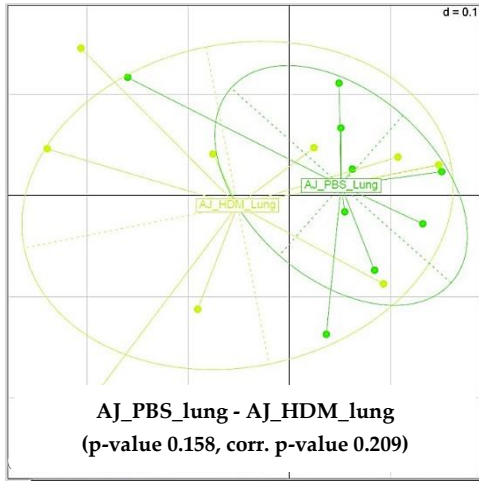
Figure 4.24: Alpha diversity (Simpson effective values) of lung samples.

Alpha diversity (Simpson effective values) of lung samples among differently treated groups. Statistics: animals per group ($n=9$); controls ($n=12$); mock=mock community ($n=3$), Kruskal-Wallis Rank Sum Test, multiple testing by Mann-Whitney Test, and correction of p -values by Benjamini-Hochberg method.

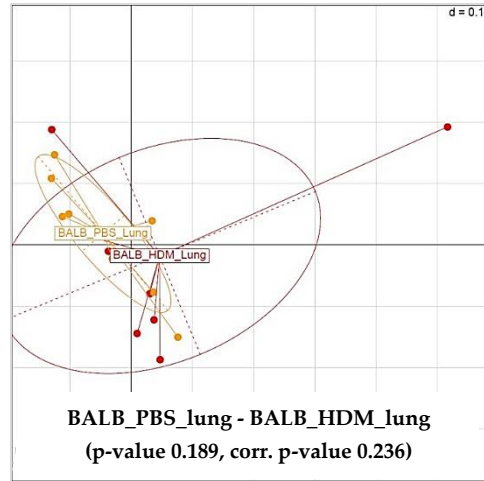
4.2.2.1.3 Beta diversity

Beta diversity values provide a measure for the similarity between microbial profiles of different groups. Generalized UniFrac distance values are calculated, as beta diversity measures, to test for differences between the PBS- and HDM-treated group of the same strain. A significant difference of the generalized UniFrac distance, in this case a corrected p value of 0.03, could be detected for the C3H/HeJ lung samples comparing the PBS- to HDM-treated group (Figure 4.25 C). This finding confirms that in response to the HDM-treatment the microbial profile is altered significantly. No significant difference between the PBS- vs. HDM-treated groups in the remaining three strains (AJ, BALB/cJ and C57BL/6J) was calculated based on generalized UniFrac distance (Figure 4.25 A, B and D). Figure 4.25 E shows all samples combined in one MDS plot, each sample is assigned to the corresponding treatment group. The overall difference among the treatment groups was calculated and a corrected p value of $p=0.001$ detected. In addition, the same value for the overall statistical difference was detected clustering the samples based on their three different sample types: RNA, control vs. mock (mock community) (Figure 4.25 F). Further, the generation of significantly different clusters were detected for the pairwise comparison of firstly RNA vs. controls (Figure 4.25 G); secondly RNA vs. mock communities (Figure 4.25 H) and thirdly controls vs. mock communities (Figure 4.25 I).

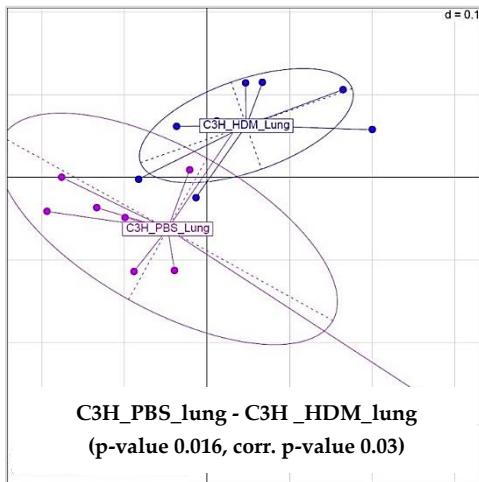
A



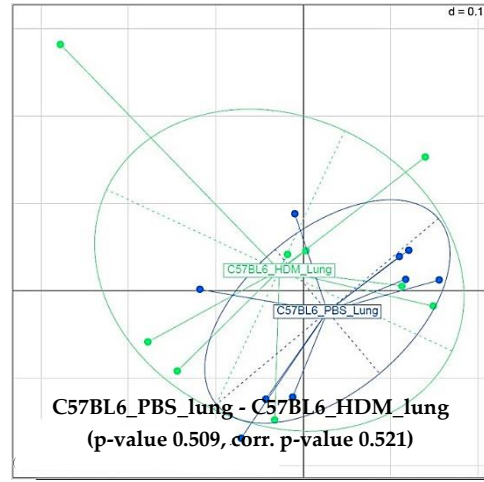
B



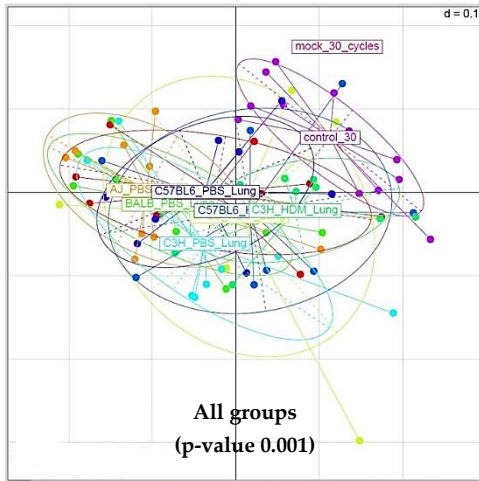
C



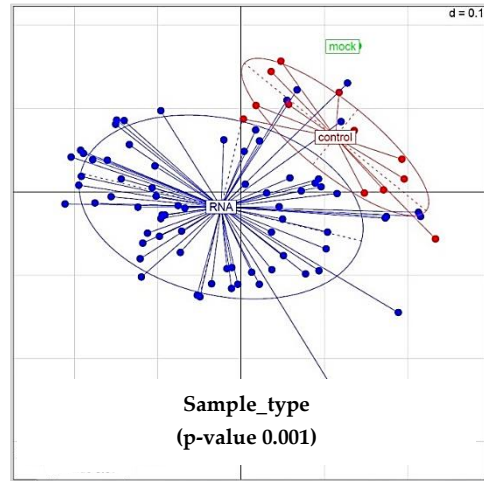
D



E



F



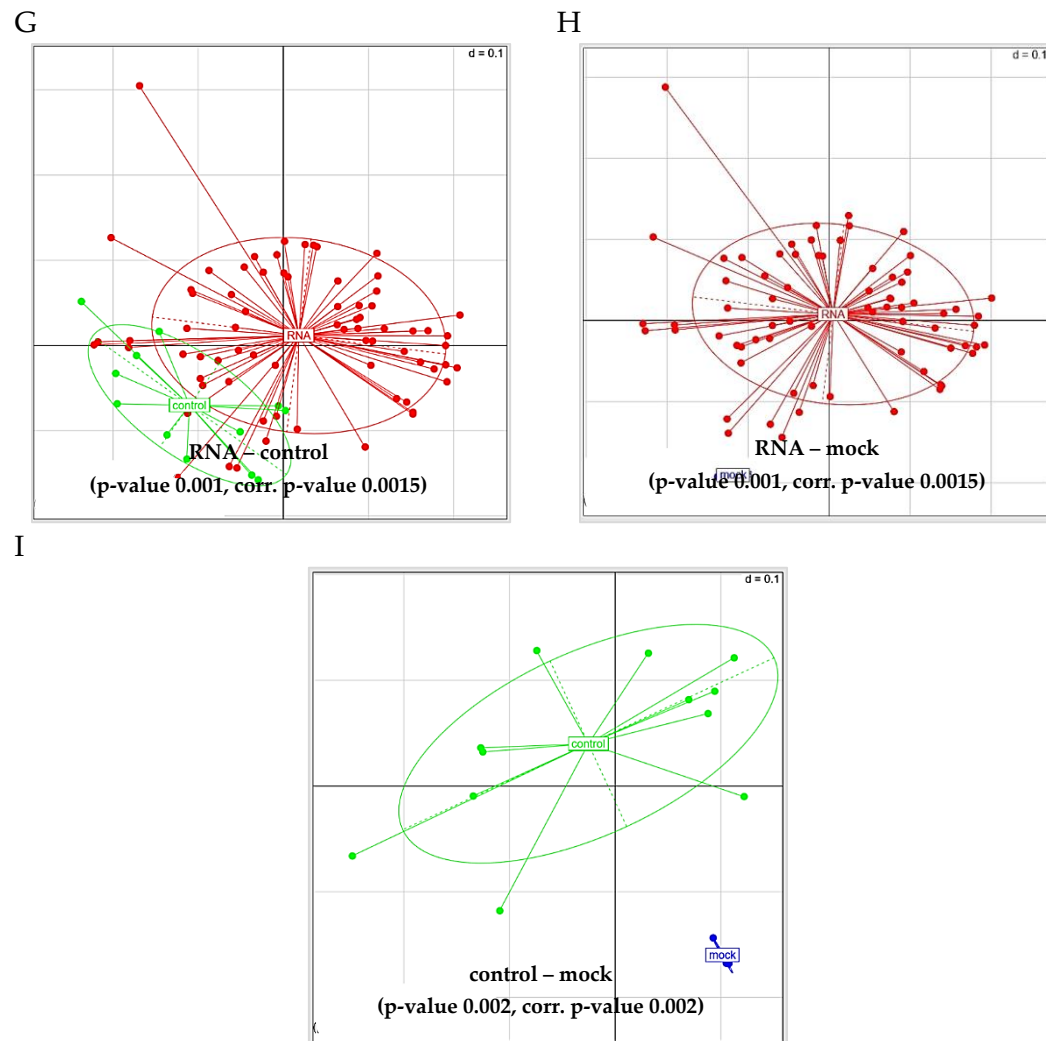


Figure 4.25: MDS plots comparing beta diversity in lung samples.

MDS plots representing the beta diversity comparing among different groups ($n=9$ animals per group; mock=mock community ($n=3$); controls ($n=12$)); A. A/J; B. BALB/cJ; C. C3H/HeJ; D. C57BL/6J; E. all groups; F. clustering based on sample type; G. pairwise comparison of RNA vs. controls. H. pairwise comparison of RNA vs. mock (mock community). I. pairwise comparison of control vs. mock (mock community).

Distances matrices calculated with `vegan::adonis`, subsequently PERMANOVA was applied, followed by Benjamini-Hochberg method for multiple testing for corr. p value. MDS plots annotate the p values of the PERMANOVA, and $d=0.1$ represents 10% of dissimilarity in the grid distance.

4.2.2.1.4 Correlation plots

The correlation plot detects correlations between different alpha diversity measures and taxa identified in lung samples. The results shown are in line with the findings for the caecum samples. The abundance of the following taxa: phylum-level: Firmicutes, class-level: *Clostridia*, order-level: *Clostridiales* and family-level: *Lachnospiraceae* and *Ruminococcaceae* were positively correlated with increased alpha diversity measures calculated based on Shannon effective and Simpson effective values. In contrast to this finding, the following taxa were negatively associated with the identical

parameters: phylum-level: Proteobacteria, class-level: *Gammaproteobacteria*, order-level: *Enterobacteriales*, family-level: *Enterobacteriaceae*, *Pseudomonadaceae* and on genus-level: *Escherichia/Shigella* and *Pseudomonas*. Overall, in the lung samples the presence of bacteria assigned to the phylum Proteobacteria is negatively correlated with the Shannon effective and Simpson effective values, whereas bacteria assigned to Firmicutes are rather positively correlated.

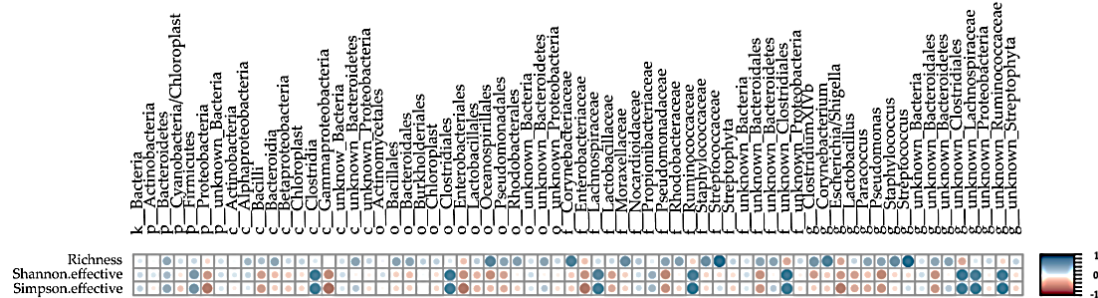


Figure 4.26: Correlation plot of alpha diversity in lung samples.

Correlation plot of alpha diversity measures and taxonomy of lung samples. Dot color states direction of the correlation (blue, positive; red, negative), circle size represents uncorrected p value of correlation. Correlation calculated based on Pearson's coefficient of correlation.

4.2.2.2 Phyloseq

4.2.2.2.1 Top10 assignments to taxonomic hierarchy

Top10 detected taxa on different taxonomic levels: phylum-, family- and genus-level in lung samples are presented in Figure 4.27. The microbial composition visualized based on major community members assigned to phylum-level appears similar in the four different strains for the PBS-treated groups (Figure 4.27 A, lower part). Closer inspection of these barplots have shown that the ratio of Bacteroidetes is higher for the A/J strain and Verrucomicrobia is slightly more abundant in C57BL/6J than in the other strains. The phylum Firmicutes dominated all lung samples irrespectively of the treatment the mice received, besides one striking observation from the data comparing the HDM-treated groups. This comparison has revealed that the ratio of Proteobacteria detected in C3H/HeJ HDM-treated group presents the main proportion and the abundance of Firmicutes and Proteobacteria was virtually reversed for the C3H/HeJ HDM-treated group. This is an interesting outcome and an indication that either the disease or the treatment has provoked this change in the lung microbial composition. A similar trend could be observed for the C57BL/6J for which the proportions of Firmicutes and Proteobacteria converge in the HDM-treated group and

show almost the same abundance. Specifically, the enhancement of the phylum Proteobacteria in all mice receiving the “asthma-inducing” treatment was characteristic. Therefore, it can be summarized that the phyla Firmicutes, Bacteroidetes are decreased, whereas the proportion of Proteobacteria, Actinobacteria and Cyanobacteria/Chloroplast are increased comparing the lung microbiome of the HDM vs. PBS treatment group. The most relevant changes within the phylum Proteobacteria in the HDM-treated C3H/HeJ group can be linked to an increase of the genus *Escherichia/Shigella*, belonging to the family *Enterobacteriaceae* and the decrease within the phylum Firmicutes which was mainly induced by a lower abundance of the families *Lachnospiraceae* and to a lower extent by *Ruminococcaceae*. Additionally, the presence of bacteria assigned to the order *Clostridiales* were reduced in the C3H/HeJ HDM-treated group. Furthermore, the proportion of the genus *Lactobacillus* was detected to be increased in the HDM-treated group of the A/J strain, in contrast to the respective PBS-treated group (Figure 4.27 C).

In summary, these results show the most pronounced changes for the composition of lung microbiome for the C3H/HeJ strain associated with the treatment they received. This treatment related effect, which was exclusively observed for the C3H/HeJ strain was previously described by significant differences of beta diversity comparing the two treatment groups. Overall, the results indicate that the asthma group’s lung microbiome is associated with a higher proportion of Proteobacteria and decreased abundance of Firmicutes.

Following negative controls were included during the sample processing: includes NEC/ Trizol/ NRNA/ NRT control samples. In addition, two mock community samples were isolated and one mock community DNA standard included for library preparation. Single controls included throughout the processing of the lung samples revealed high read numbers and contaminations which were not all removed by rarefying to 10,000 reads. The eight bacteria contained in the mock community were detected accordingly by the performed analysis for the three individual samples included (Figure 4.28 A).

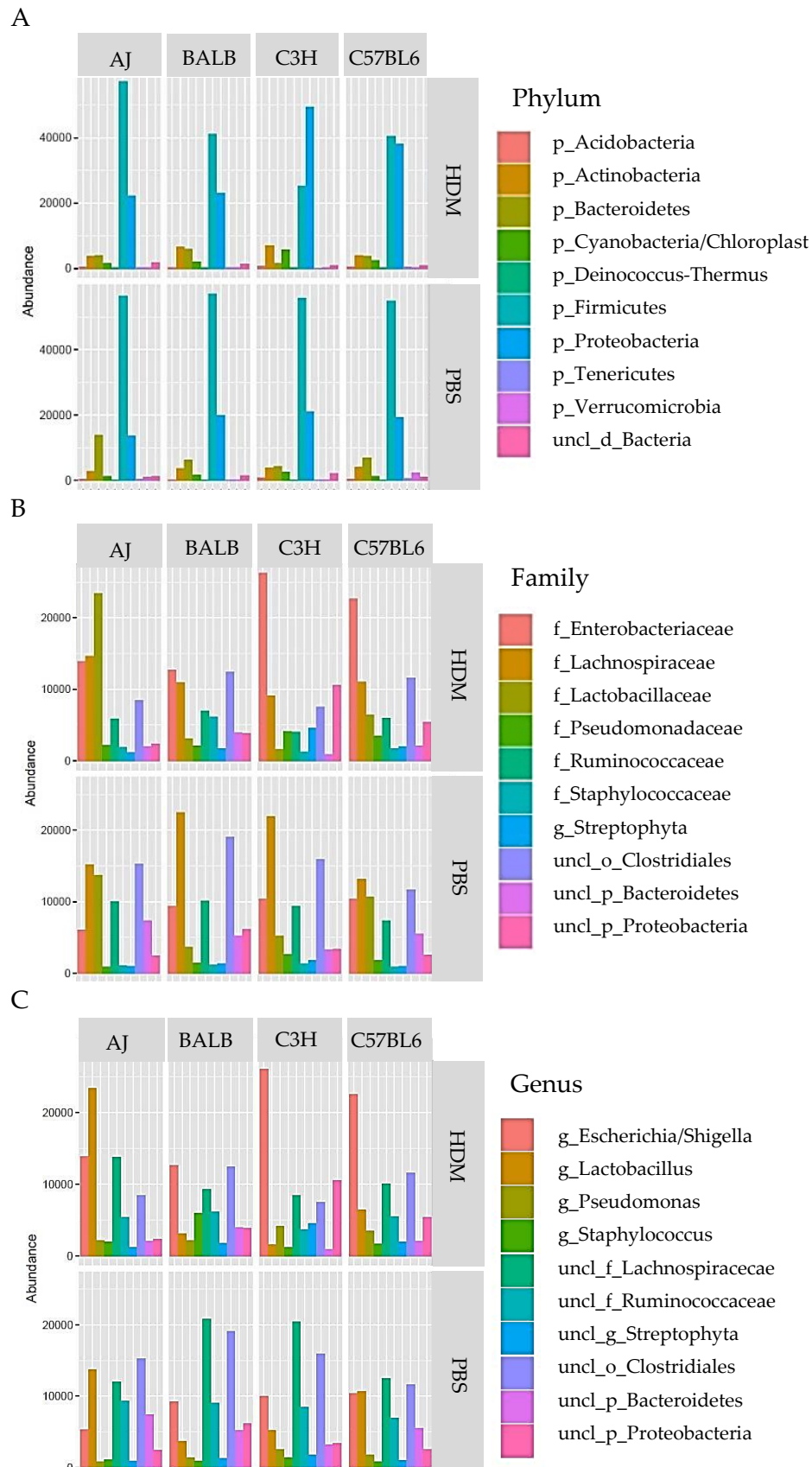


Figure 4.27: Top10 detected Taxonomy in lung samples

A: Phylum-level, B: Family-level; C: Genus-level.

n=9 animals per group; generated using Phyloseq in R.

The assignment was in line with the product specification of the ZymoBIOMICS™ Microbial Community Standard. The major contamination detected in the mock community samples without rarefying (exclusion of samples <10,000 reads) was the genus *Methylobacterium* (Figure 4.28 A). This contamination has been identified among all controls. After rarefying, *Acinetobacter* was identified among the Top10 genera in the controls, this can be related to the contamination of the NEC showing a high abundance of *Acinetobacter* (Figure 4.28 B).

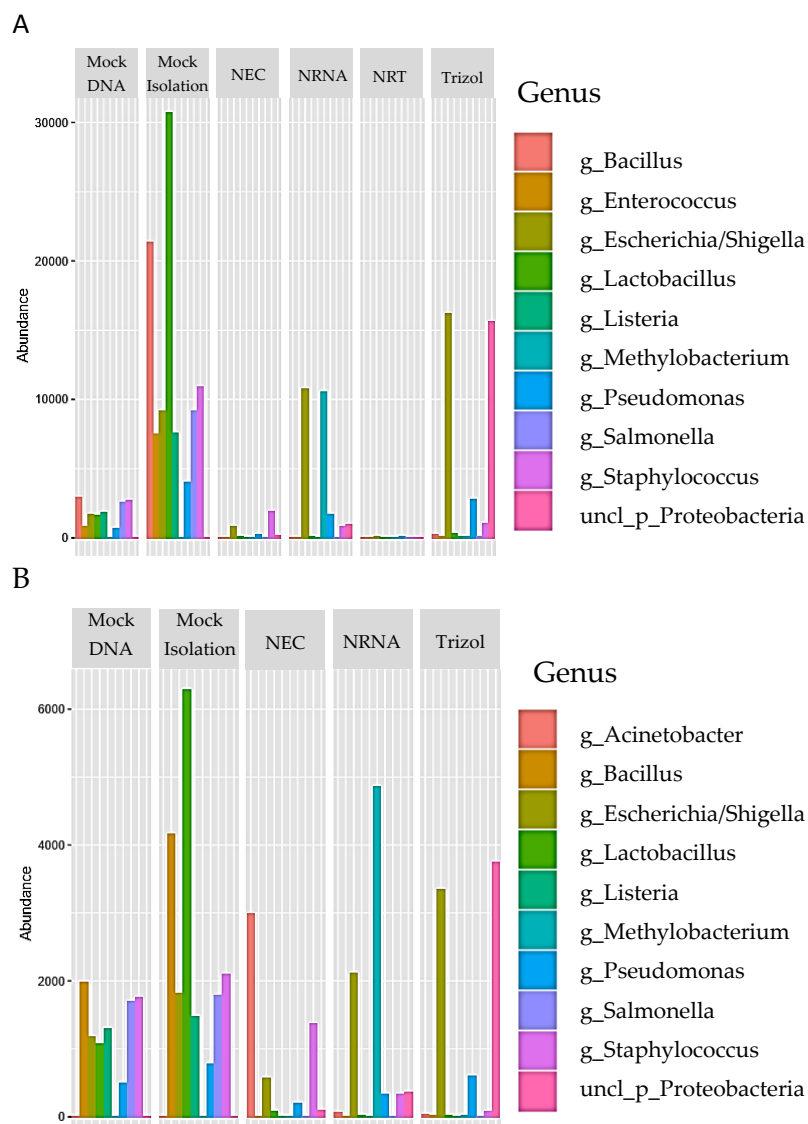


Figure 4.28: Top10 detected Genera in different subgroups of control lung samples.

A. Raw reads without normalization B. Post normalization to 10,000 reads per samples.

(Mock DNA=Mock community DNA used for dual-index amplicon PCR ($n=1$), Mock Isolation=Mock community isolated starting from Fastprep step onwards ($n=2$); NEC ($n=1$); NRNA ($n=3$); NRT ($n=5$); Trizol=Trizol extraction control, post Fastprep isolation ($n=3$)). Generated using Phyloseq in R.

The NRT controls showed almost no contamination with <250 reads in all controls (Figure 4.28 A). Highest contaminations were detected in the NEC, one of the NRNA

control and one Trizol control. Among the identified Top10 genera in these contaminated controls were *Escherichia/Shigella*, *Staphylococcus*, *Methylobacterium*, *Pseudomonas*, *Actinobacter* and unclassified Proteobacteria (Figure 4.28).

The analysis of the lung and gut microbiomes in four different strains was performed separately for the two organs. This separation was necessary because of differences, mainly the increased amplicon PCR cycle number for the lung samples, during the library preparation. For the caecum microbiome the OTU number was identified to be in the range of 150 to 350 identified OTUs. Alpha diversity was measured to be significantly lower for the sequencing controls than for the RNA samples isolated from the mice. These results applied when calculations were done according to the sample type. For the beta diversity measure no statistical relevant difference was observed among all strains and treatment groups. Also, here sequencing controls clustered differently based on the beta diversity values compared to caecum samples of the strains. Contaminations were only detected in very low ratios and the mock community was assigned correctly. Approximately 90% of the Top10 detected phyla were assigned to the Firmicutes, followed by Bacteroidetes as the second most common phyla. The remaining eight phyla (Proteobacteria, Acidobacteria, Actinobacteria, Cyanobacteria/Chloroplast, Deinococcus_Thermus, Tenericutes, Verrucomicrobia) were detected in much lower ratios.

Lung microbiome samples showed an overall sufficient sequencing depth, with 150 to 450 OTUs detected per sample, as most reached a plateau. The range for the number of detected OTUs was slightly increased compared to the caecum samples. Part of the explanation for this might be that due to the increased number of amplification cycles rare OTUs and artefacts are more likely to be detected as a sequence. Three of the negative controls which were processed in parallel with the lung samples revealed *Methylobacterium*, *Acinetobacter*, *Escherichia/Shigella*, *Pseudomonas* and *Staphylococcus* as the main contaminations. For alpha diversity a similar trend as in the caecum samples could be observed. These values have shown a slight increase in PBS-treated compared to the HDM-treated animals in the same strain. Based on the generalized UniFrac distance all isolated lung RNA sample of the mice vs. different sequencing controls vs. the mock community were clustered significantly different. The most

striking observation emerging from these data is that the lung microbiomes of the PBS- vs. the HDM-treated group of the C3H/HeJ strain form significantly different clusters based on their beta diversity measures, as presented in Figure 4.25 C. This finding demonstrates an effect of the intranasal treatment on the microbial composition of the lung. The beta diversity changes in response to the HDM treatment. Correlation plots have shown that the Shannon as well as the Simpson effective values, both measuring the alpha diversity, are positively associated with the ratio of Firmicutes and inversely with the Proteobacteria ratio. The barplots of Top10 identified Taxa revealed that for the HDM-treated group the number of Firmicutes and Bacteroidetes decreased, whereas the number of Proteobacteria and Actinobacteria was more abundant after the induction of the “asthmatic” phenotype. By taking the taxonomy in the barplots into consideration and linking it to our previous observation, which revealed significant differences in beta diversity measures for the C3H/HeJ strain in treatment dependence, it may be presumed to be caused by an increase in Proteobacteria (most abundant *Escherichia/Shigella*) and the decline of Firmicutes (probably mostly belonging to *Lachnospiraceae* and *Ruminococcaceae* family).

Overall, it can be summarized that the most abundant phyla detected in all strains among different treatment groups were different for the two organs (caecum vs. lung). Firstly, in all caecum samples Firmicutes was the major phyla detected followed by Bacteroidetes. Effects of the different treatments (HDM vs. PBS) on the microbial composition were not found. This holds at least true for the assignment at the phylum and family level. Secondly, the composition of lung microbiomes at baseline harbored other abundant phyla besides Firmicutes. For the mice which received the PBS treatment the microbial composition was dominated the phyla Firmicutes, and further the lungs were colonized with Proteobacteria and Bacteroidetes. Except for the A/J and C57BL/6J PBS groups no differences were detected among strains. Overall, it can be concluded that the lung microbiome of mice treated with HDM showed an increase of the phyla Proteobacteria. Significant differences in response to the HDM treatment were only observed for the C3H/HeJ strain. This calculation was based on the beta diversity measures, and most likely can be linked to the increase of bacteria belonging to the Proteobacteria phyla.

5 Discussion

The present thesis aimed to obtain insight into the interplay of host genetics, and potential changes of the gut and lung microbial composition and the response to allergens. To this end, asthma was experimentally induced in A/J, BALB/cJ, C57BL/6J and C3H/HeJ mice by intranasal HDM application. The asthma phenotypes were evaluated, and lung and gut microbiomes were sequenced. At the time of writing this dissertation, no data were found on the association of different murine asthma phenotypes and the microbial colonization in treated vs. control groups.

5.1 Characterization of asthma phenotypes

Asthma phenotypes are highly variable in humans and are not fully reproduced in animal models. So far, most experimental asthma models reflect allergic asthma. A common protocol is the ovalbumin (OVA) model in which mice are injected intraperitoneally with OVA and an adjuvant, followed by exposure to OVA via the airways¹⁵⁵⁻¹⁵⁹. However, as both the sensitization route and the allergen source do not reflect the human situation, protocols with inhalant allergens that are more relevant for humans, such as *Aspergillus fumigatus*¹⁶⁰, cockroach antigens¹⁶¹ and ragweed extracts¹⁶² as well as HDM have been developed. The latter is widely applied as it is a naturally occurring inhalant allergen source against which a majority of asthma patients is sensitized¹⁶³⁻¹⁶⁵. For these reasons HDM was selected for the present work.

To analyze how genetics influence asthma development, all animal strains were treated identically with HDM for three weeks. This experimental protocol has been established previously in the frame of a doctoral thesis of the same group in BALB/c mice¹⁶⁶ and induces a rather mild acute asthma. This mild phenotype was chosen as the induction of stronger inflammatory responses and airway hyperreactivity might override the influence of the genetic backgrounds. In fact, different phenotypes were visible in the four strains and allowed to characterize distinct asthma phenotypes, ranging from BALB/cJ as low-eosinophilic, Th2-low over an Th17-high plus IL-1 β expressing phenotype with intermediate severity in C57BL/6J to a severe mainly eosinophilic, Th2-dominated phenotype with pronounced goblet cell hyperplasia in A/J and C3H/HeJ.

The selection of the four different mouse strains has been made based on a previous study in which the identical four strains were used¹⁶⁷. In this publication mice were treated according to two different schemes. In the first protocol, mice were immunized three and one week prior to the challenge with 10 µg OVA plus Alum by two i.p. injections. Subsequently, the challenge was performed five times a week over a duration of four weeks with an OVA aerosol, analyses of mice were performed weekly starting before the first challenge. The highest absolute number of eosinophils was observed in C3H/HeJ and A/J, it peaked at week one and decreased constantly after this time point. BALB/cJ reached lower overall levels but peaked in week two and the decline of eosinophils was slower, similar findings could be observed in C57BL/6J except that eosinophil levels were comparable in week one and two and declined after this.

In the second model mice of the same strains were treated intranasally with OVA for three days per week for up to 12 weeks. A/J showed clearly the strongest increase in eosinophil numbers in week four, eight and 12, beyond that A/J was the only strain developing an AHR. Both the eosinophilic inflammation as well as the AHR were persistent over the period of 12 weeks in A/J but not in the remaining three strains. Interestingly, eosinophil numbers in the BAL of C3H/HeJ were very low, even though the IgE reached rather high levels. The detection of high IgE in serum of C3H/HeJ is in line with increased levels detected in our HDM model. However, in our model high IgE levels were further accompanied by a strong increase of inflammatory cells in the BAL, mainly caused by eosinophils. Altogether Shinagawa et al. could show that major strain-dependent differences exist applying the identical treatment in the four strains. The second treatment scheme used in this study, which is an exclusively intranasal treatment has been proven to be more sufficient to avoid tolerance development. Consequently, the response to the treatment does not only vary based on the selected mouse strain but further the applied treatment scheme, even though same allergen is administered, widely affects the disease persistence and severity. In addition to variance in immunological responses, also the difference in the structure of the respiratory system in the strains can play a role in the manifestations/characteristics of the disease¹⁶⁸. Reinhard et al. measured lung function of untreated animals in commonly used laboratory inbred strains¹⁶⁹. Among the strains studied were also the

strains of the present thesis. Their results confirm the proposed hypothesis that the heritable genetic traits impact the function of the lungs. By measuring the total lung capacity, C3H/HeJ was identified to possess a significant larger lung size compared to the A/J and C57BL/6J strain, this result is similarly reflected in the present study in which the IC was measured. Within the frame of the current thesis the baseline compliance values were measured in the PBS-treated control groups and revealed that C3H/HeJ has significantly higher values than the remaining three strains. These findings broadly support the results of Reinhard et alii's observations, disregarding the values for BALB/cJ¹⁶⁹.

Of note, C57BL/6J mice developed significantly higher levels of IL-17A in BALF than the other three strains and further IL-1 β levels were increased in contrast to the low eosinophilic BALB/cJ strain. The association of IL-1 β with IL-17A has been reported in a previous study in C57BL/6, which demonstrated that elevated IL-1 β concentrations induce an increase of IL-17A cytokines¹⁷⁰. The current study found that only the C57BL/6J strain developed an AHR. AHR is generally defined by two significantly increased values for airway resistance compared to PBS controls. Surprisingly, the identification of an AHR for C57BL/6J only and not the A/J strain is contradictory to findings of previous studies, describing A/J to develop very pronounced changes in lung function and being characterized as a hyperresponsive strain both under naïve and antigen-induced conditions¹⁷¹⁻¹⁷³. Using acetylcholine as a reagent to examine the contraction of the smooth muscle cells in response to the provocation revealed strong differences between the A/J and C3H/HeJ strain, explained by recessive inheritance of one gene responsible for the airway response. Defining the A/J strain as hyperreactive and the C3H/HeJ strain as hyporeactive, these findings are conflicting with our observations as due to the intrastrain variations no significant differences in the airway resistance could be identified¹⁷¹. The dissociation of AHR and other inflammatory characteristics characterizing asthma has not only been shown in mouse model but humans as well¹⁷⁴. Another study demonstrated that five HDM instillations intranasally are insufficient to induce AHR in BALB/cJ but requires up to ten instillations. This could explain why no robust response was seen in the present work since the treatment protocol was much shorter¹⁷⁵.

In the remaining three strains an increase in airway resistance post treatment can be noted as a trend, but it did not reach statistical significance and was not sufficient to define an AHR.

Multiple reports investigated “asthma” phenotypes in murine models and measured the lung function without detecting an AHR^{152,176,177} or completely neglected the measurement^{178,179}. Mack et al. were interested in addressing the perimenopausal phenotype in C57BL/6 female mice, they were able to observe a 3-fold increase in inflammatory cells in the nine months compared to the three months old mice and this finding was further accompanied by an increased neutrophilia, reflecting the human situation of perimenopausal women being at higher risk to develop a neutrophilia driven phenotype of asthma¹⁷⁷. Applying an intranasal HDM administration over two weeks did not lead to an AHR (based on central airway resistance) in the HDM-treated group compared to same aged PBS-treated mice, but they were able to identify that there are significant differences for all recorded lung parameters based on the age, suggesting an age-related decline¹⁷⁷. Different intranasal HDM-treatment protocols (over two, four and eight weeks) with either 10 µg or 25 µg of HDM were used in Woo et alii’s investigation and only for the four-week HDM application scheme with 25 µg an AHR, showing two or more significantly increased values of the total respiratory resistance compared to control was detected¹⁷⁶. Other reports on the variations in asthma phenotypes did not assess the lung function during their experimental set up. One study interested in the sex-specific effect in a HDM-model¹⁸⁰ found that females develop a more pronounced phenotype with higher HDM-spec. IgE levels, eosinophils in the BAL and effector T cells¹⁸⁰ than males but no lung function has been measured, same holds true for a recent study characterizing different phenotypic manifestation in BALB/c mice, a more detailed description will be given in the following section¹⁷⁹. Further another group could also not observe an AHR in a BALB/c mouse model using a slightly weaker HDM model than in the present thesis¹⁵². In BALB/cj mice relative numbers of eosinophils in the BAL were lower than expected. It is generally assumed that BALB/c are characterized by a high eosinophilia after allergen exposure. However, this observation is only true for OVA-models^{181–183}, while lower eosinophils in BALB/c mice have been described in HDM-models^{180,184}

one of which used 25 µg HDM (20 µg in our protocol) applying the same whole body HDM extract from Greer as in this thesis¹⁸⁰.

In the present work, C3H/HeJ displayed the strongest Th2-prone asthma phenotype, characterized by high numbers of total cells and eosinophils in BAL as well as increased serum IgE levels. In OVA-models low doses of lipopolysaccharide (LPS) are necessary to provoke a Th2-driven inflammation¹⁸⁵. Toll-like receptor 4 (TLR4) is the receptor for LPS mediating signal transduction together with cluster of differentiation (CD) 14 and MD-2¹⁸⁶. C3H/HeJ mice carry a functional genomic mutation in the toll-like receptor 4 (*tlr4*) gene locus which renders them non-responsive to endotoxin, a component of LPS. Therefore, the strong Type-2 response is surprising. In consequence this mutation causes the mice to be resistant to endotoxin, which is a relevant component of the HDM extract and can act as an adjuvant, especially used in OVA models^{187,188}. Nonetheless, our findings that C3H/HeJ despite the *tlr4* mutation are clearly Th2-prone is in line with a recent study using C57BL/6J *tlr4* knockout mice that still had a comparable eosinophil response¹⁸³. Similar to C3H/HeJ, the A/J strain showed a strong Th2-driven phenotype with prominent airway inflammation and increased serum IgE levels compared to PBS. Consistent with other studies, eosinophilic asthma, such as found in the A/J, C57BL/6J and C3H/HeJ strains is accompanied by an increase in mucin and goblet cell hyperplasia and these changes in histological features are associated with increased IL-13 levels in BALF¹⁸⁹.

The animal models developed in this dissertation have several limitations as known factors influencing asthma in humans such as sex differences and age at disease onset age were not considered.

In experimental asthma induction numerous factors can shape the resulting phenotype. These include firstly the allergen or allergen source used, secondly whether an adjuvant is applied or not, and thirdly the treatment scheme^{156,179,190}. The application of HDM in different doses and intervals in the same sex led only to minor differences where only T cell numbers differed significantly¹⁸⁰. This underscores the relevance of using different mouse strains to produce different phenotypes. A study of Draijer et al. used a similar three-week HDM model as in our experimental set-up, the applied dose of HDM being only higher. The number of the eosinophils in the BAL of BALB/c

is nearly consistent with our results in the same strain¹⁸⁰. These results suggest that the applied dose in this particular setting does not lead to major alterations and provokes a rather robust phenotype in the strains. A recent study evaluated the influence of involved immune genes, gender aspect, OVA vs. HDM and the different treatment protocols. On one hand, they observed that all models show a dependency to CD4+ cells and thymic stromal lymphopoietin receptor (TSLPR) and on the other hand they found that sex, TLR-4 receptor and Natural Killer T cells involvement differ pending on the mode of immunization and selected allergen¹⁸³. Deficiency of the TLR4 gene has not led to a distinct change compared to the wild-type (WT) mice neither in OVA nor in HDM models. This finding questions the relevance of the *tlr4* mutation in C3H/HeJ mice with regard to the assessment of the phenotypes in the present thesis. Woo et al. used different periods of HDM treatment (two, four and eight weeks) in a BALB/c mouse model, as well as different doses: the prolongation of the treatment from four to eight weeks allowed to enhance the airway inflammation as well as the collagen deposition, but also four weeks were sufficient for the development of an asthmatic response. However, 25 µg HDM instead of 10 µg five times a week over the time course of four weeks clearly enhanced collagen deposition. Still the four-week model was sufficient to induce the asthmatic characteristics. The number of inflammatory cells, as well as the ratio of neutrophils was much higher than in our experiment, although the same extract has been used¹⁷⁶. Apart from that, an experimental set-up characterizing three different phenotypes in BALB/c (eosinophilic, mixed as well as a neutrophilic phenotype) has been published. This study does not use the frequently applied Greer extract, but standardized Der f (*Dermatophagoides farinae*) and Der p (*Dermatophagoides pteronyssinus*) allergens. To induce distinct phenotypes, three times intraperitoneal sensitization with Alum as an adjuvant was followed by an intranasal challenge over three days and triggered an eosinophilic dominated phenotype. The application of a low vs. a high dose of allergens once per week over four weeks leads to the mixed and the neutrophilic phenotype, respectively¹⁷⁹. The mixed neutrophilic phenotype was reported to be associated with unique genes for IL-5 signaling. However, in the present thesis different strains were utilized and the BALB/cJ did not reveal increased IL-5 levels in BAL compared to the remaining three strains, thus this finding complements the previous study. Despite this, they

found a link of IL-1 β gene expression in lungs being characteristic for the neutrophilic phenotype, this association could not be identified in the present thesis using BALB/cJ mice but it is not a mainly neutrophilic phenotype. In addition, MUC5B was significantly overexpressed in their mixed and neutrophilic phenotypes. The present study detected highest ddCp values of MUC5B not in BALB/cJ but for A/J and C3H/HeJ mice, which both were characterized as strong Th2-eosinophilic responders in the present thesis. Thus, in the present thesis increased MUC5B expression can be more linked to eosinophilic phenotypes than to low eosinophilic phenotypes. Furthermore, Tan et al. reported the neutrophilic phenotype to be accompanied by higher levels of Th17-derived cytokines, whereas the present thesis measured significantly higher levels of IL-17A only in the C57BL/6J mice, which were identified as eosinophilic phenotypes with increased IL-1 β compared to BALB/cJ and IL-17A levels. IL-4 responsive genes were equally represented in the eosinophilic and neutrophilic phenotype in their study¹⁷⁹, in contrast to this the present investigations found BALB/cJ to be the only strain to develop no IL-4 levels in the HDM-treated group¹⁷⁹. BALB/cJ was the strain showing highest neutrophil levels both for the PBS- and the HDM-treated group, especially compared to the predominately eosinophilic C3H/HeJ strain. Further, related to mucus production we could identify the following order of mucus production, based on the CAST analysis: A/J > C3H/HeJ > C57BL/6J > BALB/cJ in this study. This research has shown that different mouse strains in response to the identical treatment protocol develop distinct phenotypes, it can therefore be assumed that the genetic background has an influence on the development of asthma, as severity of different readouts differed widely among the strains. Therefore, it appears that the genetics should not be neglected, although in humans it has not been identified as a major risk factor for asthma development. There against, the colonization with microbes in lung research has gained substantial attention in the past ten years and is still increasing.

5.2 Microbial composition in a murine asthma model

An association of asthma with pulmonary microbial dysbiosis has already been demonstrated in several human studies^{83,120,122,191–194}. Furthermore, an altered microbial composition and the presence of potentially pathogenic bacteria in early childhood

have been linked to an increased risk to develop asthma later in life^{195–197}. Studies utilizing germ-free mice demonstrated that the microbial composition very early in life can affect the development of asthma later in life^{93,198,199}. Thus, the aim of the second part of this thesis was to investigate if the observed asthma phenotypes in the four different mouse strains are linked to differences in the gut and lung microbial composition.

5.2.1 The murine gut and lung microbiome – methodological challenges

5.2.1.1 Collection of biomaterials

In humans, the collection of biomaterial from the lung such as BALF or lung tissues is invasive and this especially reduces the availability of biomaterial from healthy controls²⁰⁰. Studies have used a variety of different sample material as no universal optimal specimen has been defined for asthma. These include bronchial brushes collected from different sides, sputum, saliva, breath condensate, tissue removed during surgery or BALF in humans²⁰¹.

Mouse models on the other hand, allow the collection of the entire lung or defined parts thereof and further enable the analysis of allergen responses in a very controlled environmental setting with regards to e. g. food, water, cage bedding, day-night cycle, SPF conditions although remaining confounders need to be considered²⁰². Notwithstanding, mouse models provide a very good possibility to disentangle the influence of genetic and environmental factors on the microbial composition. This way a highly defined and characteristic lung specimen is available for the analysis of the lung microbial composition²⁰³ for later potential confirmation in human surrogate tissues such as nasal swabs or sputum.

Similar to humans²⁰⁴, the murine microbiome undergoes highly dynamic developmental structural changes during early life that do not stabilize before age of eight weeks^{200,205}. Further, important developmental processes that could influence the microbiome are completed at this age: firstly, the transition to solid food after breastfeeding occurs around day 21 and secondly, the sexual maturity is reached at approximately week six²⁰⁵. For these reasons, animals aged 8 weeks were selected for the experiment to start the treatment with HDM and they were analyzed three weeks

later. The age of approximately three months on the day of scarification has been proposed to represent roughly the age of 20 years in humans^{206,207}.

As outlined above whole lung tissues apart from the post-caval lobe (collected for gene expression analysis) was used to ensure the generation of reliable data²⁰².

The composition of the gut microbiome shows substantial shifts along the intestinal tract²⁰⁸⁻²¹⁰. For the standardized analysis of the gut microbiome, the caecal content was selected here. The murine caecum is much larger compared to humans and mainly responsible for the digestion and vitamin production²¹¹.

5.2.1.2 Microbiome analysis

Regarding the analysis of the structural composition of the microbiome, most of the scientific community working on the lung microbiome selects DNA as a template for 16S rRNA gene sequencing²¹². The DNA is more stable than RNA and can be used directly for further amplification of the targeted region on the bacterial genome for subsequent assignment to a database. Nonetheless, RNA was selected as a template in the present thesis, as RNA detection reflects the recent transcription from the DNA template and thereby it was initially intended to give first insight into the potential functional status of the detected bacteria^{213,214}. But the results obtained in this study did not allow a functional statement.

Currently, there is no standardized research pipeline for sequencing the 16S rRNA gene. During the 16S amplicon sequencing approach various biases can be introduced that need be recognized and minimized as far as possible.

First of all, the lung is a low biomass sample, especially in contrast to the gut microbiome^{215,216}. Accordingly, the risk of contamination with eukaryotic RNA on the one hand and non-related bacteria on the other is very high. Contaminations can be introduced at each single step during sample processing by multiple factors. Firstly, by background contaminations present in RNA/DNA extraction kits, cDNA transcription and PCR kits; secondly, by contaminations introduced by the lab environment through personnel, room air and technical equipment, and thirdly, recently described the well-to-well contamination during the amplification of multiple samples on the

same plate or tubes at the same time. Nevertheless, different studies strongly recommend not to remove detected contaminations bioinformatically from all samples as these identified taxa might be of biological relevance in the other samples, e. g. if they were detected in one NEC but introduced by the contamination by an adjacent sample^{215,217,218}.

In the present study, control samples handled along with caecum samples were almost negative of contamination. Sequencing results from lung samples have to be viewed more critically as a variety of contaminations were identified in the negative controls. Those are most probably caused by the extraction kit and Trizol used. These contaminations were not removed for the analysis for the reason explained above. One major contaminant detected in the present study was assigned to the genus *Escherichia/Shigella*. *Escherichia* belong to the family *Enterobacteriaceae*. *Enterobacteriaceae* are known to be difficult to be assigned specifically on the genus level. This is explained by the evolutionary relationship of *Shigella* and *Escherichia* which has been proposed to be very close. *Shigella* and *Escherichia* are hardly or not at all separated by 16S sequencing²¹⁹. However, a contamination linked to the reagents should be detected in all samples processed with the same routine, thus it would be suggested that the observed contaminations would be distributed evenly among all lung samples and the differences identified should still be considered biologically relevant. Further *Methylobacterium*, *Staphylococcus*, *Pseudomonas* and *Acinetobacter* were identified in lung control samples only, the two last-mentioned have been identified as potential environmental contaminants in human bronchoscopy¹¹⁵. Due to the increased cycle number these contaminations show up and specifically *Methylobacterium* has been known as a major contaminant from soil and water found in extraction kits, especially used for low burden biomass samples such as the lungs²¹⁵.

Additionally, many other factors were considered carefully as they can introduce a sequencing bias: sample collection, transport and storage, extraction method, primer pair selected for the region of the gene²²⁰ and the approach for the bioinformatic data analysis^{215,218,221,222}. In a previous publication the V1-V3 or the V3-V5 region have been found to be sufficient and the V1-V3 region was selected in this thesis²²³. Furthermore, these methods enable the detection of fungi and archaea which are suggested to play

a role in asthma pathogenesis as well²²⁴. Last critical point to mention when working in mouse models is the so-called cage effect which can be a relevant cofounder working on microbiome studies. Mice are coprophagic animals and lung and gut microbial compositions are mainly influenced by co-housed animals^{202,216,225}. To minimize this effect in the present thesis the animals for each treatment group were housed in three different cages. Finally, the lung microbiome research field is a very dynamic one and throughout the last three years a lot of improved methods have been described, which should be considered carefully in future experiments focused on the lung microbiome²²⁶.

5.2.2 Analysis of lung and gut microbiome in healthy mice

Before experimental asthma induction, the gut microbial alpha and beta diversity as well as the abundance of Top10 identified phyla did not differ among the four different strains in the PBS control groups. Firmicutes and Bacteroidetes were the dominant phyla. These findings are in good agreement with most previous studies²²⁷⁻²³⁰ with the exception of one study that reported a lower alpha diversity in C57BL/6J than BALB/c²²⁹. The authors proposed that genetic differences between the two inbred strains influence their ability to produce IgA subsequently such that enhanced IgA production in BALB/c supports a more diverse microbiome²²⁹.

At the family level, gut bacteria were mainly assigned to *Lachnospiraceae*, *Ruminococcaceae*, *Lactobacillaceae* plus *Bacteroidetes* on order level, which is in accordance with previous studies that found most detected genera to be assigned to the order *Clostridiales*, *Bacteroidales* and *Lactobacillales*^{227,229,230}.

Similar to the gut, the lung microbial alpha diversity did not differ among strains. Equally the beta diversity did not differ among PBS groups, except for A/J vs. C57BL/6J (Figure 7.2, page 102, supplement).

At present, no specific "healthy" human lung microbiome has been defined, as the variation among healthy individuals is very high^{98,231,232}. In healthy adults the most abundant phyla are Bacteroides, Firmicutes followed by Proteobacteria, and in some cases Actinobacteria^{83,94,96,107,191}. The composition of the murine lung microbiome has been shown to be comparable to humans based on detected phyla^{200,233}. Thus, the most abundant phyla in mouse lungs have been Proteobacteria, Firmicutes, Actinobacteria,

and Bacteroidetes²⁰⁰. Another study gave similar results but additionally identified Cyanobacteria²²⁷. In the present work, murine lung bacteria were assigned to the phyla Firmicutes, Proteobacteria, Bacteroidetes, Actinobacteria and Cyanobacteria, Verrucomicrobia, Tenericutes, Acidobacteria and Deinococcus-Thermus. The latter four phyla were detected in very low ratios. Thus, the taxonomic assignment to phyla for the lung microbial composition in this thesis is in full agreement with the previous research. Kostric et al. identified *Delftia* and *Rhodococcus* to form an age-independent core microbiome in their study²⁰⁵ investigating the development of the murine lung microbiome. However, these genera were not found in the present work.

The microbiome composition of the gut and lung investigated here differed strongly based on the assigned genera. This difference has already been examined in more detail by Barfod et al.²²⁷.

The observed trend that the median for alpha diversity measures is lower in lungs than in caecum agrees with the results previously found²²⁷. The authors of the same study found a number of observed OTUs with a median of < 150 OTUs which appears much lower compared to the results obtained in this thesis. This low number might be partly explained by the large group of outliers with approximately 500 detected OTUs which they exclude²²⁷. As shown in the rarefaction curve, lung samples contain species within the range of 150 to 400 in this thesis. Initially, it was speculated that the microbial composition among the strains differs for both organs already at baseline. The results clearly demonstrate now that the microbiomes do not differ significantly based on alpha diversity, beta diversity and also taxonomic composition. In summary, this indicates that the differences in asthma phenotypes observed earlier in this thesis cannot be explained by gross differences microbiome a priori.

5.2.3 Analysis of lung and gut microbiome in murine experimental asthma

Comparing the gut microbial composition of the same mouse strain before and after experimental asthma induction did not reveal differences neither on alpha nor on beta diversity level. Taxonomic assignment to the ten most abundant bacteria based on phylum, family and genus levels was not found to be altered in response to the treatment. Arrieta et al. reported earlier that the increased risk of developing asthma later

in life correlates with a reduced abundance of the four genera *Faecalibacterium*, *Lachnospira*, *Veillonella* and *Rothia* during the first 100 days of a newborn²³⁴. The authors confirmed these results further in an germ-free mouse model, by showing that induced airway inflammation could be ameliorated by inoculation with these genera²³⁴. Although the genus composition was altered in the newborns the alpha diversity measures did not differ among the different groups, which is in line with the results of this thesis where the alpha diversity remained unchanged. Further, the different asthmatic phenotypes were not linked to a distinct gut microbiome composition. However, it is emphasized by scientists in the field that the maximum achievable resolution using 16S rRNA sequencing allows the assignment at best to the genus-level. However, many reads can only be assigned to a higher taxonomic level^{201,235}. Many reads within this project were assigned only to high taxonomic levels, which implies that many bacteria remained undetected on the genus level. Kozik et al. stated in a recent review²³⁶ that there is currently only limited evidence for an association between gut dysbiosis and asthma phenotypes in adults. Such an association would be of high clinical interest. To this date first animal studies provided evidence that modulations of the gut microbiome can positively influence allergic airway inflammation (AAI). These changes are suggested to be generally mediated by the presence of a complex commensal flora in the gut^{93,237}. Further, the increase of circulating short chain fatty acids (SCFAs) in the blood by high fiber nutrition or oral supplementation with SCFA²²⁸ and infections with helminths²³⁸ was suggested to decrease the severity of the AAI.

The lung alpha diversity did not differ at baseline and after asthma induction in a given strain and also not among four groups receiving HDM treatments except that there was a slight decline in Simpson effective values in the HDM groups for all strains apart from BALB/cJ. The correlation plot generated for the lung samples found Proteobacteria to be associated with decreased Shannon and Simpson effective diversity, on the other hand taxa assigned to Firmicutes rather lead to an increase in the same diversity measures. The relationship between lung microbial diversity and asthma in human patients is very controversial within the scientific community as recently reviewed by Loverdos et al.¹⁰¹. Previous investigations in humans have reported an increased diversity in asthmatics compared to healthy individuals on alpha

diversity levels^{117,191,192}. This may however not be true for all patients as shown by a study where the airway microbiome of patients with eosinophilic, neutrophilic, paucigranulocytic, or mixed neutrophilic-eosinophilic asthma phenotypes was analyzed. Patients with neutrophilic asthma had a lower alpha diversity as compared to the other groups and in particular to eosinophilic asthma¹²². Finally, others did not identify any differences among different phenotypes of asthma and the healthy individual at all¹²⁰. The causes for these contradictory findings in asthmatics are unclear at present. One potential explanation is the wide variety of parameters applied to judge diversity within a sample such as Shannon diversity index^{191,192,239}, Faith's index¹¹⁷ or multiple parameters^{119,120,122} which might yield different results.

The most marked observation based on the beta diversity measure in this thesis was identified for the C3H/HeJ strain. The experimental asthma induction provoked a significant difference in the beta diversity measures (generalized UniFrac distance) comparing the whole community structure of the PBS- vs. the HDM-treated group. This was exclusively seen in C3H/HeJ but not in the three remaining strains. On the phyla level, the abundance of Proteobacteria was increased in all of the strains after experimental asthma induction. This change was most pronounced in C3H/HeJ where the ratio of Proteobacteria and Firmicutes was reversed after asthma induction. C57BL/6J also showed an equal abundance of the Firmicutes and Proteobacteria. This finding of an overall increase of Proteobacteria agrees very well with the available scientific evidence that Proteobacteria are increased in asthmatic lungs, both in humans and in mouse models^{83,116,120,121,240}. Nonetheless, the study by Li et al. did not find an increase of Proteobacteria in patients with different asthma severities compared to healthy individuals¹⁰⁹. Others performed a more detailed analysis, and found the severity of asthma to be correlated with a higher presence of family members of *Pseudomonadaceae* and *Enterobacteriaceae*. The dominance of the latter was also confirmed in this thesis¹⁰⁹. Huang et al. identified an increase of the relative abundance of *Enterobacteriaceae* and *Moraxellae* to correlate with number of leucocytes in the sputum¹⁹³. This observation was in line with this study, showing that *Enterobacteriaceae* and its higher abundance observed in HDM-treated groups of A/J, C57BL/6J and C3H/HeJ was associated with higher total cell numbers in the collected BAL. The same holds true for the HDM-treated BALB/cJ group in this thesis as reduced *Enterobacteriaceae* in the

lungs compared to other strains were in line with reduced BAL cells in the lungs¹⁹³. Zhang et al. found *Streptococcus* to be associated with eosinophilia, which however could not be detected in any of the mouse strains¹²⁰. The ratio of *Enterobacteriaceae* increased within the HDM groups and was most strongly found in C3H/HeJ and C57BL/6J and to the lowest extent in BALB/cJ. The genus *Streptophyta* was represented at equal levels in both the PBS and HDM groups, except a slight increase in the HDM-treated C3H/HeJ. This genus belonging to phylum Cyanobacteria has been identified to expand in single asthmatics in one study²³⁹. The strongest increase on genus level can be correlated with the detected *Escherichia/Shigella* and the decrease of *Lachnospiraeceae*. The biological relevance of the detected *Escherichia* is questionable, as it is a likely contaminant and has been the most prominent contamination identified in lung controls.

5.3 Conclusion

In conclusion, to the best of knowledge this is the first study investigating asthma phenotypes in mice of four different genetic backgrounds and further analyzing the corresponding gut and lung microbial composition in response to the identical HDM treatment. This work identified distinct asthma phenotypes in four different mouse strains. The phenotypes could be characterized as followed: BALB/cJ was identified as a relatively mild phenotype (low-eosinophilic, Th2-low); A/J as well as C3H/HeJ developed a more severe (high-eosinophilic, Th2-high) phenotype with pronounced goblet cell hyperplasia. In contrast C57BL/6J was identified as a phenotype with intermediate severity as distinguished by higher IL-17A concentrations in the BAL supernatant compared to all other strains. The analysis of the gut microbial composition was mainly composed of the phyla Firmicutes and Bacteroidetes and did not differ among the four mouse strains. No alterations of the microbial composition in the gut were observed in response to HDM treatment. Aside from the A/J and C57BL/6J, the lung microbial composition in the healthy mice showed no marked variation among the strains. An increase of the phylum Proteobacteria was found in all HDM groups compared to the PBS groups, whereas the microbial composition was altered significantly only for the C3H/HeJ strain in response to HDM treatment. These results indi-

cate that the mouse strains' genetics have an impact on the developing asthma phenotype, whereas the genetics appear to have only a minor impact on the microbial composition in healthy mice. The microbial alterations in the lungs occurred differently in the strains in response to the HDM treatment and thus suggest an involvement of the lung microbiomes that is at least in part strain-dependent. This observation addresses the unmet need to disentangle the influences of genetics and microbial changes during disease development further.

5.4 Future perspective

Due to the very different characteristics the human asthma phenotypes present with, it is considered a very heterogenous disease. Thus, it is very important to develop mouse models that mimic the wide range of asthma phenotypes. Until now, the large variety of human asthma phenotypes is by far not covered by existing mouse models. The development of these models is still ongoing and the resulting phenotypes can be affected by various parameters such as genetic background of mouse strains, allergens, treatment scheme, age of mice, gender, etc.^{178,179,181}. Establishing suitable mouse models will help to investigate especially those phenotypes for which only insufficient treatment options are available. Of course, the mouse as model organism faces limitations and can never resemble the complete human nature, but many characteristic features of inflammatory, structural and physiological pathology can depict parts of the clinical manifestation in humans.

By using different genetic backgrounds of mice in this study, the C57BL/6J strain was found to be a good model for IL-17A dependent mouse models, as this strain represented highest levels of IL-17A in response to the HDM challenge. A/J and C3H/HeJ, on the other hand, represent a Th2-high phenotype accompanied by high IgE levels, strong mucus production and inflammatory cells in the airways. Taking these results into consideration for future experiments will allow to select the strain to target the research question best.

In the past ten years the perspective on the relevance of the lung microbiome changed due to deeper insight into microbial compositions by applying new culture-independent sequencing technologies. Recent reviews have summarized studies finding

the lung microbiome to be affected in asthmatics, as the bacterial diversity and composition was altered in the disease state^{100,101}. Further, there are multiple studies that have investigated microbial changes in different phenotypes in humans^{118–120,236,247,248}. It is assumed that the respiratory homeostasis converts into a state of dysbiosis which can be characterized by the outgrowth of specific disease associated taxa. Disentangling the description of the lung microbiomes structural and functional features, as well as determining the role of single members' function, remains a major challenge.

The results obtained by the analysis of the microbiomes are merely descriptive in this thesis. For deeper investigation of the functional relevance of the detected microbial changes a quantitative approach of the total 16S rRNA, e. g. by qPCRs, should be included to enable not only an estimation of the abundance of single taxa but also their functional roles in health and disease. For distinguishing relevant species or strains further studies should include sequencing approaches with higher taxonomic resolution, e. g. whole genome sequencing or shot gun sequencing^{225,239}. These are useful tools to ensure the certain identification of bacteria, including the detection of known and even finding unknown genes. For mechanistic studies the application of germ-free mice models will be of great importance. Causal and functional insight can be gained by using genetically identical germ-free mice and potentially knockout germ-free mice to study newly proposed pathways involved in disease pathogenesis. These mice can be colonized with single bacteria (protective vs. pathogenic) with or without a previous colonization with a standardized mock community. Subsequently, the induced asthmatic phenotype can be evaluated and linked to the microbial composition, irrespective of the genetics, as all animals would have an identical background. Additionally, this would allow the investigation of the interaction and communication of single bacteria with each other.

The long-term overarching goal would be to understand the detailed interactions between the microbial composition and the asthma development and severity to enable preventive strategies or therapeutic manipulations of the gut or lung microbiome in the future.

6 Bibliography

1. Global Initiative for Asthma. *Global Strategy for Asthma Management and Prevention* (2019).
2. European Respiratory Society. Adult Asthma. in *The European Lung White Book* 138–147 (2013).
3. European Respiratory Society. Childhood Asthma. in *The European Lung White Book* 126–137 (2013).
4. Asher, M. I. *et al.* Worldwide time trends in the prevalence of symptoms of asthma, allergic rhinoconjunctivitis, and eczema in childhood: ISAAC Phases One and Three repeat multicountry cross-sectional surveys. *Lancet* **368**, 733–743 (2006).
5. Global Asthma Network. *The Global Asthma Report 2018*. (2018).
6. Fuchs, O., Bahmer, T., Rabe, K. F. & von Mutius, E. Asthma transition from childhood into adulthood. *Lancet Respir. Med.* **5**, 224–234 (2017).
7. Fuhlbrigge, A. L., Jackson, B. & Wright, R. J. Gender and asthma. *Immunol Allergy Clin N Am* **22**, 753–789 (2002).
8. The Lancet. A plea to abandon asthma as a disease concept. *Lancet* **368**, 705 (2006).
9. Kuruvilla, M. E., Lee, F. E.-H. & Lee, G. B. Understanding Asthma Phenotypes, Endotypes, and Mechanisms of Disease. *Clin. Rev. Allergy Immunol.* **56**, 219–233 (2019).
10. Wark, P. A. B. & Gibson, P. G. Asthma exacerbations · 3: Pathogenesis. *Thorax* **61**, 909–915 (2006).
11. Singh, A. M. & Busse, W. W. Asthma exacerbations · 2: Aetiology. *Thorax* **61**, 809–816 (2006).
12. Anderson, S. D. How does exercise cause asthma attacks? *Curr. Opin. Allergy Clin. Immunol.* **6**, 37–42 (2006).
13. Pillai, P. *et al.* Allergen-specific IgE is not detectable in the bronchial mucosa of nonatopic asthmatic patients. *J. Allergy Clin. Immunol.* **133**, 1770-1772.e11 (2014).
14. Bel, E. H. Clinical phenotypes of asthma. *Curr. Opin. Pulm. Med.* **10**, 44–50 (2004).

15. Moore, W. C. *et al.* Identification of Asthma Phenotypes Using Cluster Analysis in the Severe Asthma Research Program. *Am. J. Respir. Crit. Care Med.* **181**, 315–323 (2010).
16. Wenzel, S. E. Asthma phenotypes: the evolution from clinical to molecular approaches. *Nat. Med.* **18**, 716–725 (2012).
17. Woodruff, P. G. *et al.* T-helper Type 2–driven Inflammation Defines Major Subphenotypes of Asthma. *Am. J. Respir. Crit. Care Med.* **180**, 388–395 (2009).
18. Braido, F. *et al.* Phenotypes/endotypes-driven treatment in asthma. *Curr. Opin. Allergy Clin. Immunol.* **18**, 184–189 (2018).
19. Miranda, C., Busacker, A., Balzar, S., Trudeau, J. & Wenzel, S. E. Distinguishing severe asthma phenotypes: Role of age at onset and eosinophilic inflammation. *J. Allergy Clin. Immunol.* **113**, 101–108 (2004).
20. Steinke, J. W., Payne, S. C. & Borish, L. Eosinophils and Mast Cells in Aspirin-Exacerbated Respiratory Disease. *Immunol. Allergy Clin. North Am.* **36**, 719–734 (2016).
21. Lumme, A. *et al.* Airway inflammation, bronchial hyperresponsiveness and asthma in elite ice hockey players. *Eur. Respir. J.* **22**, 113–117 (2003).
22. Pham, D. Le, Lee, J. H. & Park, H. S. Aspirin-exacerbated respiratory disease: An update. *Curr. Opin. Pulm. Med.* **23**, 89–96 (2017).
23. Taniguchi, M. *et al.* Aspirin-exacerbated respiratory disease (AERD): Current understanding of AERD. *Allergol. Int.* **68**, 289–295 (2019).
24. Dixon, A. E. *et al.* Effects of obesity and bariatric surgery on airway hyperresponsiveness, asthma control, and inflammation. *J. Allergy Clin. Immunol.* **128**, 508–515.e2 (2011).
25. Thomson, N. C. & Chaudhuri, R. Asthma in smokers: challenges and opportunities. *Curr. Opin. Pulm. Med.* **15**, 39–45 (2009).
26. Amelink, M. *et al.* Three phenotypes of adult-onset asthma. *Allergy* **68**, 674–680 (2013).
27. Shaw, D. E. *et al.* Association Between Neutrophilic Airway Inflammation and Airflow Limitation in Adults With Asthma. *Chest* **132**, 1871–1875 (2007).
28. McKinley, L. *et al.* T H 17 Cells Mediate Steroid-Resistant Airway Inflammation and Airway Hyperresponsiveness in Mice. *J. Immunol.* **181**,

- 4089–4097 (2008).
29. Manni, M. L. *et al.* The complex relationship between inflammation and lung function in severe asthma. *Mucosal Immunol.* **7**, 1186–1198 (2014).
 30. Pavord, I. D., Brightling, C. E., Woltmann, G. & Wardlaw, A. J. Non-eosinophilic corticosteroid unresponsive asthma. *Lancet* **353**, 2213–2214 (1999).
 31. Green, R. H. *et al.* Analysis of induced sputum in adults with asthma: Identification of subgroup with isolated sputum neutrophilia and poor response to inhaled corticosteroids. *Thorax* **57**, 875–879 (2002).
 32. Tliba, O. & Panettieri, R. A. Paucigranulocytic asthma: Uncoupling of airway obstruction from inflammation. *J. Allergy Clin. Immunol.* **143**, 1287–1294 (2019).
 33. Wills-Karp, M. Immunologic Basis of Antigen-Induced Airway Hyperresponsiveness. *Annu. Rev. Immunol.* **17**, 255–281 (1999).
 34. Lopez, A. F. *et al.* RECOMBINANT HUMAN INTERLEUKIN 5 IS A SELECTIVE ACTIVATOR OF HUMAN EOSINOPHIL FUNCTION. *J. Exp. Med.* **167**, 219–224 (1988).
 35. Del Prete, G. *et al.* IL-4 IS AN ESSENTIAL FACTOR FOR THE IgE SYNTHESIS INDUCED IN VITRO BY HUMAN T CELL CLONES AND THEIR SUPERNATANTS. *J. Immunol.* **140**, 4193–4198 (1988).
 36. Poulsen, L. K. & Hummelshoj, L. Triggers of IgE class switching and allergy development. *Ann. Med.* **39**, 440–456 (2007).
 37. Haldar, P. & Pavord, I. D. Noneosinophilic asthma: A distinct clinical and pathologic phenotype. *J. Allergy Clin. Immunol.* **119**, 1043–1052 (2007).
 38. Choy, D. F. *et al.* TH 2 and TH 17 inflammatory pathways are reciprocally regulated in asthma. *Sci. Transl. Med.* **7**, 301ra129-301ra129 (2015).
 39. Mosmann, T. R., Cherwinski, H., Bond, M. W., Giedlin, M. A. & Coffman, R. L. TWO TYPES OF MURINE HELPER T CELL CLONE I. Definition According to Profiles of Lymphokine Activities and Secreted Proteins. *J. Immunol.* **136**, 2348–2357 (1986).
 40. Mosmann, T. R. & Coffman, R. L. TH1 AND TH2 CELLS: Different Patterns of Lymphokine Secretion Lead to Different Functional Properties. *Annu. Rev.*

- Immunol.* **7**, 145–173 (1989).
41. Glimcher, L. H. & Murphy, K. M. Lineage commitment in the immune system: The T helper lymphocyte grows up. *Genes Dev.* **14**, 1693–1711 (2000).
 42. Cazzola, M. & Polosa, R. Anti-TNF- α and Th1 cytokine-directed therapies for the treatment of asthma. *Curr. Opin. Allergy Clin. Immunol.* **6**, 43–50 (2006).
 43. Ouyang, W., Kolls, J. K. & Zheng, Y. The Biological Functions of T Helper 17 Cell Effector Cytokines in Inflammation. *Immunity* **28**, 454–467 (2008).
 44. Brightling, C. E. *et al.* MAST-CELL INFILTRATION OF AIRWAY SMOOTH MUSCLE IN ASTHMA. *N. Engl. J. Med.* **346**, 1699–1705 (2002).
 45. Carroll, N., Elliot, J., Morton, A. & James, A. The Structure of Large and Small Airways in Nonfatal and Fatal Asthma. *Am. Rev. Respir. Dis.* **147**, 405–410 (1993).
 46. Aikawa, T., Shimura, S., Sasaki, H., Ebina, M. & Takishima, T. Marked Goblet Cell Hyperplasia with Mucus Accumulation in the Airways of Patients Who Died of Severe Acute Asthma Attack. *Chest* **101**, 916–921 (1992).
 47. Ordoñez, C. L. *et al.* Mild and Moderate Asthma Is Associated with Airway Goblet Cell Hyperplasia and Abnormalities in Mucin Gene Expression. *Am. J. Respir. Crit. Care Med.* **163**, 517–523 (2001).
 48. Holgate, S. T. *et al.* Invited lecture: Activation of the epithelial mesenchymal trophic unit in the pathogenesis of asthma. *Int. Arch. Allergy Immunol.* **124**, 253–258 (2001).
 49. Thomson, R. J., Bramley, A. M. & Schellenberg, R. R. Airway muscle stereology: Implications for increased shortening in asthma. *Am. J. Respir. Crit. Care Med.* **154**, 749–757 (1996).
 50. Little, S. A. *et al.* High resolution computed tomographic assessment of airway wall thickness in chronic asthma: reproducibility and relationship with lung function and severity. *Thorax* **57**, 247–253 (2002).
 51. Martinez, F. D. & Holt, P. G. Role of microbial burden in aetiology of allergy and asthma. *Lancet* **354**, 12–15 (1999).
 52. Von Mutius, E. The microbial environment and its influence on asthma prevention in early life. *J. Allergy Clin. Immunol.* **137**, 680–689 (2016).
 53. Ng, S. P. & Zelikoff, J. T. Smoking during pregnancy: Subsequent effects on

- offspring immune competence and disease vulnerability in later life. *Reprod. Toxicol.* **23**, 428–437 (2007).
54. Xu, B., Pekkanen, J., Hartikainen, A. L. & Järvelin, M. R. Caesarean section and risk of asthma and allergy in adulthood. *J. Allergy Clin. Immunol.* **107**, 732–733 (2001).
55. Lambert, K. A. *et al.* Residential greenness and allergic respiratory diseases in children and adolescents – A systematic review and meta-analysis. *Environ. Res.* **159**, 212–221 (2017).
56. Ball, T. M. *et al.* SIBLINGS, DAY-CARE ATTENDANCE, AND THE RISK OF ASTHMA AND WHEEZING DURING CHILDHOOD T. *N. Engl. J. Med.* **343**, 538–543 (2000).
57. Kull, I., Almqvist, C., Lilja, G., Pershagen, G. & Wickman, M. Breast-feeding reduces the risk of asthma during the first 4 years of life. *J. Allergy Clin. Immunol.* **114**, 755–760 (2004).
58. Almqvist, C. *et al.* Direct and indirect exposure to pets - risk of sensitization and asthma at 4 years in a birth cohort. *Clin. Exp. Allergy* **33**, 1190–1197 (2003).
59. Moffatt, M. F. *et al.* A Large-Scale, Consortium-Based Genomewide Association Study of Asthma. *N. Engl. J. Med.* **363**, 1211–1221 (2010).
60. Ramasamy, A. *et al.* Genome-Wide Association Studies of Asthma in Population-Based Cohorts Confirm Known and Suggested Loci and Identify an Additional Association near HLA. *PLoS One* **7**, e44008 (2012).
61. Moffatt, M. F. *et al.* Genetic variants regulating ORMDL3 expression contribute to the risk of childhood asthma. *Nature* **448**, 470–473 (2007).
62. Hirota, T. *et al.* Genetic polymorphism regulating ORM1-like 3 (*Saccharomyces cerevisiae*) expression is associated with childhood atopic asthma in a Japanese population. *J. Allergy Clin. Immunol.* **121**, 769–770 (2008).
63. Halapi, E. *et al.* A sequence variant on 17q21 is associated with age at onset and severity of asthma. *Eur. J. Hum. Genet.* **18**, 902–908 (2010).
64. Ferreira, M. A. R. *et al.* Association between ORMDL3, IL1RL1 and a deletion on chromosome 17q21 with asthma risk in Australia. *Eur. J. Hum. Genet.* **19**, 458–464 (2011).
65. Berlivet, S. *et al.* Interaction between genetic and epigenetic variation defines

- gene expression patterns at the asthma-associated locus 17q12-q21 in lymphoblastoid cell lines. *Hum. Genet.* **131**, 1161–1171 (2012).
66. Toncheva, A. A. *et al.* Childhood asthma is associated with mutations and gene expression differences of ORMDL genes that can interact. *Allergy* **70**, 1288–1299 (2015).
67. Wu, H. *et al.* Genetic variation in ORM1-like 3 (ORMDL3) and gasdermin-like (GSDML) and childhood asthma. *Allergy* **64**, 629–635 (2009).
68. Meyers, D. A. *et al.* Genome screen for asthma and bronchial hyperresponsiveness: Interactions with passive smoke exposure. *J. Allergy Clin. Immunol.* **115**, 1169–1175 (2005).
69. Bouzigon, E. *et al.* Effect of 17q21 Variants and Smoking Exposure in Early-Onset Asthma. *N. Engl. J. Med.* **359**, 1985–1994 (2008).
70. Loss, G. J. *et al.* The Early Development of Wheeze Environmental Determinants and Genetic Susceptibility at 17q21. *Am. J. Respir. Crit. Care Med.* **193**, 889–897 (2016).
71. Eder, W. *et al.* Toll-like receptor 2 as a major gene for asthma in children of European farmers. *J. Allergy Clin. Immunol.* **113**, 482–488 (2004).
72. Viinanen, A. *et al.* The protective effect of rural living against atopy in Mongolia. *Allergy Eur. J. Allergy Clin. Immunol.* **62**, 272–280 (2007).
73. Sozańska, B., Błaszczyk, M., Pearce, N. & Cullinan, P. Atopy and allergic respiratory disease in rural Poland before and after accession to the European Union. *J. Allergy Clin. Immunol.* **133**, 1347–1353 (2014).
74. Stein, M. M. *et al.* Innate Immunity and Asthma Risk in Amish and Hutterite Farm Children. *N. Engl. J. Med.* **375**, 411–421 (2016).
75. Kilpeläinen, M., Terho, E. O., Helenius, H. & Koskenvuo, M. Farm environment in childhood prevents the development of allergies. *Clin. Exp. Allergy* **30**, 201–208 (2000).
76. Gill, S. R. *et al.* Metagenomic Analysis of the Human Distal Gut Microbiome. *Science* **312**, 1355–1359 (2006).
77. Turnbaugh, P. J. *et al.* The Human Microbiome Project. *Nature* **449**, 804–810 (2007).
78. Gao, Z., Tseng, C. -h., Pei, Z. & Blaser, M. J. Molecular analysis of human

- forearm superficial skin bacterial biota. *Proc. Natl. Acad. Sci.* **104**, 2927–2932 (2007).
79. Aas, J. a, Paster, B. J., Stokes, L. N., Olsen, I. & Dewhirst, F. E. Defining the Normal Bacterial Flora of the Oral Cavity. *J. Clin. Microbiol.* **43**, 5721–5732 (2005).
80. Bik, E. M. *et al.* Molecular analysis of the bacterial microbiota in the human stomach. *Proc. Natl. Acad. Sci.* **103**, 732–737 (2006).
81. Zhou, X. *et al.* Characterization of vaginal microbial communities in adult healthy women using cultivation-independent methods. *Microbiology* **150**, 2565–2573 (2004).
82. Eckburg, P. B. *et al.* Diversity of the human intestinal microbial flora. *Science* **308**, 1635–1638 (2005).
83. Hilty, M. *et al.* Disordered Microbial Communities in Asthmatic Airways. *PLoS One* **5**, e8578 (2010).
84. Woese, C. R. & Fox, G. E. Phylogenetic structure of the prokaryotic domain: The primary kingdoms. *Proc. Natl. Acad. Sci.* **74**, 5088–5090 (1977).
85. Fox, G. *et al.* The phylogeny of prokaryotes. *Science* **209**, 457–463 (1980).
86. Olsen, G. J., Lane, D. J., Giovannoni, S. J., Pace, N. R. & Stahl, D. A. MICROBIAL ECOLOGY AND EVOLUTION: A RIBOSOMAL RNA APPROACH. *Annu. Rev. Microbiol.* **40**, 337–365 (1986).
87. Lane, D. J. *et al.* Rapid determination of 16S ribosomal RNA sequences for phylogenetic analyses. *Proc. Natl. Acad. Sci.* **82**, 6955–6959 (1985).
88. Voelkerding, K. V., Dames, S. A. & Durtschi, J. D. Next-Generation Sequencing: From Basic Research to Diagnostics. *Clin. Chem.* **55**, 641–658 (2009).
89. Nyren, P., Pettersson, B. & Uhlen, M. Solid Phase DNA Minisequencing by an Enzymatic Luminometric Inorganic Pyrophosphate Detection Assay. *Anal. Biochem.* **208**, 171–175 (1993).
90. Ronaghi, M., Karamohamed, S., Pettersson, B., Uhlén, M. & Nyren, P. Real-time DNA sequencing using detection of pyrophosphate release. *Anal. Biochem.* **242**, 84–89 (1996).
91. Bentley, D. R. *et al.* Accurate whole human genome sequencing using

- reversible terminator chemistry. *Nature* **456**, 53–59 (2008).
92. Huffnagle, G. B. The Microbiota and Allergies/Asthma. *PLoS Pathog.* **6**, e1000549 (2010).
 93. Herbst, T. *et al.* Dysregulation of Allergic Airway Inflammation in the Absence of Microbial Colonization. *Am. J. Respir. Crit. Care Med.* **184**, 198–205 (2011).
 94. Erb-Downward, J. R. *et al.* Analysis of the Lung Microbiome in the “Healthy” Smoker and in COPD. *PLoS One* **6**, e16384 (2011).
 95. Beck, J. M., Young, V. B. & Huffnagle, G. B. The microbiome of the lung. *Transl. Res.* **160**, 258–266 (2012).
 96. Dickson, R. P., Erb-Downward, J. R. & Huffnagle, G. B. The role of the bacterial microbiome in lung disease. *Expert Rev. Respir. Med.* **7**, 245–257 (2013).
 97. Chambers, D. C., Gellatly, S. L., Hugenholtz, P. & Hansbro, P. M. JTD special edition ‘Hot Topics in COPD’-The microbiome in COPD. *J. Thorac. Dis.* **6**, 1525–1531 (2014).
 98. Charlson, E. S. *et al.* Topographical Continuity of Bacterial Populations in the Healthy Human Respiratory Tract. *Am. J. Respir. Crit. Care Med.* **184**, 957–963 (2011).
 99. Kuo, C.-H. S. *et al.* T-helper cell type 2 (Th2) and non-Th2 molecular phenotypes of asthma using sputum transcriptomics in U-BIOPRED. *Eur. Respir. J.* **49**, 1602135 (2017).
 100. Ver Heul, A., Planer, J. & Kau, A. L. The Human Microbiota and Asthma. *Clin. Rev. Allergy Immunol.* **57**, 350–363 (2019).
 101. Loverdos, K. *et al.* Lung Microbiome in Asthma: Current Perspectives. *J. Clin. Med.* **8**, 1967 (2019).
 102. Faner, R. *et al.* The microbiome in respiratory medicine: current challenges and future perspectives. *Eur. Respir. J.* **49**, 1602086 (2017).
 103. Budden, K. F. *et al.* Functional effects of the microbiota in chronic respiratory disease. *Lancet Respir. Med.* **7**, 907–920 (2019).
 104. Caverly, L. J., Huang, Y. J. & Sze, M. A. Past, Present, and Future Research on the Lung Microbiome in Inflammatory Airway Disease. *Chest* **156**, 376–382

- (2019).
105. Dickson, R. P. *et al.* Spatial Variation in the Healthy Human Lung Microbiome and the Adapted Island Model of Lung Biogeography. *Ann. Am. Thorac. Soc.* **12**, 821–830 (2015).
 106. Dickson, R. P., Erb-Downward, J. R., Martinez, F. J. & Huffnagle, G. B. The Microbiome and the Respiratory Tract. *Annu. Rev. Physiol.* **78**, 481–504 (2016).
 107. Charlson, E. S. *et al.* Assessing Bacterial Populations in the Lung by Replicate Analysis of Samples from the Upper and Lower Respiratory Tracts. *PLoS One* **7**, e42786 (2012).
 108. Pragman, A. A., Kim, H. B., Reilly, C. S., Wendt, C. & Isaacson, R. E. The Lung Microbiome in Moderate and Severe Chronic Obstructive Pulmonary Disease. *PLoS One* **7**, e47305 (2012).
 109. Li, N. *et al.* Sputum microbiota in severe asthma patients: Relationship to eosinophilic inflammation. *Respir. Med.* **131**, 192–198 (2017).
 110. Fujimura, K. E. & Lynch, S. V. Microbiota in allergy and asthma and the emerging relationship with the gut microbiome. *Cell Host Microbe* **17**, 592–602 (2015).
 111. Ott, S. J. *et al.* Reduction in diversity of the colonic mucosa associated bacterial microflora in patients with active inflammatory bowel disease. *Gut* **53**, 685–693 (2004).
 112. Kamada, N., Seo, S.-U., Chen, G. Y. & Núñez, G. Role of the gut microbiota in immunity and inflammatory disease. *Nat. Rev. Immunol.* **13**, 321–335 (2013).
 113. Lee, S. Y. *et al.* Airway microbiome composition correlates with lung function and arterial stiffness in an age-dependent manner. *PLoS One* **14**, e0225636 (2019).
 114. Dickson, R. P. & Huffnagle, G. B. The Lung Microbiome: New Principles for Respiratory Bacteriology in Health and Disease. *PLOS Pathog.* **11**, e1004923 (2015).
 115. Dickson, R. P. *et al.* Bacterial Topography of the Healthy Human Lower Respiratory Tract. *MBio* **8**, e02287-16 (2017).
 116. Huang, Y. J. & Boushey, H. A. The microbiome in asthma. *J. Allergy Clin. Immunol.* **135**, 25–30 (2015).

117. Durack, J. *et al.* Features of the bronchial bacterial microbiome associated with atopy, asthma, and responsiveness to inhaled corticosteroid treatment. *J. Allergy Clin. Immunol.* **140**, 63–75 (2017).
118. Green, B. J. *et al.* Potentially Pathogenic Airway Bacteria and Neutrophilic Inflammation in Treatment Resistant Severe Asthma. *PLoS One* **9**, e100645 (2014).
119. Simpson, J. L. *et al.* Airway dysbiosis: Haemophilus influenza and Tropheryma in poorly controlled asthma. *Eur. Respir. J.* **47**, 792–800 (2016).
120. Zhang, Q. *et al.* Airway Microbiota in Severe Asthma and Relationship to Asthma Severity and Phenotypes. *PLoS One* **11**, e0152724 (2016).
121. Sverrild, A. *et al.* Eosinophilic airway inflammation in asthmatic patients is associated with an altered airway microbiome. *J. Allergy Clin. Immunol.* **140**, 407-417.e11 (2017).
122. Taylor, S. L. *et al.* Inflammatory phenotypes in patients with severe asthma are associated with distinct airway microbiology. *J. Allergy Clin. Immunol.* **141**, 94-103.e15 (2018).
123. Pawankar, R. Allergic diseases and asthma: a global public health concern and a call to action. *World Allergy Organ. J.* **7**, 12 (2014).
124. Yeatts, K. *et al.* A Brief Targeted Review of Susceptibility Factors, Environmental Exposures, Asthma Incidence, and Recommendations for Future Asthma Incidence Research. *Environ. Health Perspect.* **114**, 634–640 (2006).
125. Dominguez-Bello, M. G. *et al.* Delivery mode shapes the acquisition and structure of the initial microbiota across multiple body habitats in newborns. *Proc. Natl. Acad. Sci.* **107**, 11971–11975 (2010).
126. Tanaka, S. *et al.* Influence of antibiotic exposure in the early postnatal period on the development of intestinal microbiota. *FEMS Immunol. Med. Microbiol.* **56**, 80–87 (2009).
127. Penders, J. *et al.* Quantification of Bifidobacterium spp., Escherichia coli and Clostridium difficile in faecal samples of breast-fed and formula-fed infants by real-time PCR. *FEMS Microbiol. Lett.* **243**, 141–147 (2005).
128. Penders, J. *et al.* Factors Influencing the Composition of the Intestinal

- Microbiota in Early Infancy. *Pediatrics* **118**, 511–521 (2006).
129. Tamburini, S., Shen, N., Wu, H. C. & Clemente, J. C. The microbiome in early life: implications for health outcomes. *Nat. Med.* **22**, 713–722 (2016).
130. Bioinformatics, B. FastQC a quality tool for high throughput sequence data. <https://www.bioinformatics.babraham.ac.uk/projects>
131. R Development Core Team, Vienna, A. R: A language and environment for statistical computing. R Foundation for Statistical Computing. <http://www.R-project.org/> (2014).
132. Oksanen, J. *et al.* vegan: Community Ecology Package - version 2.5. <https://github.com/vegandevs/vegan> (2018).
133. McMurdie, P. J. & Holmes, S. phyloseq: An R Package for Reproducible Interactive Analysis and Graphics of Microbiome Census Data. *PLoS One* **8**, e61217 (2013).
134. Lagkouvardos, I., Fischer, S., Kumar, N. & Clavel, T. Rhea: a transparent and modular R pipeline for microbial profiling based on 16S rRNA gene amplicons. *PeerJ* **5**, e2836 (2017).
135. Cole J.R., Wang, Q., Chai, B. & Tiedje, J. M. The Ribosomal Database Project: sequences and software for high-throughput rRNA analysis. in *Handbook of Molecular Microbial Ecology I: Metagenomics and Complementary Approaches* (J. Wiley & Sons, Inc., 2011).
136. Edgar, R. C. & Flyvbjerg, H. Error filtering, pair assembly and error correction for next-generation sequencing reads. *Bioinformatics* **31**, 3476–3482 (2015).
137. Morgan, E. *et al.* Cytometric Bead Array: A Multiplexed Assay Platform With Applications in Various Areas of Biology. *Clin. Immunol.* **110**, 252–266 (2004).
138. McManus, J. F. A. Histological and Histochemical Uses of Periodic Acid. *Stain Technol.* **23**, 99–108 (1948).
139. HOTCHKISS, R. D. A microchemical reaction resulting in the staining of polysaccharide structures in fixed tissue preparations. *Arch. Biochem.* **16**, 131–141 (1948).
140. Fehrenbach, H., Wagner, C. & Wegmann, M. Airway remodeling in asthma: what really matters. *Cell Tissue Res.* **367**, 551–569 (2017).

141. Bousquet, J. *et al.* Asthma: a disease remodeling the airways. *Allergy* **47**, 3–11 (1992).
142. Burgess, J. K. *et al.* Reduction of Tumstatin in Asthmatic Airways Contributes to Angiogenesis, Inflammation, and Hyperresponsiveness. *Am. J. Respir. Crit. Care Med.* **181**, 106–115 (2010).
143. Wang, Q., Garrity, G. M., Tiedje, J. M. & Cole, J. R. Naive Bayesian Classifier for Rapid Assignment of rRNA Sequences into the New Bacterial Taxonomy. *Appl. Environ. Microbiol.* **73**, 5261–5267 (2007).
144. Edgar, R. C. MUSCLE: Multiple sequence alignment with high accuracy and high throughput. *Nucleic Acids Res.* **32**, 1792–1797 (2004).
145. Callahan, B. J., Sankaran, K., Fukuyama, J. A., McMurdie, P. J. & Holmes, S. P. Bioconductor Workflow for Microbiome Data Analysis: from raw reads to community analyses. *F1000Research* **5**, 1492 (2016).
146. Jost, L. Partitioning Diversity into Independent Alpha and Beta Components. *Ecology* **88**, 2427–2439 (2007).
147. Chen, J. *et al.* Associating microbiome composition with environmental covariates using generalized UniFrac distances. *Bioinformatics* **28**, 2106–2113 (2012).
148. Anderson, M. J. A new method for non-parametric multivariate analysis of variance. *Austral Ecol.* **26**, 32–46 (2001).
149. Benjamini, Y. & Hochberg, Y. Controlling the False Discovery Rate: A Practical and Powerful Approach to Multiple Testing. *Journal of the Royal Statistical Society: Series B (Methodological)* **57**, 289–300 (1995).
150. Reynolds, A. P., Richards, G., de la Iglesia, B. & Rayward-Smith, V. J. Clustering Rules: A Comparison of Partitioning and Hierarchical Clustering Algorithms. *J. Math. Model. Algorithms* **5**, 475–504 (2006).
151. Pearson, K. Determination of the coefficient of correlation. *Science* **30**, 23–25 (1909).
152. Gregory, L. G. *et al.* Overexpression of Smad2 Drives House Dust Mite-mediated Airway Remodeling and Airway Hyperresponsiveness via Activin and IL-25. *Am. J. Respir. Crit. Care Med.* **182**, 143–154 (2010).
153. Lu, M. *et al.* Therapeutic induction of tolerance by IL-10-differentiated

- dendritic cells in a mouse model of house dust mite-asthma*. *Allergy* **66**, 612–620 (2011).
154. The Jackson Laboratory. Available at: <https://www.jax.org/strain>. (Accessed: 16th March 2020)
155. Epstein, M. M. Do Mouse Models of Allergic Asthma Mimic Clinical Disease? *Int. Arch. Allergy Immunol.* **133**, 84–100 (2004).
156. Nials, A. T. & Uddin, S. Mouse models of allergic asthma: acute and chronic allergen challenge. *Dis. Model. Mech.* **1**, 213–220 (2008).
157. Daubeuf, F. & Frossard, N. Acute Asthma Models to Ovalbumin in the Mouse. *Curr. Protoc. Mouse Biol.* **3**, 31–37 (2013).
158. Chapman, D. G., Tully, J. E., Nolin, J. D., Janssen-Heininger, Y. M. & Irvin, C. G. Animal models of allergic airways disease: Where are we and where to next? *J. Cell. Biochem.* **115**, 2055–2064 (2014).
159. Debeuf, N., Haspeslagh, E., Helden, M., Hammad, H. & Lambrecht, B. N. Mouse Models of Asthma. *Curr. Protoc. Mouse Biol.* **6**, 169–184 (2016).
160. Mehlhop, P. D. *et al.* Allergen-induced bronchial hyperreactivity and eosinophilic inflammation occur in the absence of IgE in a mouse model of asthma. *Proc. Natl. Acad. Sci.* **94**, 1344–1349 (1997).
161. Kim, J. *et al.* Eotaxin Represents the Principal Eosinophil Chemoattractant in a Novel Murine Asthma Model Induced by House Dust Containing Cockroach Allergens. *J. Immunol.* **167**, 2808–2815 (2001).
162. Wild, J. S. *et al.* IFN- γ -Inducing Factor (IL-18) Increases Allergic Sensitization, Serum IgE, Th2 Cytokines, and Airway Eosinophilia in a Mouse Model of Allergic Asthma. *J. Immunol.* **164**, 2701–2710 (2000).
163. Nelson, R. P. *et al.* Allergen-specific IgE levels and mite allergen exposure in children with acute asthma first seen in an emergency department and in nonasthmatic control subjects. *J. Allergy Clin. Immunol.* **98**, 258–263 (1996).
164. Lambrecht, B. N. & Hammad, H. The immunology of asthma. *Nat. Immunol.* **16**, 45–56 (2015).
165. Gregory, L. G. & Lloyd, C. M. Orchestrating house dust mite-associated allergy in the lung. *Trends Immunol.* **32**, 402–411 (2011).
166. Götschke, J. Entdeckung eines microRNA-basierten Biomarkers für

- allergisches Asthma. (Ludwig–Maximilians–Universität zu München, 2016).
167. Shinagawa, K. & Kojima, M. Mouse Model of Airway Remodeling: Strain Differences. *Am. J. Respir. Crit. Care Med.* **168**, 959–967 (2003).
168. Namati, J. T. Phenotype characterization of lung structure in inbred mouse strains using multi modal imaging techniques. *PhD (Doctor of Philosophy) thesis* (University of Iowa, 2009). doi:10.17077/etd.tepyrae2
169. Reinhard, C. *et al.* Inbred strain variation in lung function. *Mamm. Genome* **13**, 429–437 (2002).
170. Sutton, C. E. *et al.* Interleukin-1 and IL-23 Induce Innate IL-17 Production from $\gamma\delta$ T Cells, Amplifying Th17 Responses and Autoimmunity. *Immunity* **31**, 331–341 (2009).
171. Levitt, R. C. & Mitzner, W. Expression of airway hyperreactivity to acetylcholine as a simple autosomal recessive trait in mice. *FASEB J.* **2**, 2605–2608 (1988).
172. WILLS-KARP, M. & EWART, S. L. The Genetics of Allergen-Induced Airway Hyperresponsiveness in Mice. *Am. J. Respir. Crit. Care Med.* **156**, S89–S96 (1997).
173. Cozzi, E. *et al.* The naive airway hyperresponsiveness of the A/J mouse is Kit-mediated. *Proc. Natl. Acad. Sci.* **108**, 12787–12792 (2011).
174. Brusasco, V. *et al.* Airway responsiveness to methacholine: effects of deep inhalations and airway inflammation. *J. Appl. Physiol.* **87**, 567–573 (1999).
175. Tully, J. E. *et al.* Epithelial NF- κ B Orchestrates House Dust Mite-Induced Airway Inflammation, Hyperresponsiveness, and Fibrotic Remodeling. *J. Immunol.* **191**, 5811–5821 (2013).
176. Woo, L. N. *et al.* A 4-Week Model of House Dust Mite (HDM) Induced Allergic Airways Inflammation with Airway Remodeling. *Sci. Rep.* **8**, 6925 (2018).
177. Mack, S. *et al.* Age-dependent pulmonary reactivity to house dust mite allergen: a model of adult-onset asthma? *Am. J. Physiol. Cell. Mol. Physiol.* **316**, L757–L763 (2019).
178. Melgert, B. N. *et al.* Macrophages Regulators of Sex Differences in Asthma? *Barbro. Am. J. Respir. Cell Mol. Biol.* **42**, 595–603 (2010).

179. Tan, H.-T. T. *et al.* Tight junction, mucin, and inflammasome-related molecules are differentially expressed in eosinophilic, mixed, and neutrophilic experimental asthma in mice. *Allergy* **74**, 294–307 (2019).
180. Draijer, C., Robbe, P., Boorsma, C. E., Hylkema, M. N. & Melgert, B. N. Characterization of Macrophage Phenotypes in Three Murine Models of House-Dust-Mite-Induced Asthma. *Mediators Inflamm.* **2013**, 632049 (2013).
181. Tomkinson, A. *et al.* A Murine IL-4 Receptor Antagonist That Inhibits IL-4- and IL-13-Induced Responses Prevents Antigen-Induced Airway Eosinophilia and Airway Hyperresponsiveness. *J. Immunol.* **166**, 5792–5800 (2001).
182. McMillan, S. J., Bishop, B., Townsend, M. J., McKenzie, A. N. & Lloyd, C. M. The Absence of Interleukin 9 Does Not Affect the Development of Allergen-induced Pulmonary Inflammation nor Airway Hyperreactivity. *J. Exp. Med.* **195**, 51–57 (2002).
183. Hyde, E. J., Wakelin, K. A., Daniels, N. J., Ghosh, S. & Ronchese, F. Similar immune mechanisms control experimental airway eosinophilia elicited by different allergens and treatment protocols. *BMC Immunol.* **20**, 18 (2019).
184. Li, M. *et al.* TLR4 antagonist suppresses airway remodeling in asthma by inhibiting the T-helper 2 response. *Exp. Ther. Med.* **14**, 2911–2916 (2017).
185. Eisenbarth, S. C. *et al.* Lipopolysaccharide-enhanced, Toll-like Receptor 4–dependent T Helper Cell Type 2 Responses to Inhaled Antigen. *J. Exp. Med.* **196**, 1645–1651 (2002).
186. Jiang, Z. *et al.* CD14 is required for MyD88-independent LPS signaling. *Nat. Immunol.* **6**, 565–570 (2005).
187. Poltorak, A. *et al.* Defective LPS signaling in C3H/HeJ and C57BL/10ScCr mice: mutations in Tlr4 gene. *Science* **282**, 2085–2088 (1998).
188. Hammad, H. *et al.* House dust mite allergen induces asthma via Toll-like receptor 4 triggering of airway structural cells. *Nat. Med.* **15**, 410–416 (2009).
189. Steenwinckel, V. *et al.* IL-9 Promotes IL-13-Dependent Paneth Cell Hyperplasia and Up-Regulation of Innate Immunity Mediators in Intestinal Mucosa. *J. Immunol.* **182**, 4737–4743 (2009).
190. Chang, Y.-S. *et al.* Comparison of Asthma Phenotypes Using Different

- Sensitizing Protocols in Mice. *Korean J. Intern. Med.* **20**, 152–158 (2005).
191. Huang, Y. J. *et al.* Airway microbiota and bronchial hyperresponsiveness in patients with suboptimally controlled asthma. *J. Allergy Clin. Immunol.* **127**, 372–381.e3 (2011).
192. Marri, P. R., Stern, D. A., Wright, A. L., Billheimer, D. & Martinez, F. D. Asthma-associated differences in microbial composition of induced sputum. *J. Allergy Clin. Immunol.* **131**, 346–352.e3 (2013).
193. Huang, Y. J. *et al.* The airway microbiome in patients with severe asthma: Associations with disease features and severity. *J. Allergy Clin. Immunol.* **136**, 874–884 (2015).
194. Denner, D. R. *et al.* Corticosteroid therapy and airflow obstruction influence the bronchial microbiome, which is distinct from that of bronchoalveolar lavage in asthmatic airways. *J. Allergy Clin. Immunol.* **137**, 1398–1405.e3 (2016).
195. Bisgaard, H. *et al.* Childhood Asthma after Bacterial Colonization of the Airway in Neonates. *N. Engl. J. Med.* **357**, 1487–1495 (2007).
196. De Schutter, I. *et al.* In young children, persistent wheezing is associated with bronchial bacterial infection: a retrospective analysis. *BMC Pediatr.* **12**, 83 (2012).
197. Teo, S. M. *et al.* The Infant Nasopharyngeal Microbiome Impacts Severity of Lower Respiratory Infection and Risk of Asthma Development. *Cell Host Microbe* **17**, 704–715 (2015).
198. Gollwitzer, E. S. *et al.* Lung microbiota promotes tolerance to allergens in neonates via PD-L1. *Nat. Med.* **20**, 642–647 (2014).
199. Remot, A. *et al.* Bacteria isolated from lung modulate asthma susceptibility in mice. *ISME J.* **11**, 1061–1074 (2017).
200. Singh, N., Vats, A., Sharma, A., Arora, A. & Kumar, A. The development of lower respiratory tract microbiome in mice. *Microbiome* **5**, 61 (2017).
201. Carney, S. M. *et al.* Methods in Lung Microbiome Research. *Am. J. Respir. Cell Mol. Biol.* **62**, 283–299 (2020).
202. Dickson, R. P. *et al.* The Lung Microbiota of Healthy Mice Are Highly Variable, Cluster by Environment, and Reflect Variation in Baseline Lung Innate Immunity. *Am. J. Respir. Crit. Care Med.* **198**, 497–508 (2018).

203. Dickson, R. P. & Cox, M. J. Sampling. in *The Lung Microbiome (ERS Monography)* 1–17 (European Respiratory Society, 2019).
204. Stewart, C. J. *et al.* Temporal development of the gut microbiome in early childhood from the TEDDY study. *Nature* **562**, 583–588 (2018).
205. Kostric, M. *et al.* Development of a Stable Lung Microbiome in Healthy Neonatal Mice. *Microb. Ecol.* **75**, 529–542 (2018).
206. Flurkey, K., Curren, J. & Harrison, D. Mouse models in aging research. in *The Mouse in Biomedical Research* 637–672 (Elsevier, 2007).
207. Hagan, C. When are mice considered old? *The Jackson Laboratory* (2017). Available at: <https://www.jax.org/news-and-insights/jax-blog/2017/november/when-are-mice-considered-old>. (Accessed: 28th March 2020)
208. Sekirov, I., Russell, S. L., Antunes, L. C. M. & Finlay, B. B. Gut microbiota in health and disease. *Physiol. Rev.* **90**, 859–904 (2010).
209. Juge, N. Microbial adhesins to gastrointestinal mucus. *Trends Microbiol.* **20**, 30–39 (2012).
210. Dieterich, W., Schink, M. & Zopf, Y. Microbiota in the Gastrointestinal Tract. *Med. Sci.* **6**, 116 (2018).
211. Nguyen, T. L. A., Vieira-Silva, S., Liston, A. & Raes, J. How informative is the mouse for human gut microbiota research? *Dis. Model. Mech.* **8**, 1–16 (2015).
212. Einarsson, G. G. & Boutin, S. Techniques: culture, identification and 16S rRNA gene sequencing. in *The Lung Microbiome (ERS Monography)* 18–34 (European Respiratory Society, 2019).
213. Li, R. *et al.* Comparison of DNA-, PMA-, and RNA-based 16S rRNA Illumina sequencing for detection of live bacteria in water. *Sci. Rep.* **7**, 5752 (2017).
214. Mäki, A., Salmi, P., Mikkonen, A., Kremp, A. & Tirola, M. Sample Preservation, DNA or RNA Extraction and Data Analysis for High-Throughput Phytoplankton Community Sequencing. *Front. Microbiol.* **8**, 1848 (2017).
215. Salter, S. J. *et al.* Reagent and laboratory contamination can critically impact sequence-based microbiome analyses. *BMC Biol.* **12**, 87 (2014).
216. Kim, D. *et al.* Optimizing methods and dodging pitfalls in microbiome

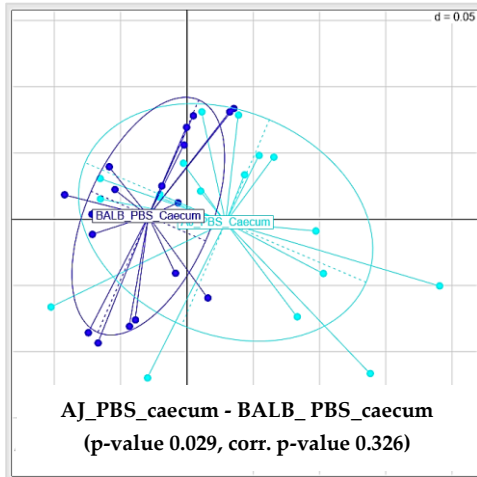
- research. *Microbiome* **5**, 52 (2017).
217. Minich, J. J. *et al.* Quantifying and Understanding Well-to-Well Contamination in Microbiome Research. *mSystems* **4**, 4:e00186-19 (2019).
218. Glassing, A., Dowd, S. E., Galandiuk, S., Davis, B. & Chiodini, R. J. Inherent bacterial DNA contamination of extraction and sequencing reagents may affect interpretation of microbiota in low bacterial biomass samples. *Gut Pathog.* **8**, 24 (2016).
219. Devanga Ragupathi, N. K., Muthuirulandi Sethuvel, D. P., Inbanathan, F. Y. & Veeraraghavan, B. Accurate differentiation of *Escherichia coli* and *Shigella* serogroups: challenges and strategies. *New Microbes New Infect.* **21**, 58–62 (2018).
220. Klindworth, A. *et al.* Evaluation of general 16S ribosomal RNA gene PCR primers for classical and next-generation sequencing-based diversity studies. *Nucleic Acids Res.* **41**, e1 (2013).
221. Knight, R. *et al.* Best practices for analysing microbiomes. *Nat. Rev. Microbiol.* **16**, 410–422 (2018).
222. Schloss, P. D. Evaluating different approaches that test whether microbial communities have the same structure. *ISME J.* **2**, 265–275 (2008).
223. Huse, S. M., Ye, Y., Zhou, Y. & Fodor, A. A. A Core Human Microbiome as Viewed through 16S rRNA Sequence Clusters. *PLoS One* **7**, e34242 (2012).
224. Kozik, A. & Huang, Y. J. Ecological interactions in asthma: from environment to microbiota and immune responses. *Curr. Opin. Pulm. Med.* **26**, 27–32 (2020).
225. Hildebrand, F. *et al.* Inflammation-associated enterotypes, host genotype, cage and inter-individual effects drive gut microbiota variation in common laboratory mice. *Genome Biol.* **14**, R4 (2013).
226. Cox, M. J., Ege, M. J. & von Mutius, E. Challenges, impact and the future. in *The Lung Microbiome (ERS Monography)* 240–244 (European Respiratory Society, 2019).
227. Barfod, K. *et al.* The murine lung microbiome in relation to the intestinal and vaginal bacterial communities. *BMC Microbiol.* **13**, 303 (2013).
228. Trompette, A. *et al.* Gut microbiota metabolism of dietary fiber influences allergic airway disease and hematopoiesis. *Nat. Med.* **20**, 159–166 (2014).

-
229. Fransen, F. *et al.* BALB/c and C57BL/6 Mice Differ in Polyreactive IgA Abundance, which Impacts the Generation of Antigen-Specific IgA and Microbiota Diversity. *Immunity* **43**, 527–540 (2015).
230. Kepert, I. *et al.* D-tryptophan from probiotic bacteria influences the gut microbiome and allergic airway disease. *J. Allergy Clin. Immunol.* **139**, 1525–1535 (2017).
231. Cui, L. *et al.* The Microbiome and the Lung. *Ann. Am. Thorac. Soc.* **11**, S227–S232 (2014).
232. Segal, L. N. *et al.* Enrichment of the lung microbiome with oral taxa is associated with lung inflammation of a Th17 phenotype. *Nat. Microbiol.* **1**, 16031 (2016).
233. Barfod, K. K. *et al.* The Murine Lung Microbiome Changes During Lung Inflammation and Intranasal Vancomycin Treatment. *Open Microbiol. J.* **9**, 167–179 (2015).
234. Arrieta, M.-C. *et al.* Early infancy microbial and metabolic alterations affect risk of childhood asthma. *Sci. Transl. Med.* **7**, 307ra152 (2015).
235. Schloss, P. D., Gevers, D. & Westcott, S. L. Reducing the Effects of PCR Amplification and Sequencing Artifacts on 16S rRNA-Based Studies. *PLoS One* **6**, e27310 (2011).
236. Kozik, A. J. & Huang, Y. J. The microbiome in asthma. *Ann. Allergy, Asthma Immunol.* **122**, 270–275 (2019).
237. Cahenzli, J., Köller, Y., Wyss, M., Geuking, M. B. & McCoy, K. D. Intestinal Microbial Diversity during Early-Life Colonization Shapes Long-Term IgE Levels. *Cell Host Microbe* **14**, 559–570 (2013).
238. Zaiss, M. M. *et al.* The Intestinal Microbiota Contributes to the Ability of Helminths to Modulate Allergic Inflammation. *Immunity* **43**, 998–1010 (2015).
239. Goleva, E. *et al.* The Effects of Airway Microbiome on Corticosteroid Responsiveness in Asthma. *Am. J. Respir. Crit. Care Med.* **188**, 1193–1201 (2013).
240. Chung, K. F. Potential Role of the Lung Microbiome in Shaping Asthma Phenotypes. *Ann. Am. Thorac. Soc.* **14**, S326–S331 (2017).

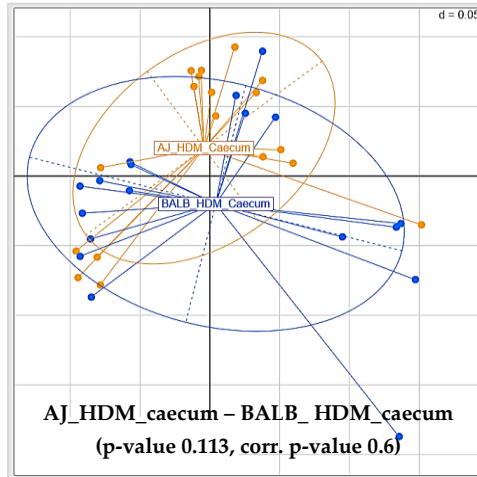
7 Appendix

7.1 Supplemental results

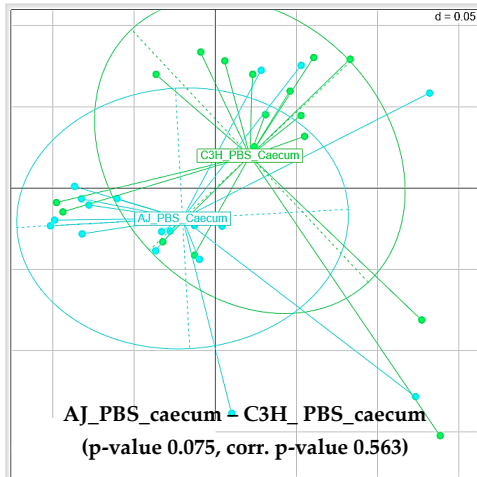
A.1



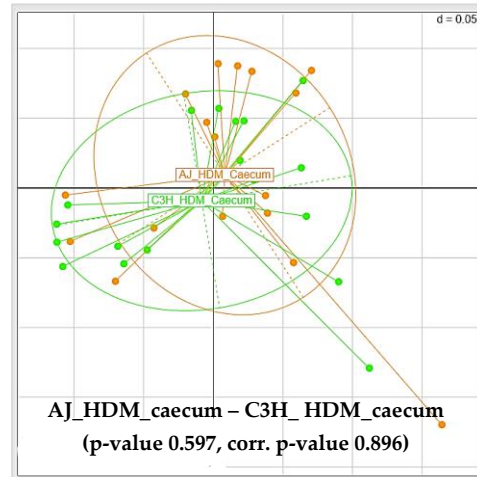
A.2



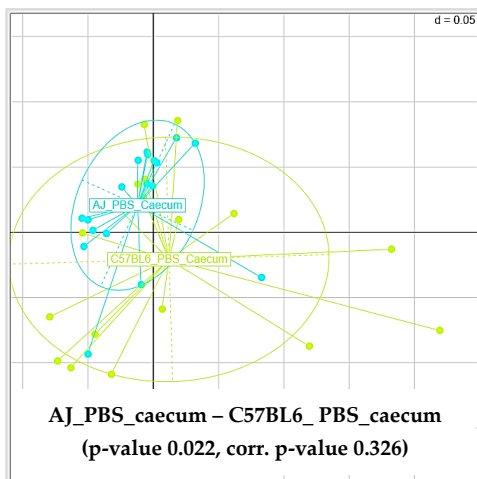
B.1



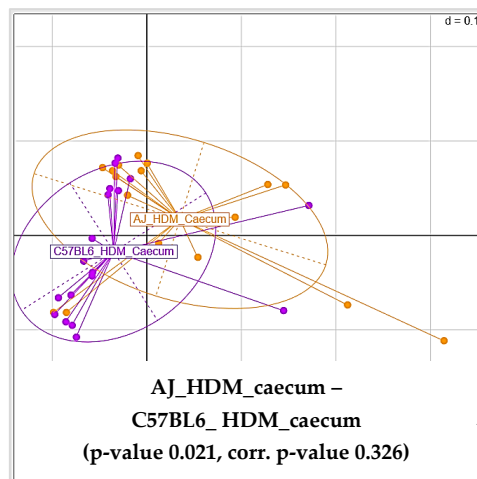
B.2



C.1



C.2



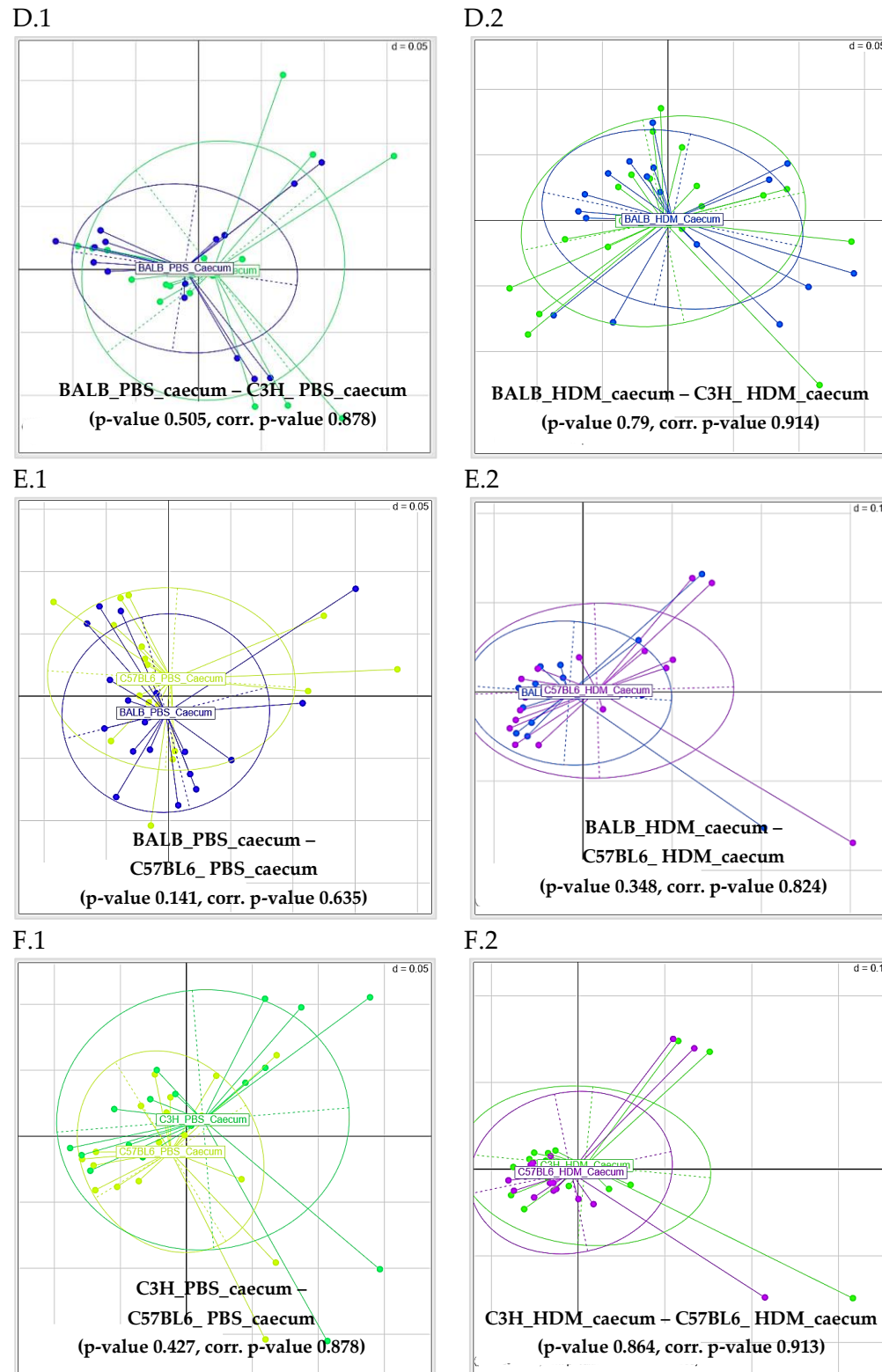
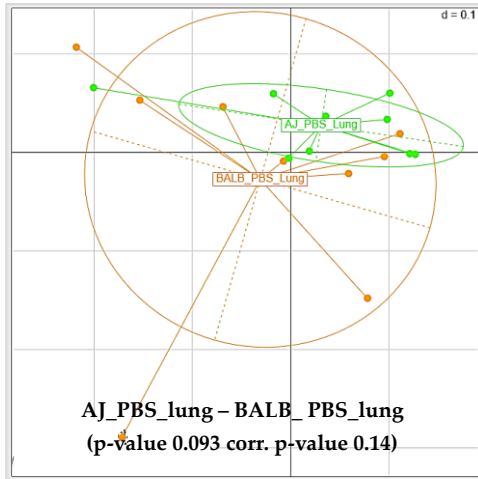


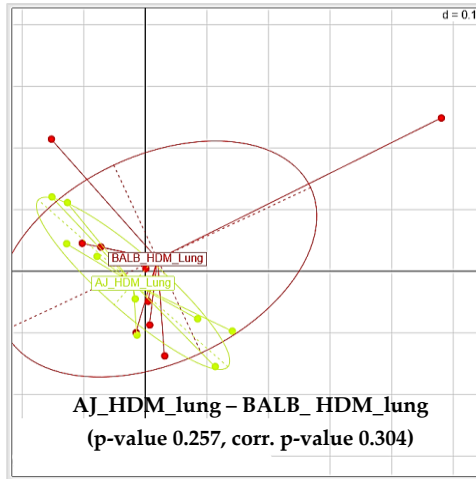
Figure 7.1: MDS plots of caecum samples comparing beta diversity.

MDS plots of caecum samples comparing beta diversity (based on generalized Unifrac distance) PBS vs. PBS (1) and HDM vs. HDM (2) among the strains A. A/J vs. BALB/c] B. A/J vs. C3H/He] C. A/J vs. C57BL/6] D. BALB/c] vs. C3H/He] E. BALB/c] vs. C57BL/6]. Animals ($n=18$ per group) Distances matrices calculated with `vegan::adonis`, subsequently PERMANOVA was applied, followed by Bonferroni-Hochberg method for multiple testing for corr. p value. MDS plots annotate the p values of the PERMANOVA, $d=0.05$ represents 5% and $d=0.1$ represents 10% of dissimilarity in the grid distance.

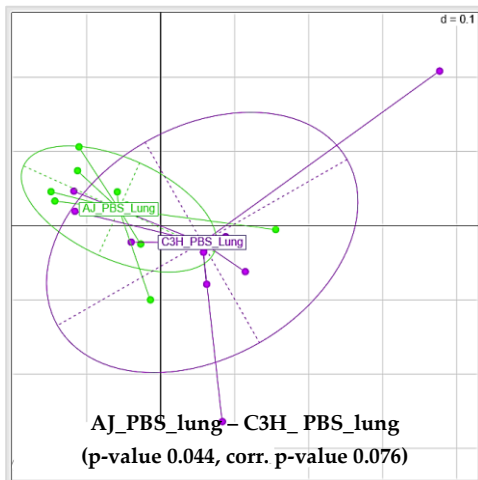
A.1



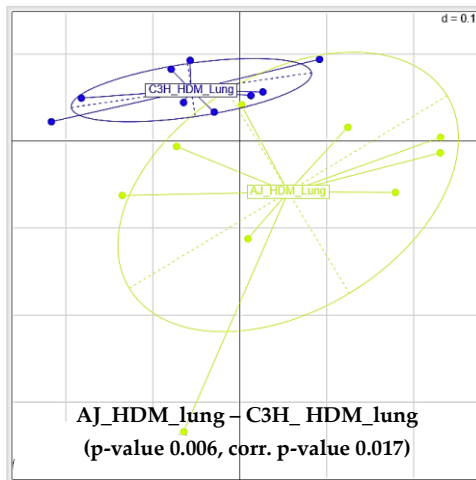
A.2



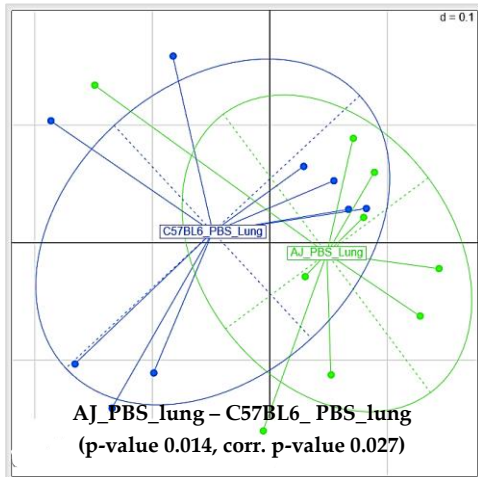
B.1



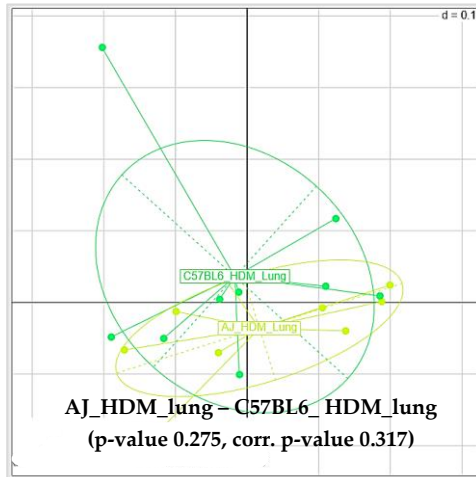
B.2



C.1



C.2



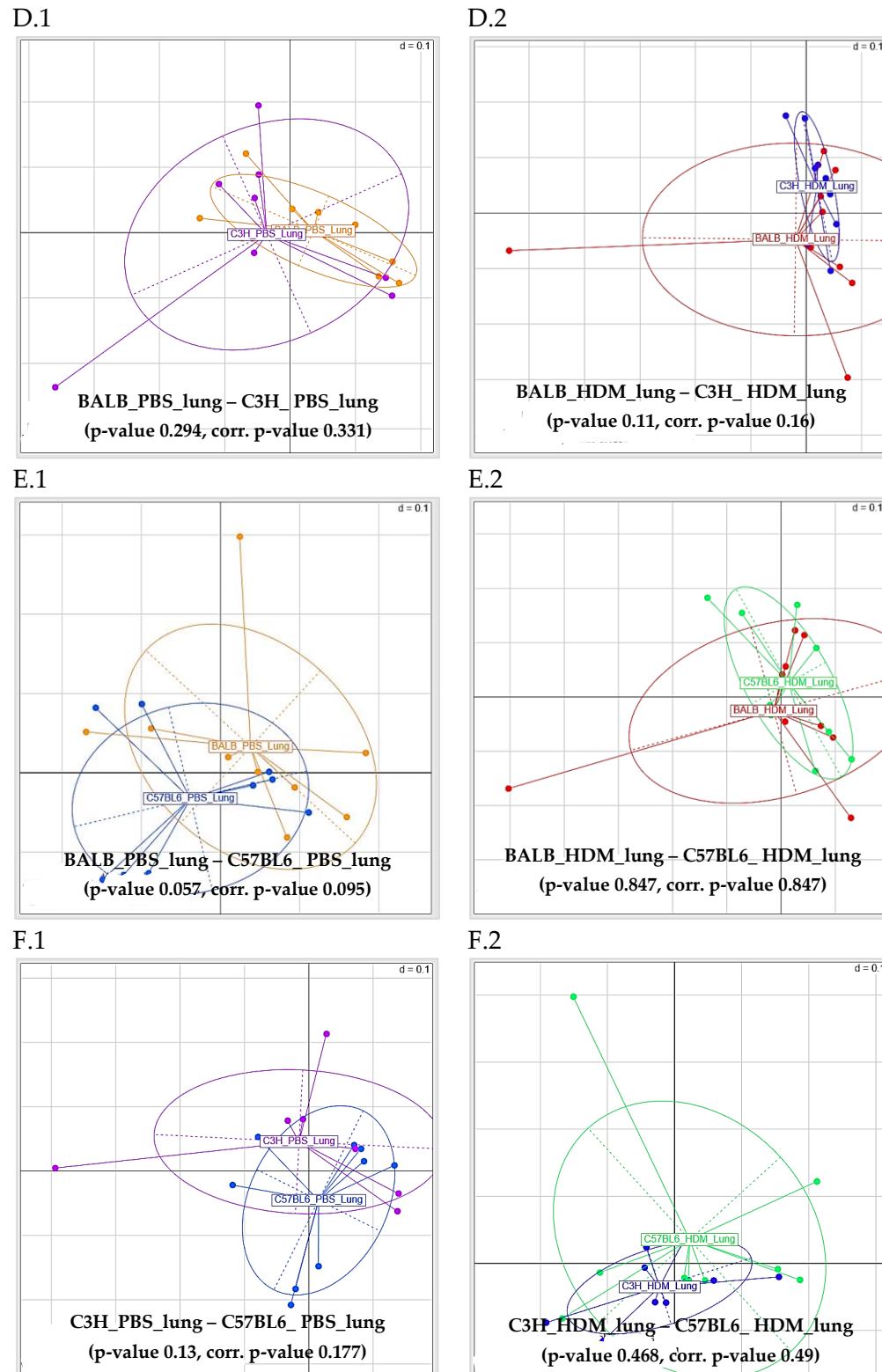


Figure 7.2: MDS plots of lung samples comparing beta diversity.

MDS plots of lung samples comparing beta diversity (based on generalized Unifrac distance) in PBS vs. PBS (1) and HDM vs. HDM (2) groups among the strains. A. A/J vs. BALB/c J B. A/J vs. C3H/HeJ C. A/J vs. C57BL/6J D. BALB/c J vs. C3H/HeJ E. BALB/c J vs. C57BL/6J. F. C3H/HeJ vs. C57BL/6J. Animals ($n=8-9$ per group) Distances matrices calculated with `vegan::adonis`, subsequently PERMANOVA was applied, followed by Bonferroni-Hochberg method for multiple testing for corr. p value. MDS plots annotate the p values of the PERMANOVA and $d=0.1$ represents 10% of dissimilarity in the grid distance.

7.2 List of Figures

Figure 1.1: Categorization of the asthma disease in Th2-high and non-Th2 phenotypes.	3
Figure 1.2: Microbiome development in early life.	9
Figure 3.1: HDM-treatment scheme to induce allergic airway inflammation.	20
Figure 4.1: Total BAL cell numbers.	32
Figure 4.2: Eosinophils in BAL.	33
Figure 4.3: Macrophages in BAL.	33
Figure 4.4: Lymphocytes in BAL.	34
Figure 4.5: Neutrophils in BAL.	34
Figure 4.6: Cytokines measured in BAL supernatant.	36
Figure 4.7: Inspiratory capacity measurement.	37
Figure 4.8: Compliance measurement.	38
Figure 4.9: Resistance measurement.	38
Figure 4.10: AHR measurement for each strain.	39
Figure 4.11: Total IgE levels in serum.	40
Figure 4.12: PAS histology staining of lung sections (10-fold magnification).	41
Figure 4.13: PAS histology staining of lung sections (2-fold magnification).	41
Figure 4.14: CAST analysis of histological features.	42
Figure 4.15: Gene expression of MUC5B and CCL11 in lung homogenates.	43
Figure 4.16: Characterization of asthma phenotypes in four strains.	44
Figure 4.17: Rarefaction curve of all caecum samples.	45
Figure 4.18: Alpha diversity (Simpson effective values) of caecum samples.	46
Figure 4.19: MDS plots comparing beta diversity in caecum samples.	48
Figure 4.20: Correlation plot of alpha diversity in caecum samples.	49
Figure 4.21: Top10 detected Taxonomy in caecum samples.	51
Figure 4.22: Top10 detected Genera in different subgroups of control caecum samples.	52
Figure 4.23: Rarefaction curve of all lung samples.	53
Figure 4.24: Alpha diversity (Simpson effective values) of lung samples.	54
Figure 4.25: MDS plots comparing beta diversity in lung samples.	56
Figure 4.26: Correlation plot of alpha diversity in lung samples.	57
Figure 4.27: Top10 detected Taxonomy in lung samples.	59
Figure 4.28: Top10 detected Genera in different subgroups of control lung samples.	60
Figure 7.1: MDS plots of caecum samples comparing beta diversity.	100
Figure 7.2: MDS plots of lung samples comparing beta diversity.	102

7.3 List of Tables

Table 3.1: Chemicals and reagents	11
Table 3.2: Buffer and solutions	13
Table 3.3: Antibodies.....	14
Table 3.4: Primer sequences for qRT-PCRs.....	14
Table 3.5: 16S rRNA amplicon primer	15
Table 3.6: Multiplex identifier (MID) indexes	15
Table 3.7: Commercial kits	16
Table 3.8: Consumables	16
Table 3.9: Mouse strains	17
Table 3.10: Devices and equipment.....	18
Table 3.11: Software	19
Table 3.12: Light cycler protocol for qRT-PCR	24
Table 3.13: Amplicon-PCR program	27

7.4 Eidesstattliche Erklärung

Hiermit bestätige ich, Joni Valeska Lund, an Eides statt, dass ich die hier vorliegende Dissertation mit dem Titel

“Mice of different genetic backgrounds respond to house dust mite extract with distinct asthma phenotypes and microbial changes”

selbstständig verfasst und mich außer den angegebenen Hilfsmitteln keiner anderen bedient habe und alle Erkenntnisse, die dem Wortlaut oder dem Sinn anderer Werke annähernd übernommen sind, als solche kenntlich gemacht und ihre Quelle und die Bezeichnung dieser einzeln kenntlich gemacht habe. Darüber hinaus ist die Arbeit unter der Einhaltung der Regeln guter wissenschaftlicher Praxis der Deutschen Forschungsgesellschaft entstanden.

Ich erkläre des Weiteren, dass die hier vorgelegte Dissertation nicht in gleicher oder ähnlicher Form bei einer anderen Stelle zur Erlangung eines akademischen Grades eingereicht wurde.

Ort, Datum

Unterschrift

7.5 Curriculum vitae

Name: Joni Valeska Lund

Academic education

- 09/2016 – **PhD Thesis**
 03/2020 “Mice of different genetic backgrounds respond to house dust mite extract with distinct asthma phenotypes and microbial changes”
Early Life Origins of Chronic Lung Diseases, Research Center Borstel, Leibniz Lung Center, Member of the German Lung Society (DZL), Borstel, Germany
- 04/2010 – **Third state examination (Pharmacy)**
 08/2015 Approbation as a public pharmacist
Pharmaceutical Institute of the Christian-Albrecht-University of Kiel, Kiel, Germany

Publications

- 03/2019 Lund, J., Schloter, M. & Krauss-Etschmann, S.: Die Rolle des Mikrobioms bei Lungenerkrankungen: Kausalzusammenhang zwischen verändertem Lungenmikrobiom und Lungenerkrankungen noch ungeklärt. Current congress: 60. Jahrestagung der Deutschen Gesellschaft für Pneumologie und Beatmungsmedizin e. V. 41. Jahrestagung der Gesellschaft für Pädiatrische Pneumologie e. V. (2019)
- 03/2020 Krauss-Etschmann, S., Lund, J.V., Kovacevic, D. & Schloter, M. Rolle der mikrobiellen Darm-Lungen-Achse für die Lungengesundheit: Mikrobiom – Darm-Lungen-Achse – Lungenerkrankungen – bakterielle Metabolite. Pädiatrische Praxis. Band 93 (2020)

Awards

- 05/2018 **Best Poster Award**
J. Lund, S. Bartel, Z. Orinska, L. Lunding, S. Kull, J. Baines, U. Jappe, S. Krauss-Etschmann. Distinct “asthma” phenotypes of four mouse strains correlate with different responses to house dust mite (HDM) allergens. *EACCI Annual Conference, Munich, Germany, 2018.*
- 03/2019 **Travel grant recipient**
17th ERS Lung Science Conference, Estoril, Portugal, 2019.

7.6 Acknowledgements

Finally, at the end of this work I would like to say a big thank you to all the great people who contributed to this work and without whom none of this would have been possible.

First of all, I would like to thank Prof. Susanne Krauss-Etschmann for the opportunity to work on this exciting research project and her excellent supervision. I am very thankful for your patience, support, advice and motivations during my PhD time. Especially, I would like to thank you for always having an open ear for me, although there were very busy times. You always encouraged me to attend national and international scientific conferences and taught me valuable skills throughout the past which I really appreciate.

Next, I want to give a great thank you to Dr. Sabine Bartel who guided me through the first two years and helped me to lay a solid foundation for the mouse experiments and all lab related tasks. All of your guidance was of tremendous relevance for starting this project and develop all necessary skills.

A huge thank you also applies to my fellow (present and former) lab members in the SKE lab at the Research Center Borstel: Gregor Jatzlauk, Martin Wolff, Barbara Hammer, Draginja Kovacevic, Janin Braun, Dr. Sebastian Reuter, Gabi Huß, Arne Krüger, Dr. Natalia El-Merhie, Masha Spaszus, Dr. Eistine Boateng and Huan Ma. Thanks for all the great time we spent together in the lab, office and on conferences! I could not have imagined better colleagues for my PhD project.

Furthermore, my sincere thanks goes to Prof. Holger Heine from the Research Center Borstel for his supervision and fruitful input during the meetings and discussions we had. As my additional supervisor I would like to acknowledge Dr. Machteld Hylkema for sharing her experience with me.

An important thank you goes also to my collaborators on this project. I thank my collaborators from the Max Planck institute in Plön of Prof. John Baines' group in sharing their expertise in 16S rRNA sequencing, enabling me to perform the library preparation and performing the sequencing run in their lab. Thank you, Cecilia Chung, Dr. Sven Künzel and all the other members.

Next, I would like to thank all collaborators within the Research Center Borstel. Thank you, Dr. Zane Orinska and your team, for performing the IgE analysis in your lab and the valuable input you gave me over the time. Further, I would like to thank the Wegemann group (Asthma Exacerbation and Regulations) and the Fehrenbach group (Experimental Pneumology) for their time spent on the CBA measurement and CAST analysis. Special thanks go to Juliane Alert and Franziska Beyersdorf. Furthermore, I would like to thank the Pathology for performing the PAS staining of the lung slides.

In addition, I would like to acknowledge other research groups of the Research Center Borstel for their briefing and provision of their lab space and lab equipment: Innate Immunity (Heine), Molecular and Experimental Mycobacteriology (Niemann), Cellular Microbiology (Schaible), Infection Immunology (Hölscher), Microbial Interface Biology (Reiling), as well as the animal facility workers.

Beyond this, thank you Dr. Thorsten Lange for proof reading the thesis at short notice.

Last but not least, a heartfelt thank you goes out to my family, especially my parents and siblings and their families, and my close friends, for supporting me unconditionally and always being there for me even in hard times.